UTS UNIVERSITY OF TECHNOLOGY SYDNEY

Development of Monitoring, Modelling and Control Systems for Human Physiological Assessment with Wearable Devices

by Hairong Yu

Thesis submitted in fulfilment of the requirements for the degree of

Doctor of Philosophy

under the supervision of Steven Su

University of Technology Sydney
Faculty of Engineering and Information Technology

June 2020

Declaration

I, Hairong Yu, declare that this thesis is submitted in fulfilment of the requirements for the award of Doctor of Philosophy in the Faculty of Engineering and Information Technology at the University of Technology Sydney.

This thesis is wholly my own work unless otherwise reference or acknowledged. In addition, I certify that all information sources and literature used are indicated in the thesis.

This document has not been submitted for qualifications at any other academic institution.

This research is supported by an Australian Government Research Training Program Scholarship.

Signature: Production Note:
Signature removed prior to publication.

Date: 27/06/2020

Acknowledgements

I would like to express my sincere gratitude to my supervisor A/Prof. Steven Su for his continual support, guidance, help and encouragement during my Ph.D. study. A/Prof. Steven Su has brought me into the topics of physiological modelling and system identification, and provided brilliant insights in my research work. It is my honor to have a supervisor who always inspires me to achieve higher targets and overcome difficulties. His conscientious and meticulous attitude on research has significant influence on my work.

I am grateful to all the staff in the School of Biomedical Engineering, especially to Prof. Joanne Tipper and Prof. Gyorgy Hutvagner for their help on Ph.D. skills development. I would also like to thank my co-supervisor Prof. Rob Duffield, Prof. Hung T. Nguyen (Swinburne University of Technology) and my external supervisor Dr. Ganesh Naik (Western Sydney University) for their kind support. Grate gratitude also for my supervisor during bachelor period, Prof. Rong Song (Sun Yat-Sen University, China), for his help in my Ph.D. period.

I am also grateful to my colleagues in A/Prof. Steven Su's research group, in particular, Lin Ye, Wenhui Chen, Yao Huang, Kairui Guo, etc., for their selfless help. Working together with them will be a good memory. I am also grateful to my friends in UTS, Zhichao Sheng, Ye Shi, Zhiyuan Shi, Hanjie Wu for their warm help.

My deepest gratitude goes to my parents for their immeasurable support and encouragement throughout my graduate studies.

Abstract

Physiological signals play vital roles in studying the mechanism of human body reaction during exercise and human kinetics assessment. This thesis develops a wearable exercise monitoring system to monitor and regulate human cardiorespiratory responses to moderate exercise. To describe the relationship between the body's physiological reactions and the exercise, the modelling approach has been extensively explored in a range of applications. In this thesis, the cardiorespiratory signal responses to the exercise phase are comprehensively analysed through the means of different modelling approaches. A non-parametric kernel based modelling approach has been proposed to address the complexity of the model dynamics. This thesis also develops a novel Inclination based Calibration method to address the static nonlinear modelling problem for the calibration of the sensors in an Inertial Measurement Units.

The non-parametric model is the preferable method when the system structure information is insufficient, or the system is too complex to be described by a simple parametric model. Hence, the non-parametric modelling method with kernel-based regularisation is developed to estimate the physiological signal response to the exercise phase during different types of exercise. The kernel selection and regularisation strategies are discussed, and a series of simulations are performed to compare the fitness, sensitivity and stability of different kernels.

For detecting the exercise phase, the innovative in-field calibration method for the portable tri-axial sensor is developed to calibrate the Inertial Measurement Units data. Based on the fact that the angle between the local gravity and magnetic field is invariant, this thesis proposed a new in-field calibration approach, called Inclination Based Calibration, which can reliably estimate the model parameters of the sensor with a simple linear Least Square estimator. Based on optimal experimental design, a 12-observation Icosahedron experimental

scheme has been performed for micro Inertial Measurement Units. Both the calibrated results and the simulation comparison demonstrate the effectiveness of the proposed method.

This monitoring and control system could comprehensively study human kinetics and cardiorespiratory mechanism and help to make assessments. Some general approaches for physiological signal processing and modelling, parameters estimation, sensor calibration and experiment protocol control are proposed in this work. The effectiveness and benefits of different modelling approaches are demonstrated by a range of means. This system could be applied in strategic exercise design, athletic assessment, exercise enhancement and health monitoring.

Publications

The contents of this thesis are based on the following papers that have been published, accepted, or submitted to peer-reviewed journals, conferences and book chapters.

Journal Papers:

1. Hairong Yu, Lin Ye, Ganesh R. Naik, Rong Song, Hung T. Nguyen, Steven Su*, "Nonparametric Dynamical Model of Cardiorespiratory Responses at the Onset and Offset of Treadmill Exercises." *Medical & biological engineering & computing*, vol. 56, no. 12, pp. 2337-2351, June 2018.

2. Hairong Yu, Lin Ye, Ying Guo, Steven Su*, "An Innovative 9-Parameter Magnetic Calibration Method Using Local Magnetic Inclination and Calibrated Acceleration Value", *IEEE Sensors Journal*, doi: 10.1109/ JSEN. 2020. 2995876, May 2020.

3. Lin Ye, Ahmadreza Argha, Hairong Yu, Branko G. Celler, Hung T. Nguyen, Steven Su*, "Dynamic Characteristics of Oxygen Consumption.", *Biomedical engineering online*, vol. 17, no. 1, pp. 44, December 2018

4. Lin Ye, Ying Guo, Lei Dong, Hairong Yu, Hung Nguyen, Steven Su*, "A Fast-Converge, Real-Time Auto-Calibration Algorithm for Triaxial Accelerometer." *Measurement Science and Technology*, vol. 30, no. 6, pp. 065010, February 2019.

5. Hairong Yu, Lin Ye, Hamzah M Alqudah, Kairui Guo, Branko G. Celler, Rong Song, Steven Su*, "Prediction of Cardiac-respiratory Response to Treadmill Exercise by Using Non-Parametric Modelling with Stairs Exercise based Kernel Characterization", under submission to *IEEE Transactions on Biomedical Engineering*, 2020.

6. Hairong Yu, Lin Ye, Rong Song, Yuxi Luo, Hamzah M Alqudah, Steven Su*, “Oxygen Consumption Response to Stair Exercise by Non-parametric Modelling", under review at *Biomedical Physics and Engineering Express*, 2020.

7. Hairong Yu, Lin Ye, Ying Guo, Steven Su*, “An Effective In-Field Calibration Method for Triaxial Magnetometers based on Local Magnetic Inclination", under review at *IEEE Transactions on Instrumentation and Measurement* , 2019.

Conference Papers:

1. Hairong Yu*, Kairui Guo, Hung T. Nguyen, Steven Su, “The Classification for “Equilibrium Triad” Sensory Loss based on sEMG Signals of Calf Muscles.” *2017 39th Annual International Conference of the IEEE Engineering in Medicine and Biology Society (EMBC)*. IEEE, July 2017.

2. Kairui Guo, Hairong Yu*, Rifai Chai, Hung Nguyen, Steven W. Su, “A Hybrid Physiological Approach of Emotional Reaction Detection Using Combined FCM and SVM Classifier.” *2019 41th Annual International Conference of the IEEE Engineering in Medicine and Biology Society (EMBC)*. IEEE, July 2019.

3. Kairui Guo*, Henry Candra, Hairong Yu, Huiqi Li, Hung T. Nguyen, Steven W. Su, “EEG-based Emotion Classification using Innovative Features and Combined SVM and HMM Classifier.” *2017 39th Annual International Conference of the IEEE Engineering in Medicine and Biology Society (EMBC)*. IEEE, July 2017.

4. Yao Huang, Rong Song*, Wenhui Chen, Hairong Yu, Ahmadreza Argha, Branko G. Celler ,Steven Su, “The Effects of Different Tracking Tasks on Muscle Synergy through Visual Feedback.” *2019 41th Annual International Conference of the IEEE Engineering in Medicine and Biology Society (EMBC)*. IEEE, July 2019.

5. Kairui Guo*, Hairong Yu, Yunzhu Chen, Rong Song, Steven W. Su “Puzzle-based Automated Upper Limb Functional Electrical Stimulation Strategy Using EMG Connectivity Analysis.” *2020 42th Annual International Conference of the IEEE Engineering in Medicine and Biology Society (EMBC)*. IEEE, July 2020.

Book Chapters:

Table of contents

List of figures

List of tables

Chapter 1

Introduction

This chapter starts with the motivation and scope of this thesis, then introduces some related research topics, and finally provides an outline of the thesis.

1.1 Motivation and Scope

Physiological assessment is essential for studying the metabolic demands that are placed on the human body. Physiological assessment can be developed by various means, including exercise phase evaluation, sports fitness assessment and determination of energy system utilisation. The most commonly accepted components of physiological assessment include cardiorespiratory response, energy consumption, and exercise endurance. The physiological signal is widely used in physiological assessment. The oxygen uptake ($\dot{V}O_2$) or carbon dioxide output ($\dot{V}CO_2$) are used to assess aerobic fitness. The Electrocardiogram (ECG), Electromyogram (EMG) and Electroencephalogram (EEG) are applied to analyse the physiological status of exercisers. Moreover, acceleration and magnetic data serves to detect the direction and describe status of the movement.

Some of the most significant advancements in physiological assessment have been made possible by the development of sophisticated and novel equipment. The development of wearable equipment, such as portable gas analysers, Inertial Measurement Unit (IMU) sensors and wireless ECG, EMG, EEG sensors, makes it possible to record large amounts of data unlike the limited data recording opportunities in the past. Meanwhile, modelling methods

have been enhanced with the development of the wearable devices so that they can effectively study the relationship between the exercise phase and physiological signal, especially the cardiorespiratory information. By comparison, the traditional modelling method could only map levels of fitness with a limited range of data. Hence, improved or optimised modelling methods were developed to the accommodate large datasets.

The modelling methods are divided into different types with different classification criteria. In the linear mathematical model, all of the operators must exhibit linearity, otherwise it is described as a nonlinear model. The static model is a model that calculates the system in equilibrium and is time-invariant. In contrast, the dynamic model accounts for time-dependent changes in the state of the system. Different types of models are applied in physiological assessment according to the characteristic of the physiological model. In this study, the relationship between the exercise phase and the physiological signal response is comprehensively studied by various modelling approaches.

During exercise, a vital aspect is to make sure that the IMU data are accurate enough to detect the exercise phase (such as ascending or descending). Regular calibrations are necessary to minimise the interference, such as hard iron and soft iron, to ensure the accuracy of the measurements. If the response speed of the IMU sensor is quick enough, this calibration question is a problem of a static nonlinear modelling. If the environment changes, the inertial system will not recalibrate on its own. The operating environment must be evaluated to determine if the application needs to be recalibrated. To meet this need, the application must have a user-controlled field calibration process. The in-field calibration are classified as “Attitude-Dependent" and “Attitude-Independent" approaches. The “Attitude-Dependent" approach requires high precision turntables to control the sensor orientation while the “Attitude-Independent" approach does not require this. It is necessary for these methods to solve a nonlinear estimation problem to identify the coefficients of the tri-axial accelerometers or magnetometers model. Considering these aspects, we intend to apply the linearisation approach to develop a new calibration algorithm that combines the acceleration data and magnetic data for calibration. This work proposes a novel calibration method, called Inclination based Calibration (I-Calibration). It is based on the fact that the local magnetic inclination is constant, which means that the angle between local gravity and magnetic field is invariant. The proposed I-Calibration provides a solid foundation for

the exercise phase detecting to ensure an accurate input in the kinetics-respiration reaction system.

One of the challenges for the modelling of the human physiological variable is the stimulation of the input is often limited. This prevents the use of models with high-dimensional parameters, as it usually leads to ill-posed inverse problems. The kinetics-respiration reaction system is described as a first or higher order time-invariant system in previous research. The classical system identification methods, e.g. Least Square, Maximum Likelihood and Prediction Error Method, are broadly used in modelling the first or higher order time-invariant system. However, an important issue in identification is how to design the experiment to ensure sufficient stimulation for the modelling of the system. When the structure of the system cannot be determined or it is too complicated to be described by a simple parametric model, a better method should be developed.

According to the above aspects, the non-parametric modelling method with a kernel regularisation term is proposed in this work which is applied in the system modelling for human physiological assessment as this is also considered to be a dynamic linear modelling problem. The experiment protocol is also well designed to ensure the stimulation for the system. The physiological signals collected from the wearable devices are considered as the output in this system and the aerobic exercise phase is considered as the input in order to study the cardiorespiratory response during aerobic exercise. Different phases of aerobic exercise and different performances of the various physiological signals are studied in this research.

For the first step, the cardiorespiratory response during the simply onset or offset phase of the jogging exercise on the treadmill is investigated. Treadmill exercise is similar to outdoor walking or running so it can be applied to analyse the mechanism of human exercise. Moreover, the treadmill is a good choice for exercise modelling because the model needs an accurate input to ensure a steady workload and exclude other effect factors. Various studies manifest different aspects of kinematics and the pattern of gas exchange. However, the dynamic changes of the $\dot{V}O_2$ and $\dot{V}CO_2$ during different periods of exercise and their concomitant relationships need to be more deeply investigated in order to acquire a comprehensive understanding of the human exercise mechanism.

The second step is to study the dynamic cardiorespiratory response with the continuously changing exercise phase. The intensity of the stair exercise can be adjusted by the exercise phase (ascending or descending) without causing any discomfort to the exercisers. The continuously changing protocol for the stair exercise provides more stimulation for the system, utilised as prior information for the tuning of the kernel covariance. Commonly, the system in previous articles often comes from a single onset or offset period experiment and is considered as a first-order system. However, the first-order system is not suitable when the input and output of the system becomess complicated as in our experiment. In addition, the individual difference in the treadmill onset or offset study also supports the diversity of the model due to the complexity of the human motion system and respiratory system.

The final step is to study the influence of the parameters in the kernel matrix on the estimation results. To ensure that there is sufficient stimulation, the dataset from the stairs experiment is applied in the kernel parameters selection. The selected kernel is utilised to analyse how the oxygen uptake or carbon dioxide output responds to the walking speed on the treadmills. Moreover, the advantages of using the non-parametric model, the necessity of sufficient stimulation for identification and the importance of the kernel regularisation term are also clearly demonstrated.

These aspects are combined to finalise the monitoring, modelling and control system. In this system, the modelling approaches are developed in terms of two aspects, static nonlinear modelling and dynamic linear modelling. The static nonlinear modelling method is developed by the proposed I-Calibration method to ensure an accurate exercise phase input. The dynamic linear modelling method is conducted by non-parametric modelling to identify how the physiological signal responds to the exercise phase. According to the identification results and analysis, this system could comprehensively study the human physiological performance and cardiorespiratory mechanism and help to make assessments.

The functional block diagram of this work is shown in Figure 1.1.

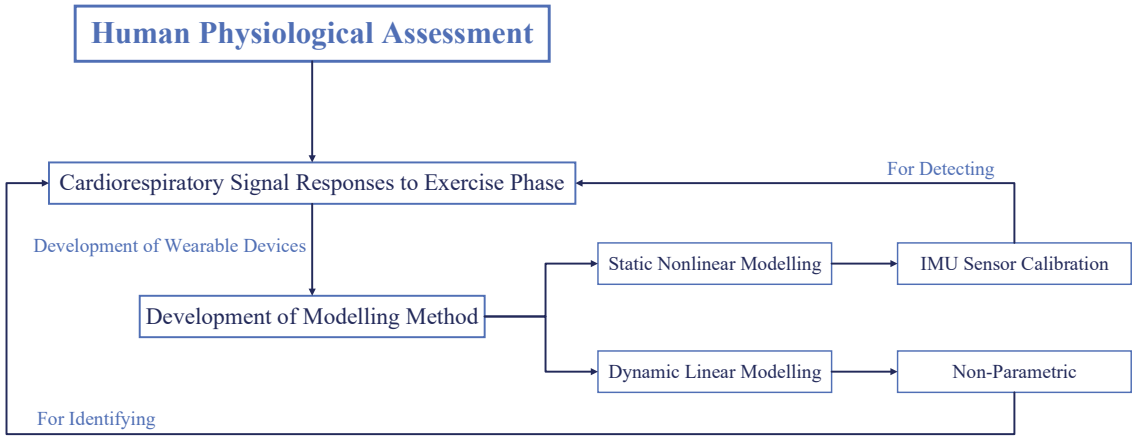

Fig. 1.1 Functional block diagram.

In general, the goals of the research in this part of the dissertation can be summarised as follows:

- Build a comprehensive human physiological assessment system which can be applied to strategic exercise design, athletic assessment, exercise enhancement and health monitoring. Provide a theoretical framework for the modelling results which will enable a comprehensive analysis of the human kinetics and cardiorespiratory mechanism and a solid means to make assessments.
- Study the different characteristic of different models with different modelling methods. The calibration for the IMU sensor is considered as a static nonlinear model while the modelling for the physiological signal response during the exercise is considered as a dynamic linear model.
- Propose a novel calibration method for the IMU sensor which will solve the acceleration or magnetic field calibration problem with a linear least square problem. This method would be particularly suitable for real-time in-field calibration for wearable devices with limited computational power.
- Prove the non-parametric model is beneficial for physiological signal modelling when the structure of the model is complicated. The non-parametric model could achieve a higher accuracy for the modelling results. In addition, it is suitable for different exercise phases and is compatible with individual difference.

- Study the relationship between $\dot{V}O_2$ and $\dot{V}CO_2$ from identification results. Demonstrate $\dot{V}O_2$ and $\dot{V}CO_2$ during exercise are related and are based on the physiological principle. The performance of different phases during exercise is different in some respects.
- Make comparison between different phases of the exercise and study the changing structure of the complicated exercise model. The structure of the system under the protocol in our experiments is of higher complexity than the first-order system or time-invariant system and this is demonstrated by the identification results.
- Investigate the importance of the kernel and its parameter selection for building the non-parametric model. The kernel matrix is the base for the regularisation term which ensures the accuracy of the modelling results.

1.2 Problems in Physiological Assessment and Aerobic Exercise

The comprehensive physiological assessment may include extensive cardiovascular evaluations with an ECG exercise tolerance test, blood chemistry analysis and blood count, maximum oxygen uptake measurement, pulmonary function tests, and orthopedic assessment [1, 2]. Among these, the cardiorespiratory evaluation is studied by different researchers in terms of various aspects. Among these studies, aerobic exercise is most commonly examined due to the close relationship between aerobic power and human physiological fitness.

Aerobic exercise is a type of exercise performed at moderate levels of intensity for extended periods and is a physical exercise which mainly depends on the aerobic energy-generating process [3]. Among various types of aerobic exercise, the interval training exercise, e.g., ascending-descending switching exercise, is one of the most commonly used protocols for enhancing cardiovascular fitness for trainers. The regular stair exercise is a good method to demonstrate the effects of the interval training exercise due to several reasons. These include improving cardiovascular fitness, calorie consumption, convenience, and low-cost [4–6]. The intensity of the stair exercise can be adjusted by the exercise phase (ascending or descending) without causing any discomfort to the exercisers [7]. The treadmill exercise is similar to walking or running in daily life so it can be applied to analyse the physiological

mechanism. It is well documented that regular treadmill exercise can greatly improve the human cardiovascular system, e.g., increase total oxygen demand and consumption (the amount of increase depending on the size of the muscles used), and VO_2 Max. Moreover, the treadmill exercise is a good choice for exercise modelling because the model needs an accurate input to ensure a steady workload and exclude other effect factors.

Some research [8] has employed the Heart Rate (HR) for the purposes of analysis, and portable sensors enable us to measure the HR conveniently while monitoring the intensity of the exercise thereby ensuring that the exercise is under aerobic conditions [7, 9, 10]. The Maximum heart rate (HR_{max}) is the highest HR that an individual can achieve without causing severe problems through exercise stress [10]. Considering the linear relationship between the HR and $\dot{V}O_2$, HR_{max} [11, 12] has been recognised as an indicator to detect the exercise intensity [13]. However, HR can easily be affected by human motion or other aspects. Accordingly, other researchers have focused on how the gas changes during exercise and this serves as their index.

The four parameters for aerobic fitness include aerobic power, or maximal oxygen uptake, work efficiency, time constant for oxygen uptake kinetics and the lactate threshold. Thus, the respiratory information, such as voluntary ventilation, oxygen uptake ($\dot{V}O_2$) or carbon dioxide output ($\dot{V}CO_2$), is also commonly used to assess the metabolism demands. In addition, the respiratory information is not affected by the participants' emotion compared with HR and hence guarantees a more accurate assessment result. The oxygen inhaled by the human body is equal to the demands during exercise and reaches a physiological balance. Aerobic exercise depends primarily on the $\dot{V}O_2$, and this intensity is related to respiratory information. It is recommended that the HR_{max} shall be kept in a proper range to ensure that the working peripheral muscles are supplied with enough oxygen.

Decades ago, some sports physiology laboratories used the Douglas bag and the Scholander gas analyser [14] to measure the oxygen (O_2) uptake and the amount of carbon dioxide (CO_2) produced before, during, and after exercise. More recently, automated portable gas analysis systems have been developed and applied in various sports fields for energy consumption assessment [15]. The study of $\dot{V}O_2$ is a traditional theme of sports physiology study and one of the paramount areas of current and future sports physiology research. Hill et al. [16] studied $\dot{V}O_2$ and investigated its recovery curve. After moderate exercise, it is a

logarithmic equation, which is equally applicable to the recovery curves of $\dot{V}CO_2$. Similarly, Wasserman illustrated the equation of $\dot{V}CO_2$ is equal to $\dot{V}O_2$. Research about the $\dot{V}O_2$ and $\dot{V}CO_2$ during the exercise have also been developed.

When people do exercise, the energy consumption, HR, $\dot{V}O_2$ and $\dot{V}CO_2$ will keep increasing until it reaches a peak. When the exercise intensity gets lower, these figures will decrease to form a valley [7]. The phase of the exercise could be considered as a square signal if we describe the exercise status as two numerical indicators. On one hand, to detect the exercise phase, the IMU sensors are widely applied in exercise experiments. The IMU sensors should be calibrated properly to ensure accuracy. The mathematical model for calibration could be considered as a static nonlinear model. On the other hand, the above physiological signals, such as HR, $\dot{V}O_2$ and $\dot{V}CO_2$, change with the phase. Accordingly, the human cardiovascular system can be described by a dynamic model whose input is the phase and output is the physiological signal.

1.3 Problems in Physiological Signal Modelling

1.3.1 Static Nonlinear Modelling Problems for Inertial Measurement Unit Calibration

The chip-based inertial sensors (e.g. Tri-Axial Accelerometers (TAs), Tri-Axial Magnetometers (TMs), Tri-Axial Gyroscopes (TGs), and Inertial Measurement Units (IMUs)) of Micro Electro Mechanical Systems (MEMS) have already been extensively utilised in wearable health monitoring devices [17, 18] and consumer electronic devices [19, 20]. These kinds of devices are also widely used and effective in terms of detecting the exercise status. Regular calibrations are necessary to minimise the interference to ensure the accuracy of the measurements, such as hard iron and soft iron [21, 22]. The calibration procedure can be considered as a static system when the sensor's output responds quickly with the input, and the mathematical model is nonlinear.

Large amounts of auto-calibration methods have recently been developed to calibrate the MEMS and are suitable for the in-field calibration [23]. The in-field calibration method is an effective approach and several convenient methods have been developed [24–27]. Compared

with “Attitude-Dependent" approaches, the “Attitude-Independent" methods do not require high precision turntables to control the sensor orientation. The parameter estimation of “Attitude-Independent" is commonly based on the nonlinear filtering approaches or nonlinear parameter estimation algorithms [24, 27]. One of the typical “Attitude-Independent" calibration methods focuses on minimising the difference between the magnitude of the measured gravity or magnetic field and that of the local gravity or magnetic field [28]. Another “Attitude-Independent" method formulates the calibration problem as an ellipsoid fitting problem [21, 29, 30]. After the ellipsoid fitting calibration, the ellipsoid of data will be mapped to a sphere [31, 32]. These methods have several advantages and only accelerometers or magnetometers data are needed. However, it is necessary for these methods to solve a nonlinear estimation problem to identify the coefficients of the tri-axial accelerometers or magnetometers model. Considering these aspects, we intend to apply the linearisation approach in developing a new calibration algorithm that combines the acceleration data and magnetic data for calibration.

The magnetic inclination is the angle between the magnetic field and horizontal plane. The inclination of a magnetic field is a form of useful angle information applied to the 3D space [33]. As the local magnetic inclination is constant, the angle between the local gravity and magnetic field is invariant. In Kok’s paper [34], it was reported that the measured accelerometers data together with magnetometers data could be used to estimate the inclination if the sensor is mounted in a static platform or its motion acceleration is much lower than the local gravity [34]. The constant inclination can be described by the magnetic field and the gravity, and this provides an idea of how to calibrate the measured value based on both the TMs and TAs.

Design of Experiment (DoE) is vital prior to the calibration to ensure the accuracy and effectiveness of the calibrated results [35–38]. DoE theory investigates the optimal selection or design of an appropriate input signal to stimulate the system significantly in order to extract the maximum system information under a limited number of experiments with physical constraints. The DoE of traditional IMU calibration problem can be addressed by using the well-established DoE theory [39–42]. The key step in experimental design is the calculation and analysis of the Fisher Information Matrix (FIM), which is related to this classical parameter estimation problem. Later, the optimal experimental design may be achieved by maximising or minimising a certain index of FIM. Such an index is often

defined in various ways, which has led to several famous design schemes, e.g., D-optimal, E-optimal, ED-optimal[43], G-optimal [39], and Ds-optimal design [44]. Based on the study of the response surface methodology [45], we have therefore developed two types of optimal experimental methods which are suitable for the calibration of the sensors model.

Well known experimental design methods include Central Composite Design (CCD), which is based on the measurements from fractional factorial points, axial points and centre points [38], and Box-Behnken Design (BBD), which is focused on the midpoints of edges and the centre [35, 38]. Generally speaking, central composite design and Box-Behnken Design are designed to reach the desired orthogonality, rotatability, and D-optimality as discussed in [46]. In this study, beside the revised BBD and CCD, we also discuss an Icosahedron design which is more suitable for this specific model. Based on the DoE for the calibration of the inertial sensor and unit [27], and considering the similarity of calibration between magnetometers and accelerometers, the Icosahedron Experiment with 12-observation DoE has been proposed [47]. In this study, we propose the 12 observation Icosahedron scheme for the calibration method as it can uniformly distribute the experiment points on experimental domains.

1.3.2 Dynamic Linear Modelling Problems for Physiological Signal Response with Exercise Phase

The modelling method is widely used in physiological signal analysis [48–50]. Among the research that spans a number of decades, $\dot{V}O_2$ and $\dot{V}CO_2$ have been measured at various sports physiological laboratories using the gas analyser [51]. With the development of new technology, the automated portable gas analysis system has been used in several sports fields for the energy consumption assessment [14]. $\dot{V}O_2$ and $\dot{V}CO_2$ analysis during exercise have been significantly developed to cover a range of aspects. According to the logarithmic equation of $\dot{V}O_2$ and $\dot{V}CO_2$, the physiological signal modelling for aerobic exercise is commonly developed to estimate the steady status and dynamic response during one simple phase of exercise.

In previous research, the respiration reaction system is often described as a first or higher order time-invariant system. To the best of our knowledge, all the existing studies only

utilised classical system identification approaches in modelling the first or higher order time-invariant system, e.g. the Least Square (LS), Maximum Likelihood (ML) and Prediction Error Method (PEM). However, the signals exerted on a human body should be carefully selected to ensure the safety. Due to this reason, when a human being is involved in an experiment, the input signals are often limited in both intensity and duration, which leads to insufficient stimulation for the modelling of the system. If this is the case, the LS/ML/PEM equipped with classical model structure selection approaches often fail to obtain an appropriate model with desired accuracy and robustness for cardiorespiratory response estimation [52–54]. An important issue in identification is how to design the experiment to ensure that there is sufficient stimulation for the modelling of the system, as the insignificantly stimulated short recording data in some system are polluted by artifacts and noise. The input signals need enough intensity and duration when participants are involved in the experiment. On the other hand, the signal applied to the human body should be well chosen to ensure safety.

The above conflicting goals can be resolved by considering the following two aspects. The first aspect is to apply a non-parametric method for identification. System structure information used in model complexity selection is a crucial step in modelling. However, when the information is insufficient to determine the parametric model structure, the system dynamics are described by non-parametric models instead of the commonly used fixed-order linear time-invariant models[55, 56]. In addition, the non-parametric model is a better method to employ when the system has massive information. Furthermore, the well-designed kernel strategies and regularisation terms can dramatically improve the accuracy and robustness of the modelling [57–59]. When the structure of the system cannot be determined or it is too complicated to be described by a simple parametric model, the non-parametric modelling method is the preferable choice [55, 56]. On the other hand, the development of wearable equipment, such as the $K4b^2$, makes it possible to record large amounts of data compared to the limited data recording opportunities that were available in the past. The traditional modelling method can achieve good fitness with a limited amount of data, while the non-parametric model is more appropriate to accommodate a large dataset. The non-parametric model with the kernel-based regularisation approach has been applied by several researchers to system identification with different demands [54, 58, 60]. This achieves high accuracy and robustness in system identification when studying the dynamics of the physiological information responses during the exercise phase.

The other aspect is to select an appropriate input with sufficient stimulation for the model. One of the challenges for the modelling of the human physiological variable is that the stimulation of the input is often limited. This prevents the use of models with high-dimensional parameters, as it usually leads to ill-posed inverse problems. Recently, the intrinsical ill-posed problem has been circumvented with kernel-based regularisation methods, which also admit a Bayesian interpretation. In particular, a non-parametric modelling approach is proposed, in which the impulse response is modelled as a zero-mean Gaussian process. In this way, prior information is introduced in the identification process by assigning a kernel covariance [52, 53, 57]. Various dynamic physiological signals are used in respiratory modelling, such as HR , $\dot{V}O_2$ and $\dot{V}CO_2$, during walking, running [61–63], or treadmill exercise [8, 64–66]. However, the physiological signal in these studies reaches a steady platform that shows an identical trend as a step response input. With this in mind, we have designed an appropriate protocol for the stairs exercise to make the signal continuously change to ensure sufficient stimulation.

Taking the above two aspects into account , the non-parametric method is applied in this study but with the condition that the protocol of the exercise experiment is designed with sufficient stimulation. The recently developed system identification approaches are not only based on plenty of physical experimental data but also emphasise more prior knowledge of the system under estimation. System prior information is often applied to model complexity selection, which is the most critical step for system modelling. In some papers [55, 56], system dynamics are depicted by non-parametric models rather than the most commonly used first/second order linear time-invariant models. Often, non-parametric methods are used when the prior information to good effect is insufficient to determine a parametric model structure. The new approach [54, 67] which well utilises the prior information is based on the kernel-based regularisation approach. By using the kernel technique, prior information is adopted in the identification process by assigning an appropriate kernel to the index function. The regularisation terms and the kernel designing strategies for non-parametric system identification are introduced in some research papers [56–59]. Based on these, the new kernel-based non-parametric approach is the best option for analysing the dynamics of the cardiorespiratory response to exercise as it greatly improves robustness and accuracy.

1.4 Thesis Contribution

A monitoring, modelling and control system for human physiological assessment with wearable devices is developed according to series modelling and estimation results analysis. This work mainly focuses on how the physiological signal responds to the exercise phase during aerobic exercise. In detecting the exercise phase, the static nonlinear modelling method is applied in IMU sensors calibration. In physiological signal identification, the dynamic linear modelling method is developed through the use of the non-parametric model with the kernel-based regularisation term.

The novel calibration method named Inclination based Calibration for IMU sensors is proposed in this work to make the problem a single calculation linear problem according to the inclination. To describe the relationship between the body's physiological reactions and the exercise phase, the system identification approach has been used in many circumstances. The non-parametric model is proposed in this work as the preferable choice when the information of the system structure is insufficient, or the system is too complex to be described by a simple parametric model. Hence, the non-parametric modelling method with kernel-based regularisation is developed to estimate the physiological signal response to the exercise phase in different types of exercise. The kernel selection and regularisation strategies have been discussed, and a series of simulations have been performed to compare the fitness, sensitivity and stability of different kernels. Based on these, the most appropriate kernel is then selected for the construction of the regularisation term.

After building the series algorithm and modelling method, the physiological signal response to the exercise phase in simply status and complicated changing status is studied. The relationship between the $\dot{V}O_2$ and $\dot{V}CO_2$, the different physiological performances in the onset and offset period, and the changing structure of the system with its continuously changing exercise phase are analysed based on the modelling results.

The contribution of this thesis can be summarised as follows:

- Different modelling methods are developed and optimised in this work for physiological assessment with different demands. The static nonlinear modelling for IMU calibration aims to detect the exercise phase. The dynamic linear modelling for physio-

logical response identification is developed for studying the relationship between the physiological signal and the exercise phase.

- A practical algorithm named Inclination based Calibration (I-Calibration) has been developed in this work to calibrate the IMU sensors. As the I-Calibration method is a single calculation linear method, with low computational costs and no divergence problems, it is more suitable for real-time in-field calibration for wearable devices with limited computational power.
- The kernel-based non-parametric modelling approach has been applied to describe the dynamics of respiratory responses to exercise. The advantage of using the non-parametric modelling method when the system structure is uncertain compared to the classical linear modelling method is proved in various ways, such as accuracy, stability and compatibility.
- Based on comprehensive comparative numerical analyses, the proper kernel has been selected as the best kernel for the identification of the dynamic response to exercise regarding the goodness-of-fit and parameter insensitivity. The regularisation term with kernel matrix plays a significate role in identification and the parameter of the kernel demonstrates that it should be selected carefully.
- According to reliable experimental data acquired from subjects, the dynamic models of the physiological signal for exercise responses for different exercise phases have been identified. The changing structure with the different phases of exercise has been demonstrated.
- Comprehensive statistical analyses are performed to compare the dynamic characteristics of the exercise status responses for the physiological signal, and several useful conclusions have been made to provide instructive guidance for exercise strategy design, athletic assessment, exercise enhancement and health monitoring.

1.5 Dissertation Outline

The outline of the dissertation is as follows:

Chapter 1

This chapter presents the motivation and scope, the research topics and the outline of the dissertation.

Chapter 2

A literature review of physiological assessment, static model Inertial Measurement Unit Calibration and dynamic model of the cardiorespiratory responses during aerobic exercise are presented.

Chapter 3

In this chapter, an innovative in-field calibration method for portable tri-axial sensors is developed to calibrate the IMU data for human exercise phase detection. Based on the fact that the angle between the local gravity and magnetic field is invariant, the Inclination Based Calibration (I-Calibration) is proposed in this work, which can reliably estimate model parameters of the sensors by simply using a linear Least Square estimator. Based on optimal experimental design, a 12-observation Icosahedron experimental scheme has been performed for a micro IMU, which contains both tri-axial accelerometers and tri-axial magnetometers. The calibrated results together with the comparison between the two methods demonstrate the effectiveness of the proposed method.

The work in this chapter has been published in:

- Hairong Yu, Lin Ye, Ying Guo, Steven Su*, “An Innovative 9-Parameter Magnetic Calibration Method Using Local Magnetic Inclination and Calibrated Acceleration Value", *IEEE Sensors Journal*, doi: 10.1109/ JSEN. 2020. 2995876, May 2020.
- Hairong Yu, Lin Ye, Ying Guo, Steven Su*, “An Effective In-Field Calibration Method for Triaxial Magnetometers based on Local Magnetic Inclination", under review at *IEEE Transactions on Instrumentation and Measurement* , 2019.
- Lin Ye, Ying Guo, Lei Dong, Hairong Yu, Hung Nguyen, Steven W Su*, “A Fast-Converge, Real-Time Auto-Calibration Algorithm for Triaxial Accelerometer." *Measurement Science and Technology*, vol. 30, no. 6, pp. 065010, February 2019.

Chapter 4

In this chapter, the simple onset and offset phase of the jogging exercise on the treadmill exercise is investigated. We compare the identified impulse response models for the two periods, as well as the relationship between oxygen uptake and carbon dioxide output. The result indicates that the steady state gain of the carbon dioxide output in the onset of exercise is bigger than that in the offset while the response time for both onset and offset are similar. Compared with oxygen uptake, the response speed of carbon dioxide output is slightly slower in both the onset and offset period while its steady state gains are similar for both periods.

The work in this chapter has been published in:

- Hairong Yu, Lin Ye, Ganesh R. Naik, Rong Song, Hung T. Nguyen, Steven W. Su*, "Nonparametric Dynamical Model of Cardiorespiratory Responses at the Onset and Offset of Treadmill Exercises." *Medical & biological engineering & computing*, vol. 56, no. 12, pp. 2337-2351, June 2018.

- Lin Ye, Ahmadreza Argha, Hairong Yu, Branko G. Celler, Hung T. Nguyen, Steven Su*, "Dynamic Characteristics of Oxygen Consumption.", *Biomedical engineering online*, vol. 17, no. 1, pp. 44, December 2018

Chapter 5

In this chapter, a mobile phone application is developed to record the physiological information during the exercise phase (i.e. ascending or descending) of stairs exercise. Our experimental dataset features ten participants and a range of different exercise periods. Based on the designed experiment protocol, a non-parametric model with an experimentally selected kernel has been established. Compared with the fixed-order models on accuracy, stability and compatibility, the modelling results demonstrate the effectiveness of the non-parametric modelling approach. The influence of exercise duration on estimated fitness reveals that the model of the phase-oxygen uptake system is not time-invariant.

The work in this chapter has been published in:

- Hairong Yu, Lin Ye, Rong Song, Yuxi Luo, Hamzah M Alqudah, Steven Su*, "Oxygen Consumption Response to Stairs Exercise by Non-parametric Modelling", under review at *Biomedical Physics and Engineering Express*, 2020.

Chapter 6

In this chapter, the kernel-based regularisation non-parametric model is utilised to analyse how the oxygen uptake or carbon dioxide output responds to the walking speed on treadmills. To ensure sufficient stimulation, the dataset from the stairs experiment with a proper protocol is applied in the kernel parameters selection, and this selection approach is compared with the numerical simulation approach. The comparison results illustrate an improvement of 4.18% for oxygen uptake and 7.63% for carbon dioxide output in a half period, and 11.00% for oxygen uptake and 12.60% for carbon dioxide output in one period when using the kernel parameter selected from the stairs exercise. Moreover, the advantages of using the non-parametric model, the necessity of sufficient stimulation for identification and the importance of the kernel regularisation term are also addressed in this work.

The work in this chapter has been published in:

- Hairong Yu, Lin Ye, Hamzah M Alqudah, Kairui Guo, Branko G. Celler, Rong Song, Steven Su*, “Prediction of Cardiac-respiratory Response to Treadmill Exercise by Using Non-Parametric Modelling with Stairs Exercise based Kernel Characterization", under submission to *IEEE Transactions on Biomedical Engineering*, 2020.

Chapter 7

This chapter summarises the work of this Ph.D. dissertation and presents the future research developments.

Chapter 2

Background

In this chapter, we first briefly describe some related knowledge about human physiological assessment. Then, the various modelling methods and assessment approaches about the cardiorespiratory response for aerobic exercise is introduced. In the aspect of detecting the human exercise status, the calibration for the IMU sensor is a vital part. With the development of wearable devices for collecting the physiological data, it is possible for researchers to record a large amount of data. According to the increasing of the amount of data, the traditional modelling method is necessary to be improved.

2.1 Human Physiological Assessment

Fitness is defined as the quality or state of being fit. It is commonly agreed that physiological and physiologically related perspective is necessary for defining fitness parameters and discussing fitness [2]. The physiological assessment could be viewed in different aspects, including cardiovascular assessment, respiratory assessment, energy assessment et al. It should be pointed out that aerobic power is an essential part of human physiological fitness assessment. Aerobic exercise is a type of exercise performed at moderate levels of intensity for extended periods. The regular aerobic exercise is with several advantages, including improving cardiovascular fitness, consuming calorie, convenience, and low-cost [4–6].

Oxygen uptake ($\dot{V}O_2$) is a vital parameter of human fitness because the maximum $\dot{V}O_2$ represents the upper limit of aerobic exercise tolerance [68]. Similarly, the respiratory

information, such as voluntary ventilation or carbon dioxide output ($\dot{V}CO_2$), is also commonly used to assess the metabolism demands and analyse the human mechanism [63, 69–75]. According to previous studies, for the $\dot{V}O_2$ during exercise, the exponential function was applied to describe the dynamic performance [62, 76, 77].

$$\dot{V}O_2(t) = \dot{V}O_2^0 + R_A[1 - e^{-(t-T_D)/\tau}]. \tag{2.1}$$

where $\dot{V}O_2(t)$ is the O_2 output at time t, $\dot{V}O_2^0$ is the initial value of O_2 output, R_A is the response amplitude, T_D is the time delay, and τ is the time constant.

Puente [62] demonstrated that the $\dot{V}CO_2$ could also be described by the same as:

$$\dot{V}CO_2(t) = \dot{V}CO_2^0 + R_A[1 - e^{-(t-T_D)/\tau}]. \tag{2.2}$$

where $\dot{V}CO_2(t)$ is the CO_2 output at time t, $\dot{V}CO_2^0$ is the initial value of CO_2 output, R_A is the response amplitude, T_D is the time delay, and τ is the time constant.

Heart Rate (HR) is the speed of the heartbeat, measured by the number of contractions (beats) of the heart per minute (bpm). HR can vary with the body's physical needs, including the need to absorb oxygen and excrete carbon dioxide. Physical exercise can provoke a change in HR. The American Heart Association states the HR of a normal resting adult human is 60 to 100 bpm. The $\dot{V}O_2$ and $\dot{V}CO_2$ is with linear relationship with HR. Meanwhile, HR_{max} [11, 12] has been recognised as an indicator to detect the exercise intensity [13]. The maximum heart rate (HR_{max}) is the highest HR that an individual can achieve without severe problems through exercise stress [10]. One representative formula of HR_{max} is introduced in Robert's research [78] as shown in Eq. (2.3):

$$HR_{max} = 205.8 - 0.685 \times age, \tag{2.3}$$

where, *age* indicates the age of participant.

The cardiovascular and respiratory characterization attracted a lot of scholars to work on this field for different demands. The first aspect is to study the respiratory mechanism. In the research of Hill et al. [16], the recovery curve of $\dot{V}O_2$ is studied. It also demonstrated that the recovery curve of $\dot{V}O_2$ is a logarithmic equation after a moderate exercise and it is equally

applicable to the recovery curves of $\dot{V}CO_2$. A similar conclusion is also drawn by Wasserman [79] that the equation of carbon dioxide elimination is equal to oxygen uptake. David's research provides a comprehensive understanding of the mechanistic bases of $\dot{V}O_2$ kinetics [77]. The mechanisms for the acceleration of pulmonary $\dot{V}O_2$ on-kinetics in human after prolonged endurance training is demonstrated in Jerzy's study [76]. The cardiorespiratory performance of human in different kinds of exercise and different periods of exercise are also demonstrated by different researches. William studied the individual differences in respiratory gas change during the recovery period of moderate exercise [80]. The threshold of anaerobic metabolism for cardiac patients during exercise is detected in Karlman's study [81]. The anaerobic threshold and respiratory gas exchange during exercise are also studied in Karlman's other study [82]. The oxygen and carbon dioxide performance of young adults at rest and after exercise are studied in Morton's paper [83].

2.2 Static Nonlinear Modelling Problems for Inertial Measurement Unit Calibration

2.2.1 In-Field Calibration Method

In the light of the rapid development of MEMS technology, the chip-based inertial sensors are rapidly improved in terms of the size reduction. Nowadays, MEMS accelerometers and magnetometers are widely used in various areas [21, 84–87]. The magnetometers measure a constant local magnetic field vector when the magnetic disturbances are not presented. Compared with the accelerometers, the magnetometers are relative with low accuracy as the results of the installation errors, sensor deficiencies and vicinity magnetic interference [31]. Hence, regular calibrations are necessary to minimise interference [21, 22].

The errors of the MEMS magnetometers are usually divided into hard iron distortion and soft iron distortion [21, 22]. Interference caused by ferromagnetic material or equipment in the magnetometers vicinity is called hard iron distortion. Soft iron distortion is the result of material that distorts a magnetic field but does not necessarily generate a magnetic field itself. In general, the MEMS magnetic sensor should be regularly calibrated to ensure its accuracy [31, 88]. The in-field calibration method is broadly used as an auto-calibration method for

calibrating the MEMES [23]. Various in-field calibration methods have been developed and showed effectiveness in calibration results [24–27].

For conventional magnetometers calibration, “Attitude-Dependent" approaches could implement calibration in a laboratory environment by comparing the measured data with the actual magnetic field. However, this method required high precision turntables to accurately control the sensor orientation and was mainly effective for high-precision navigation types of equipment [22, 25, 26]. The practical in-field calibration methods were “Attitude-Independent" approaches, whose parameter estimation was based on either nonlinear filtering approaches, e.g., extended Kalman filter (EKF) and Unscented filter (UF) [24], or nonlinear parameter estimation algorithms [27]. One of the typical “Attitude-Independent" calibration methods focuses on minimising the difference between the magnitude of the measured magnetic field and that of the local magnetic field [28]. Another “Attitude-Independent" method formulates the calibration problem as an ellipsoid fitting problem [21, 29, 30]. After the ellipsoid fitting calibration, the ellipsoid of data will be mapped to a sphere [31, 32].

These methods are with several advantages and only magnetometers data are needed. However, it is necessary for these methods to solve a nonlinear estimation problem to identify the coefficients of the tri-axial accelerometers and magnetometers model. Hence, a new linear calibration algorithm that combines the acceleration data and magnetic data together for magnetic calibration could be proposed. In Kok’s paper [34], it was reported that the measured accelerometers data together with magnetometers data could be used to estimate the inclination if the sensor is mounted in a static platform or its motion acceleration is much lower than the local gravity [34].

As for the mathematical model for the tri-axial senors, it is considered as a nonlinear model and needed to be linearized to further estimation. Commonly, the 6-parameters model is suitable in most cases. The 6-parameter model is first proposed and studied in our work. However, due to the non-orthogonality and misalignment of the tri-axial anisotropic magnetoresistive sensor, as well as the unwanted magnetic interference, the 6-parameter model may not be sufficient to obtain the desired estimation [27, 47, 89]. The 9-parameter auto-calibration model is also adopted to build the I-Calibration algorithm in our work.

2.2.2 Experimental Design

The classical Design of Experiment (DoE) theory [45] is applied to generate the experimental schemes for the calibration of TAs and TMs in order to improve the quality of the calibration method [35–38]. For response surface methodology, there are two types of well developed optimal experimental method which is suitable for the calibration of tri-axial accelerometers model and tri-axial magnetometers model.

One is Central Composite design (CCD), which was based on the measurements from fractional factorial points, axial points and centre points [38]. The CCD is a kind of response surface method to build a second-degree model. In addition, it is applied to estimate the curvature according to the measurement value from fractional factorial points, axial points, and centre points [90]. The general structure of CCD is shown in Fig. 2.1. According to the points shown in the Fig. 2.1, there will be six runs for centre points, eight runs for eight fractional factorial points and six run for six axial point for tri-axial accelerometers model and tri-axial magnetometers model.

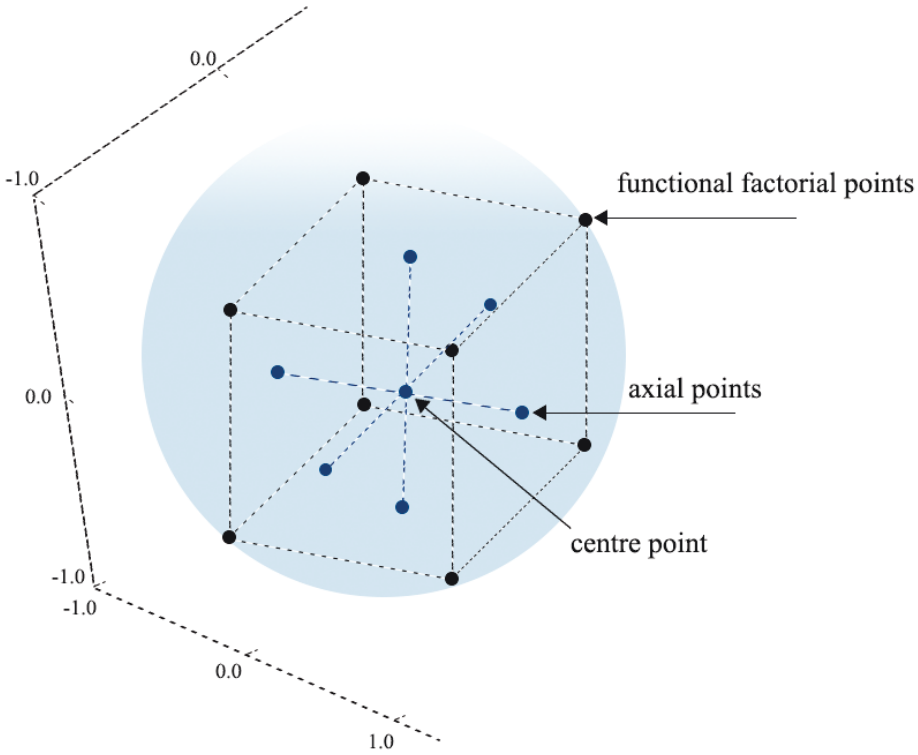

Fig. 2.1 The Structure of Central Composite Design (CCD).

The other commonly used response surface method is Box-Behnken design (BBD), which is focused on the midpoints of edges and the centre [35, 38]. The general structure of BBD is shown in Fig. 2.2. As for the points of BBD shown in the Fig. 2.2, it requires twelve runs for midpoints and three runs for center points. Normally, the BBD could be modified by reducing to twelve points due to the structure of tri-axial accelerometers model or tri-axial magnetometers model.

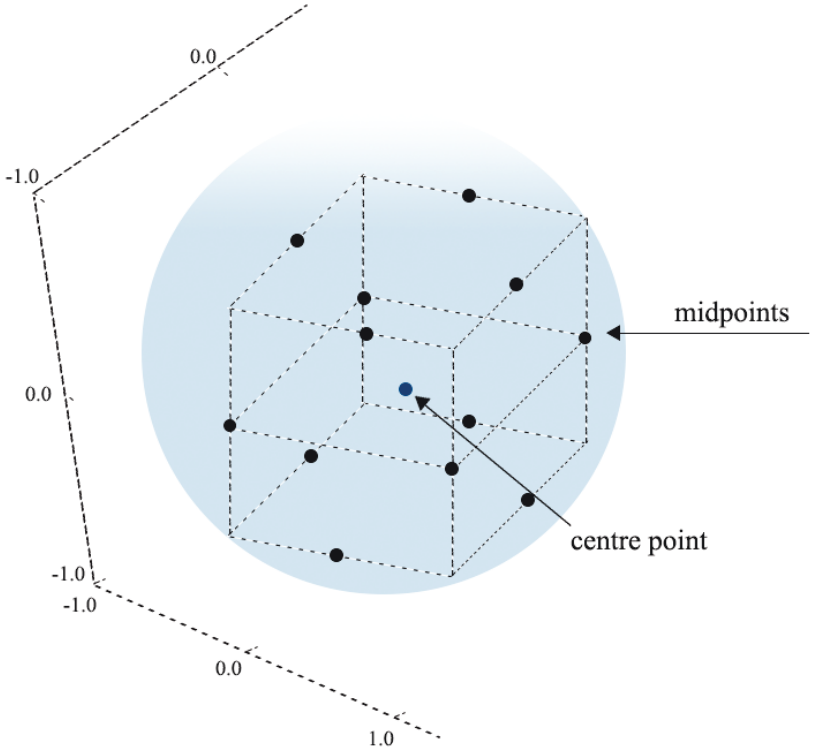

Fig. 2.2 The Structure of Box-Behnken Design (BBD).

Beside BBD and CCD, we utilise an Icosahedron Design which is more suitable for these specific models. The concept of Icosahedron Design is coming for uniform design. In order to achieve the goal that the experiment points can uniformly distribute on experimental domains for six and nine parameters models, the Icosahedron Experiment design is designed as a twelve points space-filling. The general structure of Icosahedron Design is shown in Fig. 2.3.

All the experiment points will be located on the surface of a sphere whose radius equals the local gravity or magnetic field owing to the constraint of the tri-axial accelerometers

model and tri-axial magnetometers model. Moreover, these twelve points will construct an Icosahedron whose radius of its circumcircle will be gravity or magnetic field.

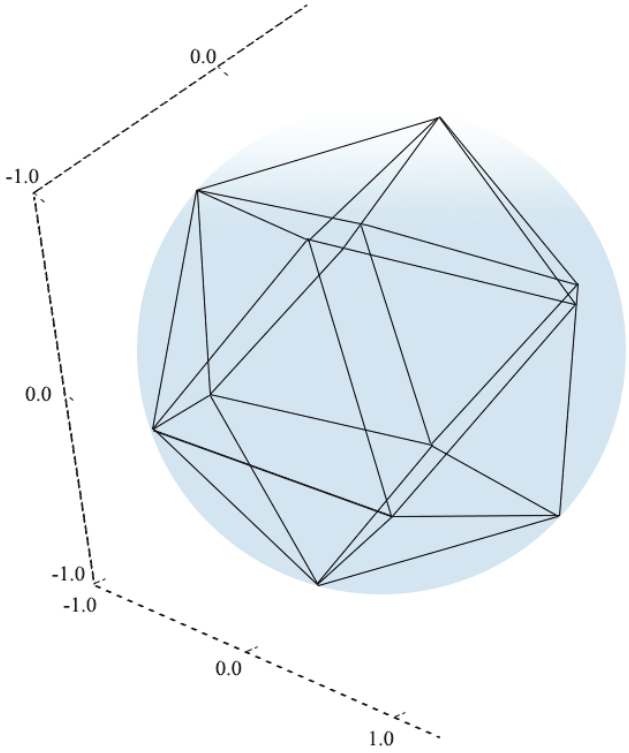

Fig. 2.3 The Structure of Icosahedron Design for TAs or TMs model.

The key step in experimental design is the calculation and analysis of the Fisher Information Matrix (FIM), which is related to this classical parameter estimation problem. The optimal experimental design may be achieved by maximising or minimising a certain index of FIM. Such an index is often defined in various ways, which lead to several famous design schemes, e.g., G-optimal, D-optimal, E-optimal, ED-optimal, and Ds-optimal design [39, 43, 44]. Among these design schemes, D-optimality (determinant) is a popular criterion, which seeks to minimise $|(X^TX)^{-1}|$, or equivalently maximise the determinant of the information matrix X^TX of the design. This criterion results in maximising the differential Shannon information content of the parameter estimates. In addition, G-optimality is also a popular criterion, which seeks to minimise the maximum entry in the diagonal of the hat matrix $X(X^TX)^{-1}X^T$. This has the effect of minimising the maximum variance of the predicted values. The 12-observation experimental design applied in our paper is proved to be both G-optimal and D-optimal in the previous study [47, 91].

2.3 Dynamic Linear Modelling Problems of Cardiorespiratory Responses of Aerobic Exercise

2.3.1 Cardiorespiratory Signal Modelling Method

Among the researches that study the relationship between exercise phase and physiological signal, especially the cardiorespiratory information, the modelling methods are widely developed and applied in these studies [48–50]. Various dynamic physiological signals are used in respiratory modelling, such as HR , $\dot{V}O_2$ and $\dot{V}CO_2$, during walking, running [61–63], or treadmill exercise [8, 64–66, 92, 93] and so on [94–96].

The step response of physiological signal can be approximated as a first-order system in these studies. However, the physiological signal changing in these studies will reach a steady platform that corresponds to the same trend as the step response. In that case, the dynamic relationship between exercise status and HR is not obvious enough. With this in mind, an appropriate protocol for the exercise is necessary to be designed to make the signal continuously changing to ensure sufficient stimulation. In another aspect, some research [8] applied Heart Rate (HR) to make the analysis, but it can easily be affected by human motion or other aspects. In this way, other researchers choose how the gas changes during the exercise as an index. However, the commonly used Least Square (LS), Maximum Likelihood (ML) and Prediction Error Method (PEM) equipped with classical model structure selection approaches often fail to obtain an appropriate model with desired accuracy and robustness for cardiorespiratory response estimation, which is based on insignificantly stimulated short recording data polluted by artifacts and noise [52–54].

Among the studies of cardiorespiratory response to exercise, researchers preferred to choose oxygen uptake as the index. Both linear and nonlinear static models [61, 97, 98] had been proposed based on the walking speed. Furthermore, some researchers modelled the VO_2 response with a monoexponential curve [62, 76, 77]. System structure information used in model complexity selection is a crucial step in modelling. However, when the information is insufficient to determine the parametric model structure, the system dynamics could be described by non-parametric models instead of the commonly used fixed-order linear time-invariant models[55, 56].

2.3.2 Development of Wearable Devices

Over the last dozens of years, automated portable gas analysis systems had been developed and applied in various sports fields for energy consumption assessment [15]. The Tissot spirometer/volumetric gas analyser system is one of the first open-circuit equipment configurations applied in measuring VO_2 during exercise [99]. The Douglas bag/volumetrix gas analyser system is a slight variation of the Tissot spirometer/volumetric gas analyser system [14]. Hereafter, the volumetric gas analysers are replaced by the electronic gas analysers. Subsequently, the meteorological balloon/electronic gas analyser system is born [2]. A portable gas analysis system that is available in the breath by breath Cosmed $K4b^2$ system, which is the latest of a series (including the K2 and K4) of portable systems Cosmed (Rome, Italy) has produced [100].

Portable sensors enable us to measure HR conveniently when monitoring the intensity of exercise so that ensures the exercise is under aerobic conditions [7, 9, 10]. In addition, $\dot{V}O_2$ and $\dot{V}CO_2$ are measured at various sports laboratories by gas analyser [14, 51, 100]. The development of wearable equipment and systems makes it possible to record large amounts of data compared to the limited data in the past. Hence, the optimised modelling method should be developed to make it suitable for large amounts of dataset.

2.3.3 Non-parametric Modelling with Optimised Kernel-Parameter Selection

In some papers [55, 56], system dynamics is depicted by non-parametric models rather than the most commonly used first/second order linear time-invariant models. Commonly, non-parametric methods are used when the prior information is insufficient to determine a parametric model structure. The new approach [54, 67] which well utilises the prior information is based on the kernel-based regularisation approach. By using the kernel technique, prior information is adopted in the identification process by assigning an appropriate kernel to the index function. Specifically, papers [56–59] introduced the regularisation terms and the kernel designing strategies for non-parametric system identification. In this way, prior information is introduced in the identification process by assigning a kernel covariance [52, 53, 57]. When the structure of the system could not be determined or it is too compli-

cated to be described by a simple parametric model, the non-parametric modelling method is a preferable choice [55, 56].

The non-parametric model with the kernel-based regularisation approach has been applied by several researchers to system identification with different demands [54, 58, 60], which achieves high accuracy and robustness in system identification when studying the dynamics of physiological information responses to exercise phase with a well-designed kernel strategy and a regularisation term. In addition, the non-parametric model has an advantage when the system is with massive information. Furthermore, the well-designed kernel strategies and regularisation terms can dramatically improve the accuracy and robustness for the modelling [57–59].

2.4 Summary

This chapter reviews the basic knowledge about the human physiological assessment. The researches that study the different performances of cardiorespiratory information during different types of exercise are introduced in Section 2.1. From the perspective of detecting the exercise status, the IMU sensors should be calibrated carefully. The development of the in-field calibration method is introduced in Section 2.2.1. The experimental design, which is a crucial step prior to the calibration, is introduced in Section 2.2.2. The modelling methods of physiological signal response to exercise in previous studies are presented in Section 2.3.1. The development of the wearable devices which is introduced in Section 2.3.2 makes it possible to record large amounts of data compared to the limited data recording circumstance in the past. In that case, the non-parameter modelling method is then developed to make an improvement in the physiological modelling problem, which is introduced in Section 2.3.3.

Chapter 3

An Effective In-Field Calibration Method for Inertial Measurement Unit based on Local Magnetic Inclination

3.1 Introduction

The application of Micro-Electro-Mechanical Systems chip-based inertial sensors is popularized in mobile navigation [21, 101] and health monitoring [85, 102, 103]. Specifically, in order to investigate the relationship between human's physiological information and the exercise status, the IMU device is widely applied in human exercise monitoring. To ensure the accuracy of the IMU device, the calibrations for accelerometers and magnetometers are vital procedures.

The magnetometers are capable of measuring vector magnetic signals and have key applications in the fields of Attitude and Heading Reference Systems (AHRS) [84, 104], ballistics measurement and Magnetic Anomaly Detection (MAD) [87]. Compared with the accelerometers, the magnetometers are relative with low accuracy as the results of the installation errors, sensor deficiencies and vicinity magnetic interference [31]. As a practical device, the existence error is inevitable. The errors of the MEMS magnetometers are usually divided into hard iron distortion and soft iron distortion [21, 22]. Interference caused by ferromagnetic material or equipment in the magnetometers vicinity is called

hard iron distortion. Soft iron distortion is the result of material that distorts a magnetic field but does not necessarily generate a magnetic field itself. To improve the accuracy, the magnetometers need to be calibrated regularly because the errors of the low cost MEMS sensors can be corrupted by various reasons, such as biases and scale factor deviations, misalignment and nonorthogonality of the sensor axes, sensor fabrication issues and the magnetic deviations induced by the host platform [25, 105]. Hence, regular calibrations are necessary to minimise the interference, such as hard iron and soft iron, to ensure the accuracy of the measurements[21, 22].

Various auto-calibration methods are recently developed to calibrate the MEMS and are suitable for the in-field calibration [23]. Several convenient effective in-field calibration methods have been developed, and as mentioned before, the hard iron [24–27] and soft iron [21, 22, 105] are eliminated through these calibration methods to minimise interference. The in-field calibration methods are classified as “Attitude-Dependent" and “Attitude-Independent" approaches. “Attitude-Dependent" approaches could implement calibration in a laboratory environment by comparing the measured data with the actual magnetic field. However, this method required high precision turntables to accurately control the sensor orientation and was mainly effective for high-precision navigation types of equipment [22, 25, 26]. Aother practical in-field calibration methods were “Attitude-Independent" approaches, whose parameter estimation was based on either nonlinear filtering approaches, e.g., extended Kalman filter (EKF) and Unscented filter (UF) [24], or nonlinear parameter estimation algorithms [27]. One of the typical “Attitude-Independent" calibration methods focuses on minimising the difference between the magnitude of the measured magnetic field and that of the local magnetic field [28]. Another “Attitude-Independent" method formulates the calibration problem as an ellipsoid fitting problem [21, 29, 30]. After the ellipsoid fitting calibration, the ellipsoid of data will be mapped to a sphere [31, 32]. These methods are with several advantages and only magnetometers data are needed. However, it is necessary for these methods to solve a nonlinear estimation problem to identify the coefficients of the tri-axial magnetometers model. Considering these aspects, we intend to develop a new calibration algorithm that combines the acceleration data and magnetic data together for magnetic calibration. The parameter estimation of the proposed method is a simple linear least square algorithm, which can be easily implemented in a wearable device with limited computational power.

This work proposed a novel calibration method for TMs, called Inclination based Calibration (I-Calibration). It was based on the fact that the local magnetic inclination is constant, which means that the angle between local gravity and magnetic field is invariant. Magnetic inclination can be determined by the angle between the local magnetic field and the horizontal plane. In Kok's paper [34], it was reported that the measured accelerometers data together with magnetometers data could be used to estimate the inclination if the sensor is mounted in a static platform or its motion acceleration is much lower than the local gravity [34]. Usually, positive values of inclination indicate that the field is pointing downward, into the earth, at the point of measurement. For the same location, the inclination is constant and can be found out on the Magnetic-Declination and Inclination Website. The inclination in Sydney (Latitude: 33°52′4.3″ S, Longitude: 151°12′26.4″ E) is 64°20′ as shown in Fig 3.1. The constant inclination can be described by the magnetic field and the gravity, and this provides an idea of how to calibrate the measured magnetic value based on both the TMs and TAs.

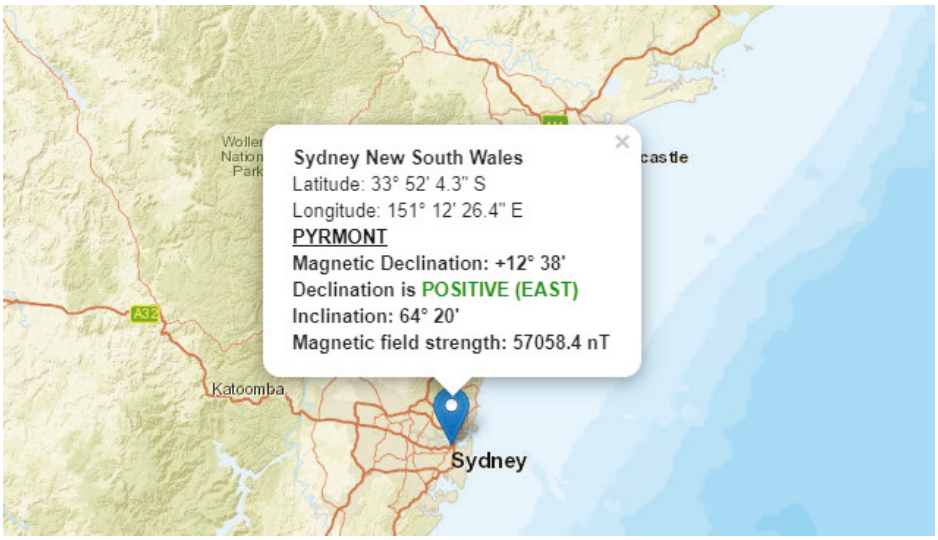

Fig. 3.1 The Inclination in Sydney New South Wales Australia (http://www.magnetic-declination.com/Australia/Sydney/124736.html).

Experimental Design (DoE) is a vital part prior to the calibration to ensure the accuracy and effectiveness of calibrated results [35–38]. Some well known experimental design methods included Central Composite Design (CCD), which was based on the measurements from fractional factorial points, axial points and centre points [38], and Box-Behnken Design (BBD), which was focused on the midpoints of edges and the centre [35, 38]. Based on the DoE for the calibration of the inertial sensor and unit [27], considering the similarity

of calibration between magnetometers and accelerometers, the Icosahedron Experiment with 12-observation DoE was proposed [47]. The DoE can be achieved by maximising or minimising a certain index of the Fisher Information Matrix (FIM), which is related to the classical parameter estimation problem. Several famous design schemes are developed to define the index of FIM, such as G-optimal, D-optimal, E-optimal, ED-optimal, and Ds-optimal design [39, 43, 44]. In this study, for the newly proposed calibration method, we adopted this 12-observation Icosahedron scheme, which can uniformly distribute the experiment points on experimental domains.

According to both numerical analysis and real-time experiments, it was demonstrated that the new method could efficiently and reliably estimate the coefficients of the tri-axial magnetometers model by simply using a linear Least Square estimator. Specifically, the robustness to the misalignments of the TAs and TMs for the proposed I-Calibration method was demonstrated by using numerical simulations. Then, the proposed approach was compared with the Magnitude Based Calibration (M-Calibration), which was based on our previous work [27]. Real-time experiments were performed according to the Icosahedron Experimental Scheme [27]. Based on the collected experimental data, the coefficients were estimated by using the two calibration methods respectively. The comparison results demonstrated the effectiveness of the proposed approach.

The above calibration is developed on the basis of the 6-parameter model. In the previous study about TAs and TMs calibration, the 6-parameter model was designed by neglecting three cross-axis sensitivity factors. However, due to the non-orthogonality and misalignment of the tri-axial anisotropic magnetoresistive sensor, as well as the unwanted magnetic interference, the 6-parameter model may not be sufficient to obtain the desired estimation [27, 47, 89]. For a further demonstration, the 9-parameter auto-calibration model is then adopted to build the I-Calibration algorithm in our work. On the other hand, in the previous study [47], it has been shown that the 12-observation can potentially reach both G-optimal and D-optimal for 9-parameter TAs or TMs model.

According to both numerical analysis and real data experiments in our work, it was demonstrated that the proposed I-Calibration method could efficiently and reliably estimate the coefficients of the triaxial magnetometers model by simply using a linear Least Square estimator. The robustness to the misalignments of the TAs and TMs for the I-Calibration

method was demonstrated by using numerical simulations. In summary, compared to the existing "Attitude-Independent" calibration methods [106, 107] and the M-Calibration method [27], the proposed I-Calibration only needs to address a simple linear static parameter estimation problem, for which a linear least square method is sufficient. It does not need to consider the issues of initial condition selection and local optima trap [34, 108]. Thus, the method can be easily implemented in a wearable device with low computational power.

3.2 Calibration Methodology

The mathematical model of the tri-axial magnetometers measurements is related to the measurement value $\mathbf{M^m} \in R^3$ and the local magnetic field $\mathbf{M^r} \in R^3$. The model could be expressed as follows:

$$\mathbf{M^r} = \mathbf{G}(\mathbf{M^m} + \mathbf{O}) + \mathbf{n}, \tag{3.1}$$

where $\mathbf{G} \in R^{3\times3}$ represents the simplified matrix from $\mathbf{G_s G_e}$ [21, 22]. The diagonal matrix $\mathbf{G_s}$ is constructed by scale factors and the matrix $\mathbf{G_e}$ stands for the nonorthogonality and misalignment of the tri-axial sensors [25, 47]. We also assume $\mathbf{G} = diag\{[G_x\ G_y\ G_z]\}$. The vector $\mathbf{O} \in R^3$ represents the offset of measurements, and $\mathbf{n} \in R^3$ stands for the Gaussian noise vector. The vector $\mathbf{M^r} \in R^3$ represents the estimated output. In this study, as the measured magnetometers value is local magnetic filed only, $\mathbf{M^r}$ should be equal to the local earth magnetic field. The vector $\mathbf{M^m} \in R^3$ represents the measured value from the magnetometers.

In order to get the calibrated magnetic value $\mathbf{M^c} \in R^3$, two principles are applied to construct the calibration procedure. In one aspect, the magnitude of the local magnetic field $\|\mathbf{M^r}\|$ remains constant when the disturbances and distortions are negligible, which leads to the Magnitude based Calibration (M-Calibration). In the other aspect, the Inclination based Calibration (I-Calibration) is due to the fact that the local inclination is constant for the same location. That means the dot product between the magnetic field $\mathbf{M^r} \in R^3$ and the acceleration field $\mathbf{A^r} \in R^3$ is also constant.

3.2.1 Magnitude Based Calibration

According to [47], the magnetometers model in Eq.(3.1) can be re-constructed so that the parameters can be estimated by using the recursive least square approach proposed in [107]. The error ε between the estimated magnetic value and the local magnetic field $\mathbf{M^r}$ can be expressed based on Eq.(3.1):

$$\varepsilon_i = \|\mathbf{M^r}\|^2 - \sum_{j=x,y,z} [G_j \cdot (M_{ji}^m + O_j)]^2, \quad i = 1,2,..,n, \tag{3.2}$$

here n is the number of data points from the experimental design, and $\|\mathbf{M^r}\|$ is the magnitude of the local magnetic field.

To linearize Eq.(3.2) and reduce the computational complexity, Eq.(3.2) can be simplified by neglecting some less significant terms at first [36, 45]. Hence, Eq.(3.2) is expanded and rewritten as follows:

$$\|\mathbf{M^r}\|^2 = 2 \sum_{j=x,y,z} G_j^2 O_j M_{ji}^m + \sum_{j=x,y,z} G_j^2 (M_{ji}^m)^2 + \sum_{j=x,y,z} G_j^2 O_j^2 + \varepsilon_i, \tag{3.3}$$

for $i = 1,2,\cdots,n$.

In Eq.(3.3), we define the third term as γ:

$$\gamma = \sum_{j=x,y,z} G_j^2 O_j^2. \tag{3.4}$$

The unknown parameter vector $\beta_M = [\beta_x \quad \beta_y \quad \beta_z \quad \beta_{xx} \quad \beta_{yy} \quad \beta_{zz}]^T$ is defined as:

$$\begin{cases} 2G_x^2 O_x = \beta_x \\ 2G_y^2 O_y = \beta_y \\ 2G_z^2 O_z = \beta_z \\ G_x^2 = \beta_{xx} \\ G_y^2 = \beta_{yy} \\ G_z^2 = \beta_{zz}. \end{cases} \tag{3.5}$$

The observation matrix $\mathbf{X_M} \in \mathbf{R}^{n\times 6}$ is constructed by the measurements M_{ji}^m in Eq.(3.3):

$$\mathbf{X_M} = \begin{bmatrix} M_{x1}^m & M_{y1}^m & M_{z1}^m & (M_{x1}^m)^2 & (M_{y1}^m)^2 & (M_{z1}^m)^2 \\ \cdots & \cdots & \cdots & \cdots & \cdots & \cdots \\ \vdots & \vdots & \vdots & \vdots & \vdots & \vdots \\ \vdots & \vdots & \vdots & \vdots & \vdots & \vdots \\ M_{xn}^m & M_{yn}^m & M_{zn}^m & (M_{xn}^m)^2 & (M_{yn}^m)^2 & (M_{zn}^m)^2 \end{bmatrix}, \tag{3.6}$$

where n is the number of data points from the experimental design.

The Eq.(3.3) could be rewritten as a matrix form based on Eq.(3.5) and Eq.(3.6), and expressed as:

$$\mathbf{Y} = \mathbf{X_M}\beta_M + \gamma + \varepsilon, \tag{3.7}$$

where $\mathbf{Y} \in \mathbf{R}^n = [y_1 \quad y_2 \quad ... \quad y_n]^T$, $\varepsilon \in \mathbf{R}^n = [\varepsilon_1 \quad \varepsilon_2 \quad ... \quad \varepsilon_n]^T$ and $\gamma \in \mathbf{R}^n = [\gamma \quad \gamma \quad ... \quad \gamma]^T$.

Eq.(3.7) could be solved by a convergence guaranteed iterative least square estimation method [32, 29], which is summarized in Algorithm 1 [107].

Algorithm 1 Convergence Guaranteed Iterative Least Square Estimation for β_M

1: The initial value of γ is assumed as zero and the initial estimation of β_M is calculated as

$$\hat{\beta}_M^{(1)} = (\mathbf{X_M}^{\mathrm{T}}\mathbf{X_M})^{-1}\mathbf{X_M}^{\mathrm{T}}(\boldsymbol{y} - \boldsymbol{\gamma}^{(0)}). \tag{3.8}$$

2: The matrix $\mathbf{G}$ and $\mathbf{O}$ could be solved by the estimated $\hat{\beta}_M$ based on Eq.(3.5) and the new $\hat{\gamma}^{(i)}$ could be estimated

$$\begin{cases} \hat{G_x^{(i)}} = \sqrt{\hat{\beta}_{xx}^{(i)}}, \\ \hat{G_y^{(i)}} = \sqrt{\hat{\beta}_{yy}^{(i)}}, \\ \hat{G_z^{(i)}} = \sqrt{\hat{\beta}_{zz}^{(i)}}, \\ \hat{O_x^{(i)}} = \frac{\hat{\beta}_x^{(i)}}{2\hat{\beta}_{xx}^{(i)}}, \\ \hat{O_y^{(i)}} = \frac{\hat{\beta}_y^{(i)}}{2\hat{\beta}_{yy}^{(i)}}, \\ \hat{O_z^{(i)}} = \frac{\hat{\beta}_z^{(i)}}{2\hat{\beta}_{zz}^{(i)}}, \\ \hat{\gamma^{(i)}} = \sum\limits_{j=x,y,z} \hat{G_j^{2(i)}} \hat{O_j^{2(i)}}, \\ \hat{\gamma^{(i)}} = [\underbrace{\hat{\gamma^{(i)}}, \hat{\gamma^{(i)}}, ..., \hat{\gamma^{(i)}}}_{n}]^T. \end{cases} \tag{3.9}$$

3: Repeat until the convergence criteria is reached.

4: The final estimator $\hat{\beta}_M^{(n)}$ could be expressed as following after n steps

$$\hat{\beta}_M^{(n)} = (\mathbf{X_M}^{\mathrm{T}}\mathbf{X_M})^{-1}\mathbf{X_M}^{\mathrm{T}}(\boldsymbol{y} - \hat{\gamma}^{(n-1)}). \tag{3.10}$$

3.2.2 Inclination Based Calibration

Algorithm for 6-parameter Inclination Based Calibration

A 6-parameter model is first applied to define the unknown parameters as it had been proved that it is sufficient to obtain desired estimation to some extend [89]. Since the angle between the local magnetic field $\mathbf{M^r} \in R^3$ and the gravity field $\mathbf{A^r} \in R^3$ is a constant, the dot product between these two vector should be a constant value. In the ideal situation, the relationship between the real acceleration value $\mathbf{A^r} = [A_x \quad A_y \quad A_z]^T$ and the real magnetic

value $\mathbf{M^r} = [M_x \quad M_y \quad M_z]^T$ can be expressed as follows based on the inclination angle θ [33]:

$$\theta = \frac{\pi}{2} - \cos^{-1}\left(\frac{A_x M_x + A_y M_y + A_z M_z}{\|\mathbf{A^r}\|\|\mathbf{M^r}\|}\right). \tag{3.11}$$

In Eq.(3.23), a constant L can be defined by $\mathbf{A^r}$ and $\mathbf{M^r}$ as:

$$\mathrm{L} = \mathrm{A_x M_x} + \mathrm{A_y M_y} + \mathrm{A_z M_z}. \tag{3.12}$$

The constant L could also be expressed as :

$$\mathrm{L} = \mathrm{A_x M_x} + \mathrm{A_y M_y} + \mathrm{A_z M_z} = \|\mathbf{A^r}\|\|\mathbf{M^r}\|\cos\left(\frac{\pi}{2} - \theta\right). \tag{3.13}$$

Based on the model of local magnetic filed and measured value from magnetometers in Eq.(3.1), the calibrated magnetic value $\mathbf{M^c} = [M_x^c \quad M_y^c \quad M_z^c]^T$ can be calculated by the measured magnetic value $\mathbf{M^m} = [M_x^m \quad M_y^m \quad M_z^m]^T$ with the following formula:

$$\begin{cases} M_x^c = G_x M_x^m + \tilde{O}_x \\ M_y^c = G_y M_y^m + \tilde{O}_y \\ M_z^c = G_z M_z^m + \tilde{O}_z, \end{cases} \tag{3.14}$$

where G_x, G_y and G_z is the diagonal elements of $\mathbf{G}$. $\tilde{\mathbf{O}} = \mathbf{GO} = [\tilde{O}_x \quad \tilde{O}_y \quad \tilde{O}_z]^T$ (the matrices $\mathbf{G}$ and $\mathbf{O}$ have been introduced in Eq.(3.1)). During calibration, the unknown parameters β_I are defined as follows:

$$\beta_I = [\tilde{O}_x \quad G_x \quad \tilde{O}_y \quad G_y \quad \tilde{O}_z \quad G_z]^T. \tag{3.15}$$

Based on Eq.(3.24) and Eq.(3.22), the calibration formula can be re-constructed by the measured acceleration $\mathbf{A^m} = [A_x^m \quad A_y^m \quad A_z^m]^T$ and $\mathbf{M^m}$ as:

$$L = A_x^m(G_x M_x^m + \tilde{O}_x) + A_y^m(G_y M_y^m + \tilde{O}_y) + A_z^m(G_z M_z^m + \tilde{O}_z) + \epsilon, \tag{3.16}$$

where $\epsilon \in R^n$ is the measurement noise.

When there are n sets of measurement data, Eq.(3.26) can be stacked to a matrix form as follows:

$$\begin{bmatrix} A_{x1}^m & A_{x1}^m M_{x1}^m & A_{y1}^m & A_{y1}^m M_{y1}^m & A_{z1}^m & A_{z1}^m M_{z1}^m \\ \cdots & \cdots & \cdots & \cdots & \cdots & \cdots \\ \vdots & \vdots & \vdots & \vdots & \vdots & \vdots \\ \vdots & \vdots & \vdots & \vdots & \vdots & \vdots \\ A_{xn}^m & A_{xn}^m M_{xn}^m & A_{yn}^m & A_{yn}^m M_{yn}^m & A_{zn}^m & A_{zn}^m M_{zn}^m \end{bmatrix} \begin{bmatrix} \tilde{O}_x \\ G_x \\ \tilde{O}_y \\ G_y \\ \tilde{O}_z \\ G_z \end{bmatrix} + \boldsymbol{\epsilon} = \begin{bmatrix} L \\ \cdots \\ L \end{bmatrix}, \tag{3.17}$$

The constant L could be estimated by the local inclination θ based on Eq.(3.23) and Eq.(3.24).

The simplified form of Eq.(3.26) can be written as:

$$\mathbf{L} = \mathbf{X_I}\beta_I + \boldsymbol{\epsilon}, \tag{3.18}$$

where

$$\mathbf{X_I} = \begin{bmatrix} A_{x1}^m & A_{x1}^m M_{x1}^m & A_{y1}^m & A_{y1}^m M_{y1}^m & A_{z1}^m & A_{z1}^m M_{z1}^m \\ \cdots & \cdots & \cdots & \cdots & \cdots & \cdots \\ \vdots & \vdots & \vdots & \vdots & \vdots & \vdots \\ \vdots & \vdots & \vdots & \vdots & \vdots & \vdots \\ A_{xn}^m & A_{xn}^m M_{xn}^m & A_{yn}^m & A_{yn}^m M_{yn}^m & A_{zn}^m & A_{zn}^m M_{zn}^m \end{bmatrix}.$$

The parameters in Eq.(3.28) can be identified by using least square estimation as follows:

$$\hat{\beta}_I = (\mathbf{X_I}^{\mathrm{T}}\mathbf{X_I})^{-1}\mathbf{X_I}^{\mathrm{T}}\mathbf{L}. \tag{3.19}$$

Algorithm for 9-parameter Inclination Based Calibration

The 9-parameter auto-calibration model is also developed in this study due to the non-orthogonality and misalignment of the tri-axial anisotropic magnetoresistive sensor, as well as the unwanted magnetic interference which lead to the limitation of 6-parameter model [27, 47, 89]. According to the mathematical model mentioned previously in Eq.(3.1), the model could be rewritten as:

$$\mathbf{M^r} = \mathbf{G_s G_e}(\mathbf{M^m} + \mathbf{O}) + \mathbf{n} = \mathbf{G M^m} + \tilde{\mathbf{O}} + \mathbf{n}, \tag{3.20}$$

where, matrix $\mathbf{G_s}$ is constructed by scale factors and the matrix $\mathbf{G_e}$ stands for the soft iron causing by the nonorthogonality and misalignment of the tri-axial sensors [25, 47]. The matrix $\mathbf{G} \in R^{3\times3}$ is simplified from $\mathbf{G_s} \times \mathbf{G_e}$ [21, 22, 105]. The offset of measurements is indicated by $\mathbf{O} \in R^3$. The matrix $\tilde{\mathbf{O}} = [\tilde{O}_x \quad \tilde{O}_y \quad \tilde{O}_z]^T$ is the product of $\mathbf{G}$ and $\mathbf{O}$. The Gaussian noise vector with zero mean is presented by $\mathbf{n} = [n_x \quad n_y \quad n_z]^T$.

The distortion matrix $\mathbf{G}$ is expressed as [34] :

$$\mathbf{G} = \begin{bmatrix} G_{xx} & G_{xy} & G_{xz} \\ G_{yx} & G_{yy} & G_{yz} \\ G_{zx} & G_{zy} & G_{zz} \end{bmatrix}. \tag{3.21}$$

According to the model of local magnetic filed and measured value from magnetometers in Eq. (3.1), the calibrated magnetic value $\mathbf{M^c} = [M_x^c \quad M_y^c \quad M_z^c]^T$ can be calculated by the measured magnetic value $\mathbf{M^m} = [M_x^m \quad M_y^m \quad M_z^m]^T$ with the following formula based on Eq. (3.1):

$$\begin{cases} M_x^c = G_{xx}M_x^m + G_{xy}M_y^m + G_{xz}M_z^m + \tilde{O}_x \\ M_y^c = G_{yx}M_x^m + G_{yy}M_y^m + G_{yz}M_z^m + \tilde{O}_y \\ M_z^c = G_{zx}M_x^m + G_{zy}M_y^m + G_{zz}M_z^m + \tilde{O}_z. \end{cases} \tag{3.22}$$

For the purpose of getting the calibrated magnetic value $\mathbf{M^c} \in R^3$ and considering the dot product between the magnetic field $\mathbf{M^r} \in R^3$ and the acceleration field $\mathbf{A^r} \in R^3$ is constant, the I-Calibration is proposed in the 9-parameter model. Ideally, the inclination angle θ could express the relationship between the real acceleration value $\mathbf{A^r} = [A_x \quad A_y \quad A_z]^T$ and the real magnetic value $\mathbf{M^r} = [M_x \quad M_y \quad M_z]^T$ [33]:

$$\theta = \frac{\pi}{2} - \cos^{-1}\left(\frac{A_xM_x + A_yM_y + A_zM_z}{\|\mathbf{A^r}\|\|\mathbf{M^r}\|}\right). \tag{3.23}$$

As mentioned before, the dot product between the local magnetic field $\mathbf{M^r} \in R^3$ and the gravity field $\mathbf{A^r} \in R^3$ is invariant, a constant L can be defined to express the relationship

between $\mathbf{A^r}$ and $\mathbf{M^r}$ in Eq. (3.23):

$$\mathrm{L} = \mathrm{A_x M_x} + \mathrm{A_y M_y} + \mathrm{A_z M_z} = \|\mathbf{A^r}\|\|\mathbf{M^r}\|\cos(\frac{\pi}{2} - \theta). \tag{3.24}$$

In order to formulate the 9-parameter model for Eq. (3.22), we assume $G_{yx} = G_{xy}$, $G_{zx} = G_{xz}$, $G_{zy} = G_{yz}$. The unknown parameter matrix β for 9-parameter I-Calibration algorithm could be expressed as:

$$\beta = [G_{xx} \quad \tilde{O}_x \quad G_{yy} \quad \tilde{O}_y \quad G_{zz} \quad \tilde{O}_z \quad G_{xy} \quad G_{xz} \quad G_{yz}]^T. \tag{3.25}$$

To ensure the accuracy of the magnetic calibration results, the measured acceleration value $\mathbf{A^m} = [A_x^m \quad A_y^m \quad A_z^m]^T$ is first calibrated by the approach which proposed in our previous work [107] and identified as $\mathbf{A^c} = [A_x^c \quad A_y^c \quad A_z^c]^T$. Based on Eq. (3.24) and Eq. (3.22), the calibration formula which expresses the relationship between the measured magnetic value $\mathbf{M^m} = [M_x^m \quad M_y^m \quad M_z^m]^T$, the calibrated acceleration value $\mathbf{A^c} = [A_x^c \quad A_y^c \quad A_z^c]^T$ and the constant L is expanded as:

$$\begin{aligned}
\mathrm{L} &= A_x^c M_x^c + A_y^c M_y^c + A_z^c M_z^c \\
&= A_x^c(G_{xx}M_x^m + G_{xy}M_y^m + G_{xz}M_z^m + \tilde{O}_x) \\
&+ A_y^c(G_{yx}M_x^m + G_{yy}M_y^m + G_{yz}M_z^m + \tilde{O}_y) \\
&+ A_z^c(G_{zx}M_x^m + G_{zy}M_y^m + G_{zz}M_z^m + \tilde{O}_z).
\end{aligned} \tag{3.26}$$

Eq. (3.26) can be stacked to a matrix form as shown in Eq. (3.27) when there are n sets of measurement data and $\epsilon \in R^n$ is the measurement noise.

$$\begin{bmatrix} A^c_{x1}M^m_{x1} & \cdots & \cdots & A^c_{xn}M^m_{xn} \\ A^c_{x1} & \cdots & \cdots & A^c_{xn} \\ A^c_{y1}M^m_{y1} & \cdots & \cdots & A^c_{yn}M^m_{yn} \\ A^c_{y1} & \cdots & \cdots & A^c_{yn} \\ A^c_{z1}M^m_{z1} & \cdots & \cdots & A^c_{zn}M^m_{zn} \\ A^c_{z1} & \cdots & \cdots & A^c_{zn} \\ A^c_{x1}M^m_{y1}+A^c_{y1}M^m_{x1} & \cdots & \cdots & A^c_{xn}M^m_{yn}+A^c_{yn}M^m_{xn} \\ A^c_{x1}M^m_{z1}+A^c_{z1}M^m_{x1} & \cdots & \cdots & A^c_{xn}M^m_{zn}+A^c_{zn}M^m_{xn} \\ A^c_{y1}M^m_{z1}+A^c_{z1}M^m_{y1} & \cdots & \cdots & A^c_{yn}M^m_{zn}+A^c_{zn}M^m_{yn} \end{bmatrix}^T \begin{bmatrix} G_{xx} \\ \tilde{O}_x \\ G_{yy} \\ \tilde{O}_y \\ G_{zz} \\ \tilde{O}_z \\ G_z \\ G_{xy} \\ G_{xz} \\ G_{yz} \end{bmatrix} + \boldsymbol{\epsilon} = \begin{bmatrix} L \\ \cdots \\ L \end{bmatrix}. \quad (3.27)$$

The constant L could be calculated by the local inclination θ based on Eq. (3.23) and Eq. (3.24) and simply written as follows based on Eq. (3.26):

$$\mathbf{L} = \mathbf{X}\boldsymbol{\beta} + \boldsymbol{\epsilon}, \quad (3.28)$$

where

$$\mathbf{X} = \begin{bmatrix} A^c_{x1}M^m_{x1} & \cdots & \cdots & A^c_{xn}M^m_{xn} \\ A^c_{x1} & \cdots & \cdots & A^c_{xn} \\ A^c_{y1}M^m_{y1} & \cdots & \cdots & A^c_{yn}M^m_{yn} \\ A^c_{y1} & \cdots & \cdots & A^c_{yn} \\ A^c_{z1}M^m_{z1} & \cdots & \cdots & A^c_{zn}M^m_{zn} \\ A^c_{z1} & \cdots & \cdots & A^c_{zn} \\ A^c_{x1}M^m_{y1}+A^c_{y1}M^m_{x1} & \cdots & \cdots & A^c_{xn}M^m_{yn}+A^c_{yn}M^m_{xn} \\ A^c_{x1}M^m_{z1}+A^c_{z1}M^m_{x1} & \cdots & \cdots & A^c_{xn}M^m_{zn}+A^c_{zn}M^m_{xn} \\ A^c_{y1}M^m_{z1}+A^c_{z1}M^m_{y1} & \cdots & \cdots & A^c_{yn}M^m_{zn}+A^c_{zn}M^m_{yn} \end{bmatrix}^T. \quad (3.29)$$

Then, a least square estimation problem could be formulated to calculate the parameter β in Eq.(3.28):

$$\hat{\boldsymbol{\beta}} = (\mathbf{X}^{\mathrm{T}}\mathbf{X})^{-1}\mathbf{X}^{\mathrm{T}}\mathbf{L}. \quad (3.30)$$

After the parameters β is calculated, the calibrated magnetic $\mathbf{M_I^c} = [M_{Ix}^c \quad M_{Iy}^c \quad M_{Iz}^c]^T$ value by I-Calibration is calculated according to Eq. (3.22) and Eq. (3.25).

3.3 Experimental Design and Simulation

3.3.1 Experimental Design

The experiment was performed by using the commercially IMU device (VICON IMeasureU, Auckland, New Zealand) as shown in Fig. 3.2. The experiment was implemented at the campus of University of Technology Sydney and was performed relatively far away from any magnetic materials to ensure a homogeneous local magnetic field. This aims to discard perturbation from the hosting platform to measure the earth's field. Meanwhile, as the experiment is performed in clean ferromagnetic surroundings, the measured value from magnetometers can be approximately equal to the local magnetic field. As mentioned previously, we adopt the 12-observation scheme [27] to calibrate the magnetometers. During the experiment, the IMU sensor was rotated to 12 positions with respect to the local horizontal frame, and was placed in each position according to the 12-observation in Fig. 3.3 for a certain period to record steady data.

Fig. 3.2 The IMU Device used in Experiment.

The x, y, z indicate the positive direction in each axis. It should be noted that the high accuracy platform was not used for the alignment of axis due to the limitation of in-field calibration. After the 12-observation experiment completed, the data were stored for further processing. This calibration procedure could be repeated to reduce the influence of sensor drift [37].

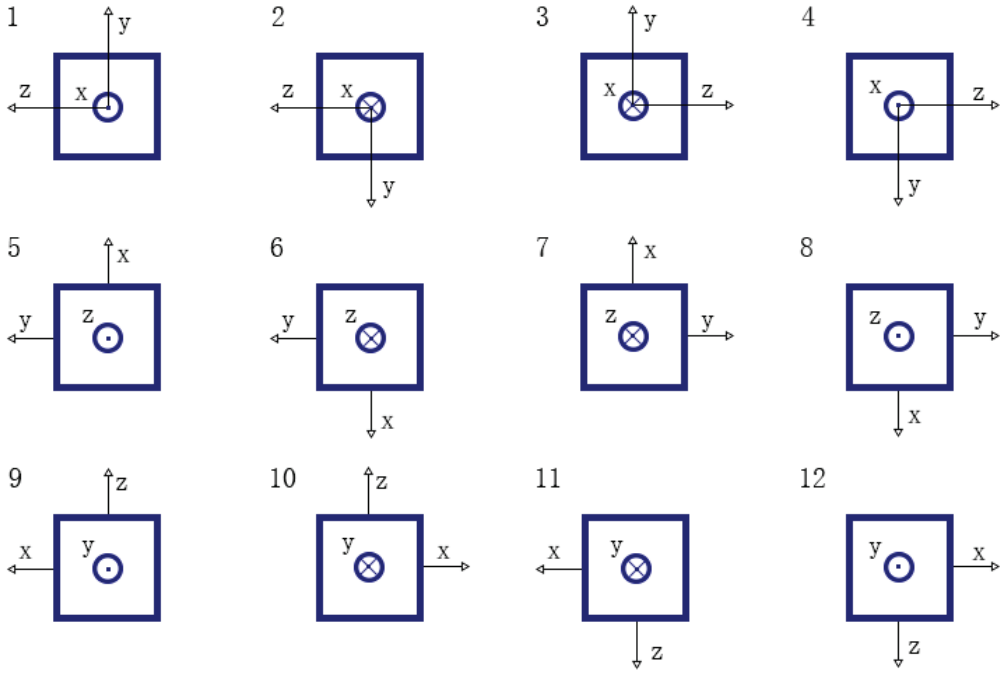

Fig. 3.3 The Arrangements of MEMS IMU for 12-Observation DoE.

3.3.2 Simulation for Inclination Based Calibration

To evaluate the I-Calibration approach, a series of simulations under different conditions are developed to study this I-Calibration method. The simulated acceleration value $\mathbf{A}^{\mathbf{s}} \in R^3$ and the simulated magnetic value $\mathbf{M}^{\mathbf{s}} \in R^3$ are generated according to real situations. Different weights of the noise level, scale factors and misalignments, offset and tolerance angle are considered to simulate different conditions for the simulated data. Each run of the simulation is obtained by the 12-observation DoE as shown in Fig. 6.1. The proposed I-Calibration method is then implemented to estimate the unknown parameters, and the simulation results are calculated and recorded.

Firstly, the simulated acceleration value $\mathbf{A}^{\mathbf{s}}$ is generated with the typical errors of scale factors and offsets are within $\pm 10\%$ and $\pm 0.1g$ [107], respectively. Next, the simulated magnetic value $\mathbf{M}^{\mathbf{s}}$ is assumed as the projection of acceleration value $\mathbf{A}^{\mathbf{s}}$ in the axis of

magnetic according to the inclination. A tolerance angle $\varphi = [\varphi_x \quad \varphi_y \quad \varphi_z]^T$ is set to study the affect of misalignment between the accelerometers axis and the magnetometers axis:

$$R_x = \begin{bmatrix} 1 & 0 & 0 \\ 0 & \cos\varphi_x & -\sin\varphi_x \\ 0 & \sin\varphi_x & \cos\varphi_x \end{bmatrix}, \tag{3.31}$$

$$R_y = \begin{bmatrix} \cos\varphi_y & 0 & \sin\varphi_y \\ 0 & 1 & 0 \\ -\sin\varphi_y & 0 & \cos\varphi_y \end{bmatrix}, \tag{3.32}$$

$$R_z = \begin{bmatrix} \cos\varphi_z & -\sin\varphi_z & 0 \\ \sin\varphi_z & \cos\varphi_z & 0 \\ 0 & 0 & 1 \end{bmatrix}. \tag{3.33}$$

The transformation matrix for a rotation about the simulated magnetic value $\mathbf{M^s}$ by a tolerance angle φ is identified as $\mathbf{M^s_\varphi} \in R^3$ and given by Eq.(3.34)[109, 110]:

$$\mathbf{M^s_\varphi} = R_x \times R_y \times R_z \times \mathbf{M^s}. \tag{3.34}$$

The 12-observation DoE is applied to obtain the observation matrix $\mathbf{X_I}$ in Eq.(3.28) after the simulated acceleration value $\mathbf{A^s}$ and the simulated magnetic value $\mathbf{M^s}$, $\mathbf{M^s_\varphi}$ have been generated. Then, the I-Calibration method can be implemented to complete the simulation.

As the calibration algorithm utilises the local gravity information, which is measured by TAs, the overall performance of the proposed calibration method is influenced by the estimated gravity. For the purpose of studying the influence of accelerometers value accuracy on the calibration results and evaluating the I-Calibration approach, the second part of simulation study is developed. Similarly, the simulated TAs output value $\mathbf{A^s} \in R^3$ is generated according to the theoretical projection of the earth gravity, and deliberately added errors to the model parameters. Specifically, the scale factors are set within $\pm 10\%$ and offsets are within $\pm 0.1g$ [107]. In order to implement the angle between the gravity and magnetic field during simulation, the simulated TMs value $\mathbf{M^s}$ is generated as the projection of acceleration value $\mathbf{A^s}$ in the magnetic axis according to the inclination angle. To make a comparison,

before calibration, we assume there are additional errors of scale factors $\pm 10\%$ and offset within $\pm 0.1g$ in the TAs model, and use $\mathbf{A_n^s}$ to stand for the uncalibrated TAs output. Then, the 12-observation DoE is adopted to acquire the observation matrix $\mathbf{X}$ as introduced in Section 3.2.2 after the simulated data have been generated. At last, $\mathbf{A^s}$ and $\mathbf{M^s}$, $\mathbf{A_n^s}$ and $\mathbf{M^s}$ are substituted in the formula of I-Calibration method respectively to obtain the simulation calibration results.

3.4 Results

3.4.1 Simulation Study

Simulation for the Tolerance Angles of Inclination Based Calibration

The simulation results about demonstrating the effectiveness and tolerance angles of I-Calibration are presented in this section. A randomly-selected example of the estimated magnetic magnitude value before and after the I-Calibration simulation is shown in Fig. 3.4. The magnitude value is calculated by the square root of the sum of squares of their vector components.

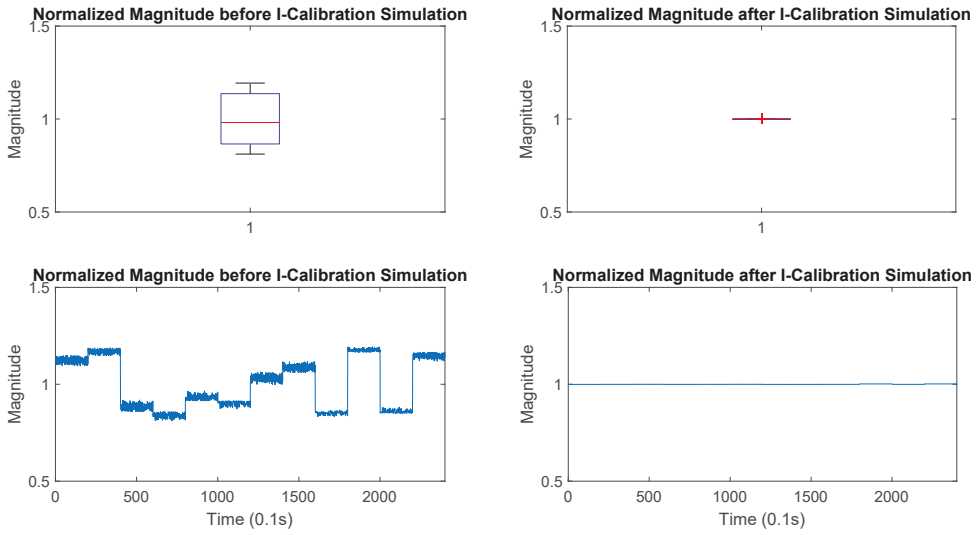

Fig. 3.4 Normalized Magnitude Value before and after I-Calibration Simulation.

In total, we have 2000 simulations and the results are generated randomly under the following conditions:

- The weights of noise level follow a uniform distribution $U(-10\%, 10\%)$,
- The scale factors and misalignments of $\mathbf{A}^{\mathbf{s}}$ follow a uniform distribution $U(-10\%, 10\%)$,
- The offsets of $\mathbf{A}^{\mathbf{s}}$ follow a uniform distribution $U(-0.1g, 0.1g)$,
- The tolerance angles are set as shown in the following four cases, and run 500 simulations for each case:
  $\varphi_x = \varphi_y = \varphi_z = 0°$;
  $\varphi_x = \varphi_y = \varphi_z = 30°$;
  $\varphi_x = \varphi_y = \varphi_z = 60°$;
  $\varphi_x = \varphi_y = \varphi_z = 90°$.

According to the magnitude of the simulated magnetic value with different tolerance angles, the range and standard deviation of magnitude are calculated and represented in Fig. 3.5 to demonstrate the degree of dispersion of magnitude.

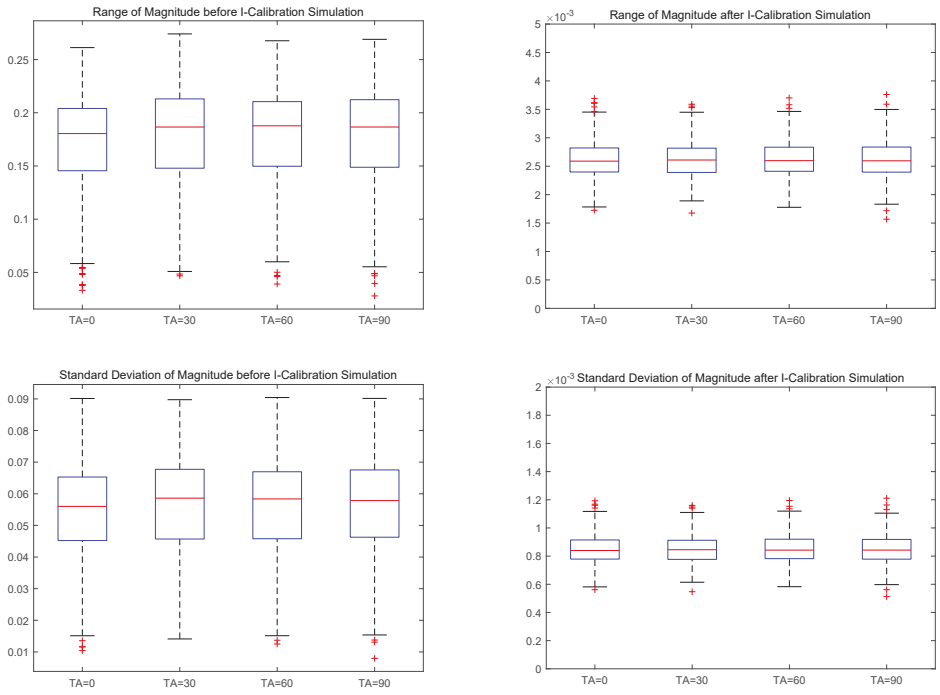

Fig. 3.5 Scaled Range and Standard Deviation of Magnitude before and after I-Calibration Simulation, where "tolerance angles" is abbreviated as "TA" to save space.

As shown in Fig. 3.5, the magnitude of the estimated local magnetic field is much more accurate after calibration, which indicates the I-Calibration is effective in calibrating tri-axial magnetometers. In addition, the tolerance angle has no significant effect on the calibration results.

Simulation for the Acceleration Calibration of Inclination based Calibration

The simulation results about how the acceleration data affect the magnetometers calibration results in I-Calibration is illustrated in this section. The sum of the square of the magnetic data is magnitude, which is a vital factor to indicate the effectiveness of calibration [111, 112]. A randomly-selected example of the simulation results is presented in Fig. 3.6 which shows the normalized magnetic magnitude value before and after the I-Calibration simulation. The calibration results calculated by the raw (measured) acceleration value and calibrated acceleration value are represented respectively.

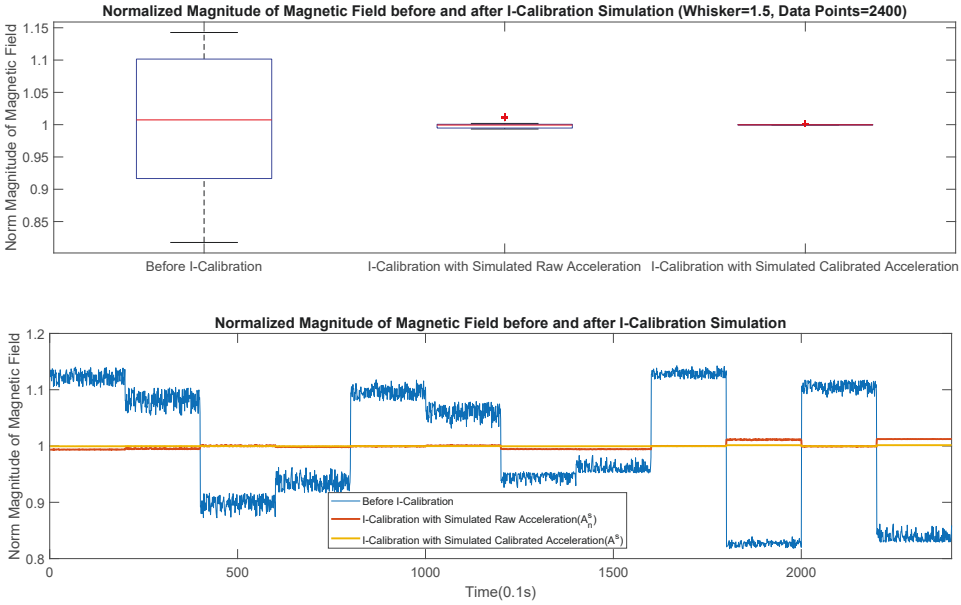

Fig. 3.6 Raw Data and Calibrated Data by I-Calibration Simulation with Measured Acceleration data and Calibrated Acceleration data.

According to the magnitude of the magnetic value after 2000 times I-Calibration simulation with different measured and calibrated acceleration values, the range and standard deviation of magnitude are calculated and represented in Fig. 3.7.

From the above results, it is demonstrated that the I-Calibration is an effective magnetic calibration method as the magnitude of the magnetic field is more accurate after calibration. In addition, the acceleration data after calibration is helpful to improve the magnetic calibration results.

3.4.2 Experimental Results

Experiment for Magnitude Based Calibration

The experiments for M-Calibration are also performed according to the 12-observation experimental scheme as shown in Fig. 3.3. It should be pointed out that the simulation study, without experimental verification, of this calibration approach was already given in our

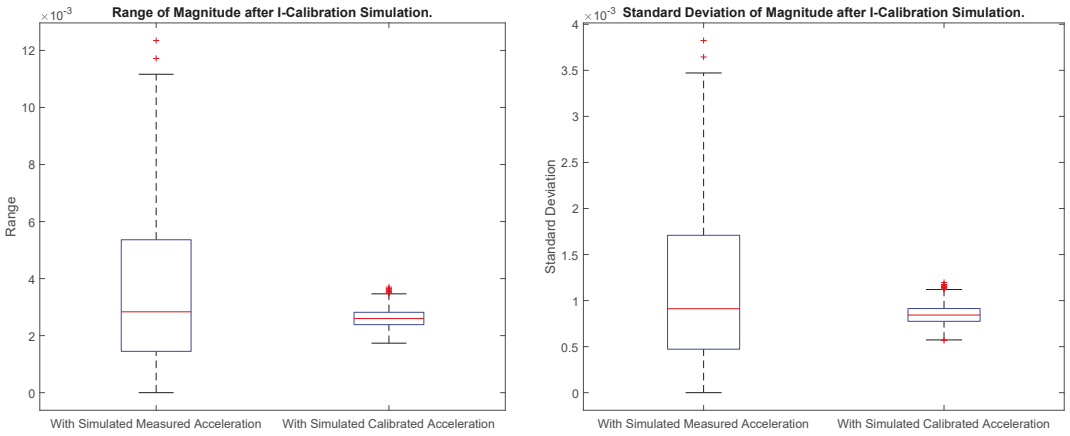

Fig. 3.7 Scaled Range and Standard Deviation of Magnitude after I-Calibration Simulation with Measured Acceleration data and Calibrated Acceleration data.

previous study [47, 107]. Here, for the first time, we experimentally examine this calibration method.

Based on the experimental data and Algorithm 1, the parameters of the model were identified recursively. The convergence rate of γ in Algorithm 1 is shown in Fig. 3.8, which indicates that the estimated value can converge to the real value within 5 iterations.

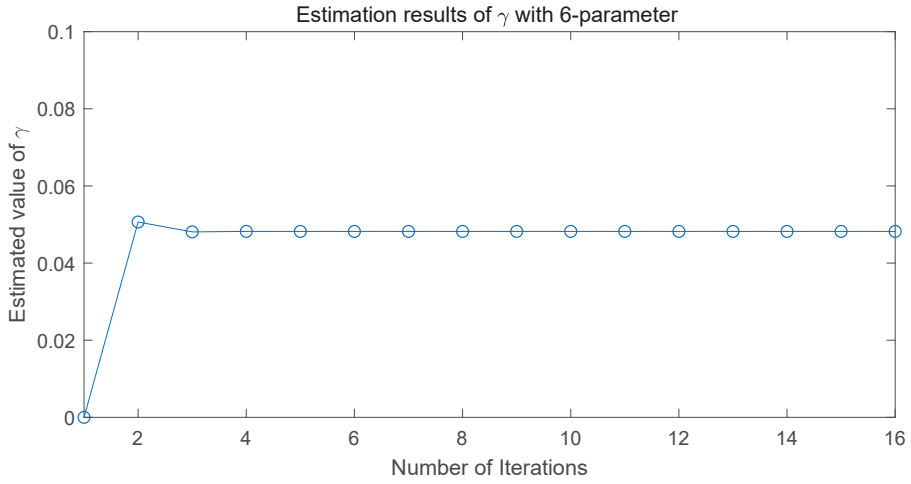

Fig. 3.8 Estimation Results of γ and Convergence.

The estimation results (e.g., convergence rate) of the parameters in the matrices **G** and **O**, during the 15 iterations, are shown in the Fig. 3.9. The calibrated magnetic value by

M-Calibration $\mathbf{M_M^c} = [M_{Mx}^c \quad M_{My}^c \quad M_{Mz}^c]^T$ can be calculated by **G**, **O** and the measured magnetic value $\mathbf{M^m}$ according to Eq.(3.1).

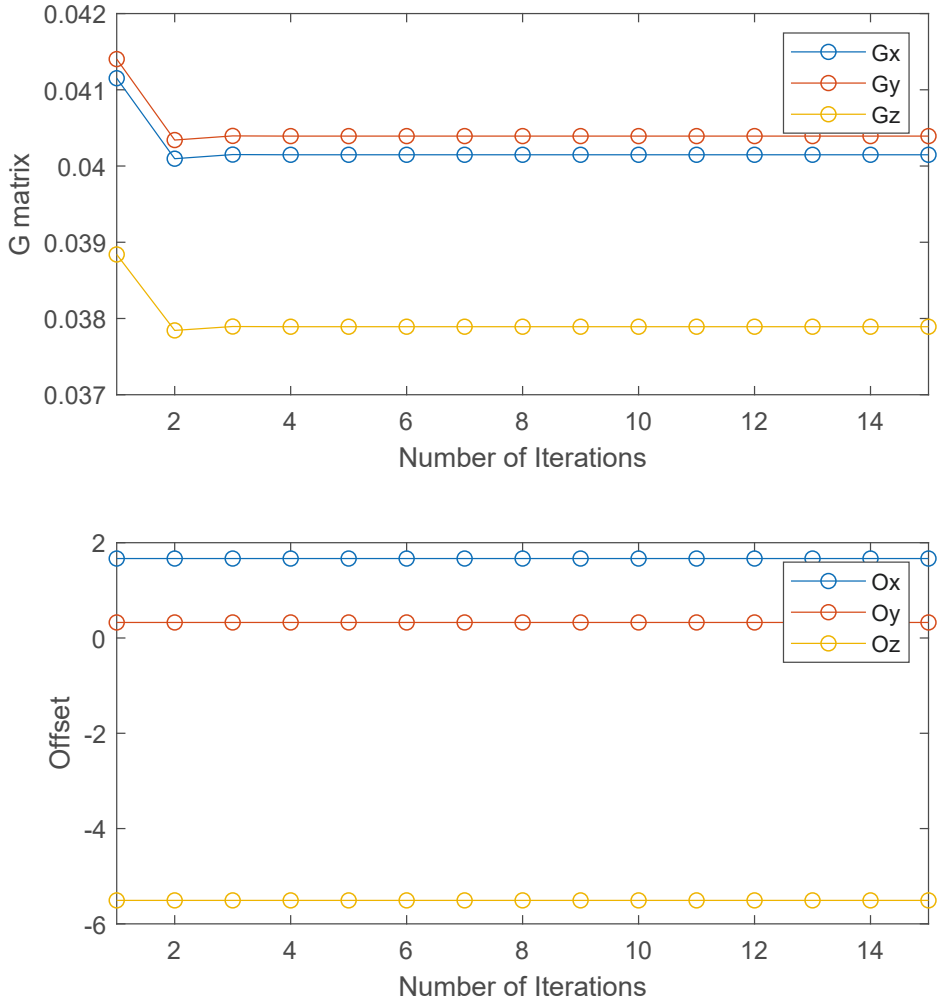

Fig. 3.9 Results of Estimated **G** and **O**.

The calibrated magnitude value of $\mathbf{M_M^c}$ (H_M) and the raw magnitude value of $\mathbf{M^m}$ (H_0) can be calculated by the square root of the sum of squares of their vector components. The normalized magnitude value before and after M-Calibration and their boxplot are shown in Fig. 3.10.

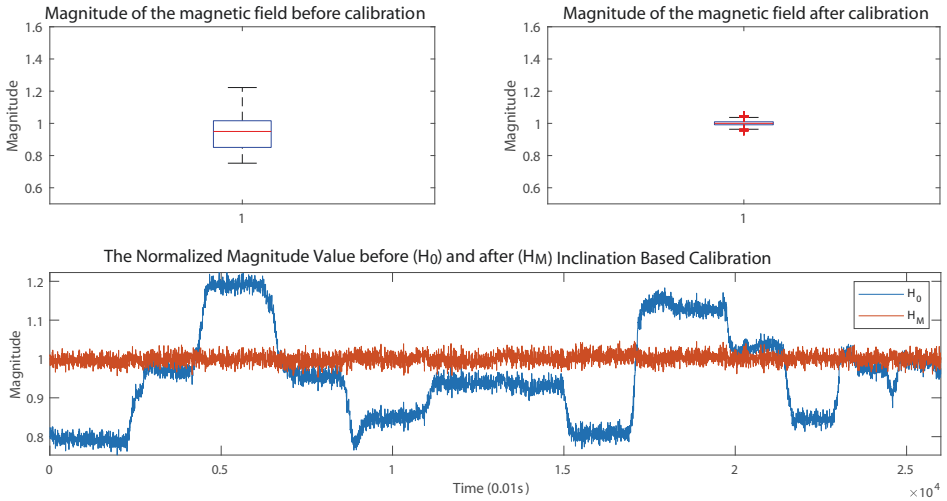

Fig. 3.10 The Normalized Magnitude Value of the Measured Magnetic Fields before (H_0) and after (H_M) Magnitude Based Calibration.

Experimental Results for 6-Parameter Inclination Based Calibration

The experiments for 6-parameter I-Calibration are performed according to the 12-observation experimental scheme as shown in Fig. 6.1. The calibrated magnetic value by using the I-Calibration method $\mathbf{M_I^c} = [M_{Ix}^c \quad M_{Iy}^c \quad M_{Iz}^c]^T$ is calculated according to Eq.(3.22) and Eq.(3.30) .

The magnitude of the calibrated data $\mathbf{M_I^c}$ (H_I) and the measured data $\mathbf{M^m}$ (H_0) were calculated by the square root of the sum of squares of their vector components. The normalized magnitude of the calibrated magnetometers data can be seen to lie around 1 as depicted in red in Fig. 3.11.

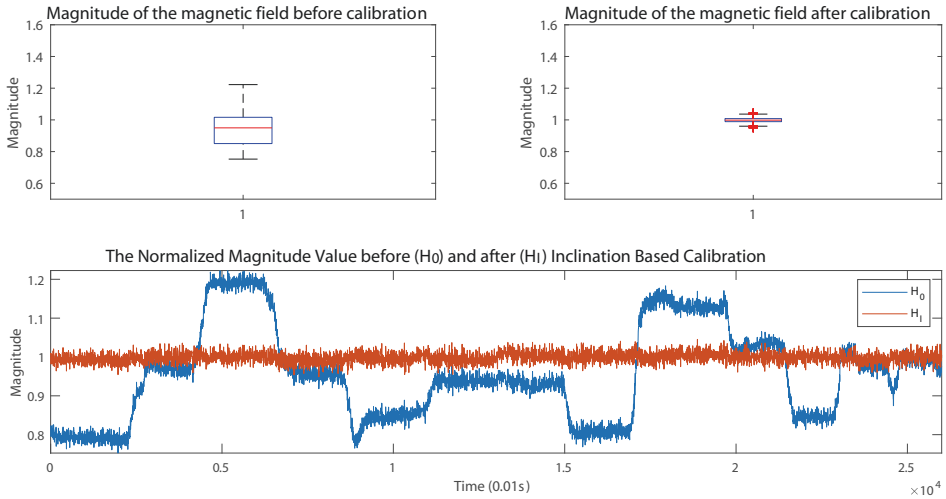

Fig. 3.11 The Normalized Magnitude Value of the Measured Magnetic Fields before (H_0) and after (H_I) Inclination Based Calibration.

As the magnitude of measured data H_0 (without calibration), the magnitude of calibrated data by M-Calibration H_M, and the magnitude of calibrated data by I-Calibration H_I, are calculated, the detailed comparisons for H_0, H_M and H_I, including the maximum value, minimum value, range, standard deviation and quartile difference ($75th$ percentile minus $25th$ percentile) are listed in Table 5.3.

Table 3.1 The Comparison of Raw Magnitude and Calibrated Magnitudes of Two Methods.

Method	H_0	H_M	H_I
Maximum	1.2226	1.0452	1.0464
Minimum	0.7527	0.9489	0.9530
Range	0.4699	0.0962	0.0934
Standard Deviation	0.1186	0.0138	0.0137
Quartile difference	0.1656	0.0192	0.0186

Based on Table 3.1, we apply the Rank Sum Test on the comparison indexes of M-Calibration (column II) and I-Calibration (column III), as they do not follow the normal distribution. Generally, if $P < 0.05$, it will be considered as statistically significant. The result of the Rank Sum Test shows that $P = 1$ means $h = 0$, which means that the distinction of the calibrated magnitude acquired from M-Calibration and I-Calibration is not significant.

If the magnetometer is properly calibrated, the magnitude of the calibrated measurement of the magnetic field will be less independent on the orientation of the platform, and the

estimated value of the local magnetic field should lie on a sphere [34, 108]. Due to sensor draft and distortion, the uncalibrated estimations of local magnetic field often lie on an ellipsoid surface. After a proper calibration for the magnetometer, the calibrated estimations will distribute in a unit sphere [34]. The calibrated data $\mathbf{M}_{\mathbf{M}}^{\mathbf{c}}$, $\mathbf{M}_{\mathbf{I}}^{\mathbf{c}}$ and raw data $\mathbf{M}^{\mathbf{m}}$ are displayed in Fig. 3.12 and compared with a reference sphere.

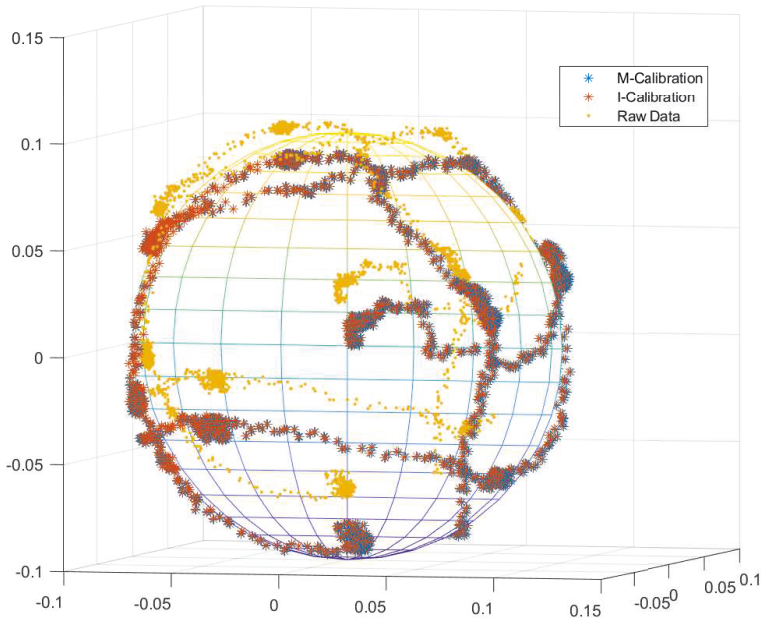

Fig. 3.12 Raw Data and Calibrated Data by M-Calibration and I-Calibration.

In addition, the Rank Sum Test was applied to the raw data ($\mathbf{M}^{\mathbf{m}}$) and calibrated data ($\mathbf{M}_{\mathbf{M}}^{\mathbf{c}}$, $\mathbf{M}_{\mathbf{I}}^{\mathbf{c}}$) to demonstrate the distinction. The comparison result between $\mathbf{M}^{\mathbf{m}}$ and $\mathbf{M}_{\mathbf{M}}^{\mathbf{c}}$, and the result between $\mathbf{M}^{\mathbf{m}}$ and $\mathbf{M}_{\mathbf{I}}^{\mathbf{c}}$ both show $P < 1 \times 10^{-103}$ and $h = 1$, which indicate the calibrated estimations from both M-Calibration and I-Calibration are significantly improved compared to the uncalibrated estimations. On the other hand, the comparison result between $\mathbf{M}_{\mathbf{M}}^{\mathbf{c}}$ and $\mathbf{M}_{\mathbf{I}}^{\mathbf{c}}$ is $P = 0.4706$ and $h = 0$, which implies that the distinction of the calibrated results from these two methods is not significant.

Experimental Results for 9-Parameter Inclination based Calibration

The magnitudes of the calibrated magnetometers data $\mathbf{M^c}$ and the measured magnetometers data $\mathbf{M^m}$ are also applied as indicators to demonstrate the effectiveness of 9-parameter I-Calibration in the experiment. The normalized magnitude of the calibrated magnetometers data can be seen to lie around 1 as depicted in yellow in Fig. 3.13.

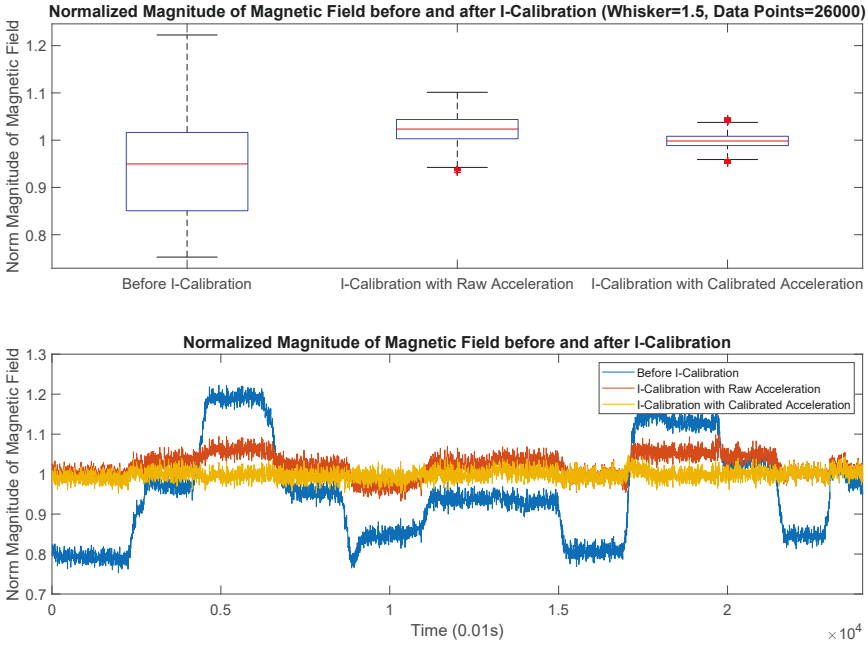

Fig. 3.13 The Normalized Magnitude Value before and after I-Calibration with Calibrated Acceleration $\mathbf{A^c}$ and Measured Acceleration $\mathbf{A^m}$.

As mentioned in Section 3.2.2, the acceleration value has been calibrated when the I-Calibration is applied to the magnetic calibration. In order to illustrate the influence of acceleration value accuracy on the calibration results, a contrast is proposed by implementing the measured acceleration value $\mathbf{A^m} = [A_x^m \quad A_y^m \quad A_z^m]^T$ without calibration in Eq. (3.26). The normalized magnitude before and after I-Calibration by using uncalibrated acceleration value are shown in red in Fig. 3.13.

Generally, if the magnetic distortion and sensor error exist, the magnetometers data without calibration will lie on an ellipsoid surface. Once the magnetic value has been calibrated properly, the calibrated magnetic data will be distributed in a unit sphere [34, 108].

In order to display the raw data, the calibrated magnetic data by I-Calibration using raw measured acceleration value $\mathbf{A^m}$ and using calibrated acceleration value $\mathbf{A^c}$ directly, Fig. 3.14 and Fig. 3.15 are presented to make a contrast for them with a sphere reference plane.

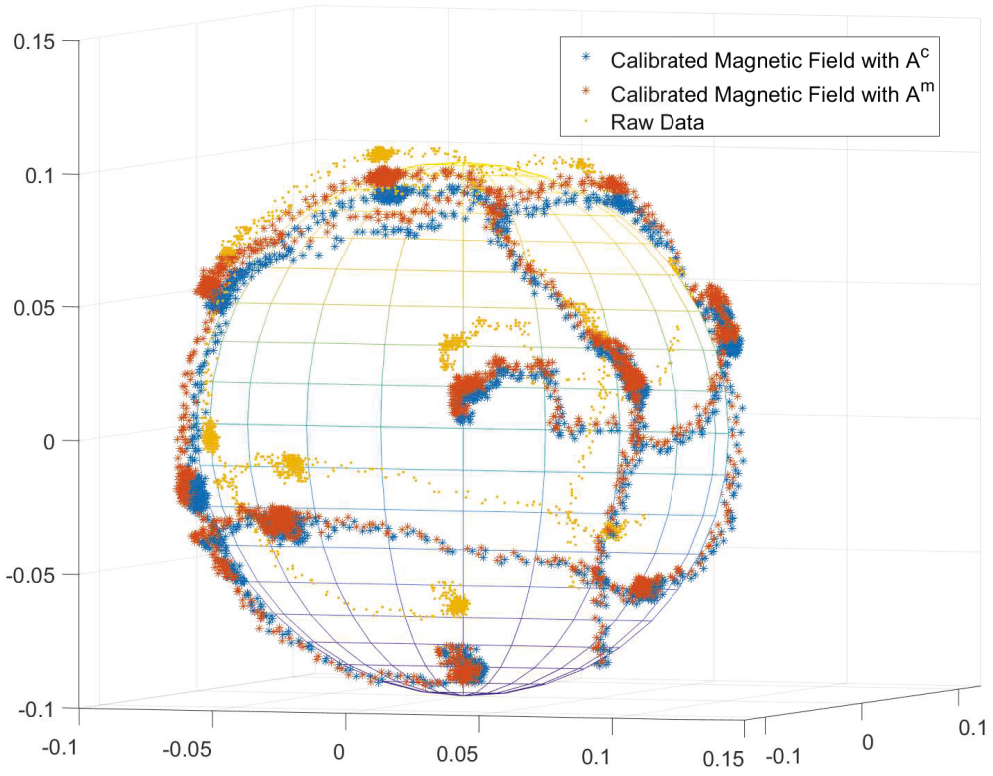

Fig. 3.14 Raw Data and Calibrated Data by I-Calibration with Calibrated Acceleration $\mathbf{A^c}$ and Measured Acceleration $\mathbf{A^m}$ (Front Review)

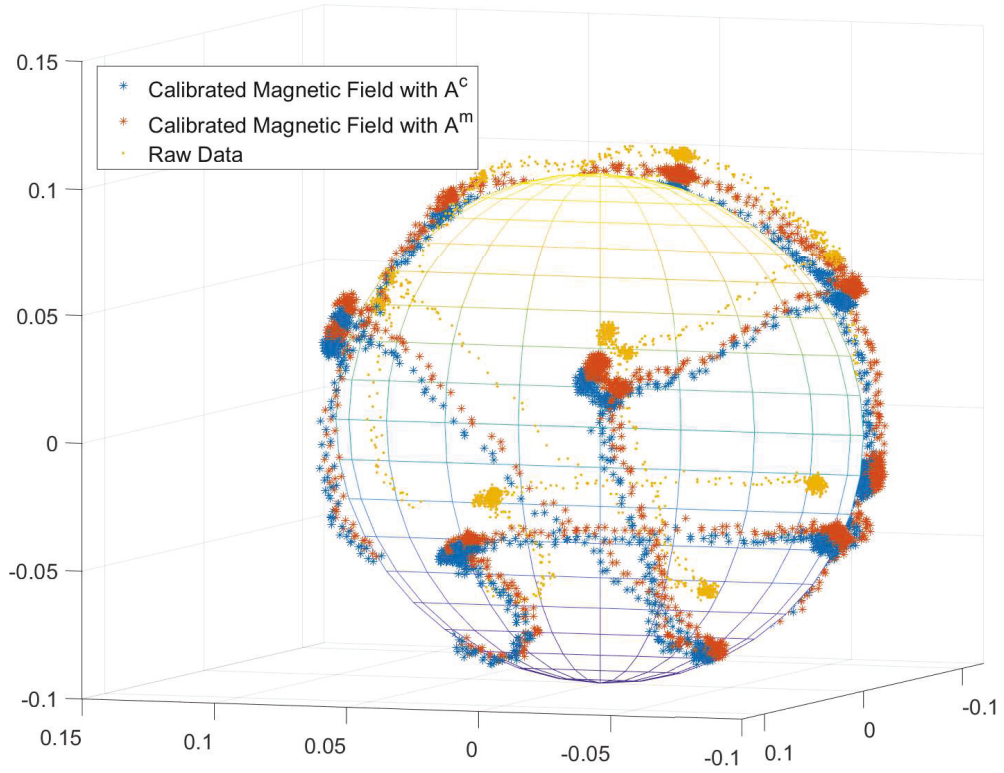

Fig. 3.15 Raw Data and Calibrated Data by I-Calibration with Calibrated Acceleration $\mathbf{A^c}$ and Measured Acceleration $\mathbf{A^m}$ (Back Review)

Notation H_0 represents the magnitude of raw magnetic data, while H_1 and H_2 stand for the magnitudes of calibrated magnetic data by I-Calibration with measured and calibrated accelerations, respectively. In Table 5.3, the range (the difference between the largest and smallest values of the magnitudes) indicates the measures of variation and the standard deviation (SD) represents the dispersion of H_0, H_1 and H_2. In addition, the mean absolute deviation (MAD) and mean absolute value (MAV) are listed in Table 5.3 to demonstrate the deviation of H_1 and H_2 from the baseline, which is defined as 1.

The improvement comparisons for the magnetic calibration by the I-Calibration method and the importance of the acceleration data calibration are listed in Table 3.3 according to the statistical indicators in Table 3.1.

Table 3.2 The Comparisons for Magnitude of Raw Data and Calibrated Data by I-Calibration with Calibrated Acceleration $\mathbf{A^c}$ and Measured Acceleration $\mathbf{A^m}$.

Method	H_0	H_1	H_2
Range	0.4699	0.1694	0.0953
SD	0.1186	0.0282	0.0142
MAD	/	0.0206	0.0098
MAV	/	0.0299	0.0115

Table 3.3 The Improvement Comparisons for the Statistical Indicators.

Comparison	H_1 *to* H_0	H_2 *to* H_0	H_2 *to* H_1
Range	63.94%	79.72%	43.76%
SD	76.20%	87.98%	49.50%
MAD	/	/	52.18%
MAV	/	/	61.44%

The experimental results lead to the same conclusion with the simulation that the I-Calibration is effective on magnetic calibration and the acceleration data should be calibrated to ensure accurate calibration results.

3.5 Discussion

The proposed I-Calibration algorithm, which associated with the measured magnetic data and calibrated acceleration data, has been applied to the simulation and experimental magnetometers calibration procedure. The effectiveness of the I-Calibration algorithm is demonstrated both by simulation and experiment. In addition, the effect of tolerance angle in 6-parameter I-Calibration and the effect of calibrated acceleration in 9-parameter I-Calibration is also demonstrated both by simulation and experiment.

In the study of 6-parameter I-Calibration and comparison with M-Calibration, it is demonstrated that the I-Calibration has the similar effectiveness as the M-Calibration in terms of calibration accuracy. This conclusion is based on the raw and calibrated data as shown in Fig. 3.12, the Rank Sum Test of comparison index in Table 3.2, and the estimated vectors ($\mathbf{M_M^c}$, $\mathbf{M_I^c}$, $\mathbf{M^m}$). However, these two methods have different advantages and disadvantages. The M-Calibration can be utilised to directly calibrate magnetometers without using the measurements from TAs. However, during calibration, the M-Calibration

needs some extra conditions to ensure the convergence of the algorithm as it is a nonlinear parameter estimation algorithm. High computational cost and appropriately selected initial conditions are required to guarantee the convergence of the iterative algorithm (see Algorithm 1). One the other hand, the I-Calibration is a simple linear method, and it is a single step linear least square estimator, i.e., without iteration. Furthermore, Fig. 3.5 illustrates that even though the frames of the tri-axial accelerometers and magnetometers are not consistent, the I-Calibration method is still valid. However, the accuracy of the tri-axial accelerometers is essential to ensure the success of I-Calibration method hence this point is discussed in the 9-parameter model.

In the study of 9-parameter I-Calibration, the magnetic field data can also be calibrated properly. From the results shown in Fig. 3.13, the normalized magnitude of the calibrated magnetometers data can be seen to lie around 1 which means the data have been calibrated effectively [108, 111, 112]. The results in Fig. 3.14 also displays that the data is mapped to a sphere after calibration [34, 105, 108]. For the purpose of demonstrating whether the acceleration data has an influence on the I-Calibration method, the simulation and experimental calibration have also been implemented by the raw acceleration data. It can be noticed that when the acceleration data is without calibration, the normalized magnitude of the magnetic field is with deviation from the baseline of 1 in Fig. 3.6 and Fig. 3.13. The deviation is proved by the decreased range and standard deviation of the magnetic field magnitude after the I-Calibration simulation in Fig. 3.7. The calibrated TMs data with raw acceleration data as shown in Fig. 3.14 are also with deviation from the reference sphere. The percentage of the improvement for the magnetic calibration results when the acceleration data is calibrated in Table 3.2 provides the statistical evidence for the deviation. As we can see, the range, standard deviation of the magnitude of the magnetic field is decreased after calibration, and the extent of decreasing when using calibrated acceleration is larger compared to that using measured acceleration. The decreased MAD and MAV by different acceleration values also illustrate the necessity of acceleration calibration. According to the results both from simulation and experiment, the improvement in the calibration results when using the calibrated acceleration data is demonstrated.

Above all, compared to the existing “Attitude-Independent" calibration methods which need some extra conditions to ensure the convergence of the algorithm [106, 107] (as it is a nonlinear parameter estimation algorithm and need appropriate selected initial condition

[34, 108]), the proposed I-Calibration is a simple linear method, i.e., it is a single step linear least square estimator without iteration. Thus, the method can be easily implemented in a wearable device with low computational power. The performance of tri-axial accelerometers is essential to ensure the success of the proposed I-Calibration method as the uncalibrated accelerometers data can affect the calibration results as shown in Section 3.4.2. To further improve the effectiveness of the two proposed methods, in the next step, the I-Calibration can be used to select the initial conditions, then the M-Calibration can be applied by using the well selected initial values to ensure the convergence of the M-Calibration [107].

3.6 Conclusion

A practical algorithm named Inclination based Calibration (I-Calibration) has been developed in this work to calibrate the tri-axial magnetometers. This algorithm is based on the fact that the angle between the local magnetic field and gravity is constant. Different from existing in-field calibration methods, the newly proposed I-Calibration could accurately estimate the coefficients of the magnetometers model by simply using a linear Least Square estimator. Both 6-parameter and 9-parameter mathematical methods associated with the 12-observation experimental design is proposed to the calibration procedure. The problem is finally formulated as a linear least square problem based on the measured magnetic value and calibrated acceleration value.

Extensive numerical simulations for 6-parameter and 9-parameter model demonstrated the effectiveness of the I-Calibration. The algorithm performs well on both the simulation study and practical experiment and is confirmed that the I-Calibration is robust to the mismatch of the frames of TAs and TMs when using 6-parameter model. Real-time experiments were also performed to compare the performance of the proposed I-Calibration and the M-Calibration. The experimental results demonstrated the two calibration methods have similar effectiveness in terms of calibration accuracy. To investigate the significance for the accuracy of the acceleration value, a contrast study is applied in the simulation and experimental procedure by 9-parameter model. It is demonstrated that the acceleration data should be calibrated well to ensure the effectiveness of the Inclination based Calibration algorithm. However, as the I-Calibration method was a single-calculation linear method, with low computational cost

and without divergence problem, it would be more suitable for real-time in-field calibration for wearable devices with limited computational power.

Chapter 4

Non-Parametric Dynamical Model of Cardiorespiratory Responses at the Onset and Offset of Treadmill Exercise

4.1 Introduction

Decades ago, some sports physiology laboratories had used the Douglas bag and the Scholander gas analyser [14] to measure the oxygen (O_2) uptake and the amount of carbon dioxide (CO_2) produced before, during, and after exercise. Over the last dozens of years, automated portable gas analysis systems had been developed and applied in various sports fields for energy consumption assessment [15]. The study of oxygen uptake was both the traditional theme of sports physiology study and one of the mainstreams of current and future sports physiology research. The characterization of gas exchanging attracted a lot of scholars to work in the field. Hill et al. [16] studied oxygen uptake ($\dot{V}O_2$) and investigated its recovery curve. After moderate exercise, it is a logarithmic equation, which is equally applicable to the recovery curves of carbon dioxide output ($\dot{V}CO_2$). Similarly, Wasserman and Berg illustrated the equation of carbon dioxide elimination is equal to oxygen uptake. Researches about the $\dot{V}O_2$ and $\dot{V}CO_2$ during the exercise also had been developed.

Modelling method is widely used in the biological signal analysis [48–50]. Several research studies for the modelling of the dynamics of physiological signal in response to

treadmill exercise were also conducted [64, 92, 93]. To the best of our knowledge, all the existing studies only utilised classical system identification approaches, e.g. the Least Square (LS), Maximum Likelihood (ML) and Prediction Error Method (PEM). However, the signals that exert on a human body should be well selected to ensure the safety. Due to this reason, when the human being is involved in an experiment, the input signals are often limited in both intensity and duration, which leads to insufficient stimulation for the modelling of the system. In this case, the LS/ML/PEM equipped with classical model structure selection approaches often fail to obtain an appropriate model with desired accuracy and robustness for cardiorespiratory response estimation, which is based on insignificantly stimulated short recording data polluted by artifacts and noise [52–54].

The recently developed system identification approaches are not only based on plenty of physical experimental data but also emphasizing more on prior knowledge of the system under estimation. System prior information is often applied to model complexity selection, which is the most critical step for system modelling. In some papers [55, 56], system dynamics is depicted by non-parametric models rather than the most commonly used first/second order linear time-invariant models. Often, non-parametric methods are used when the prior information is insufficient to determine a parametric model structure. The new approach [54, 67] which well utilises the prior information is based on the kernel-based regularisation approach. By using kernel technique, prior information is adopted in the identification process by assigning an appropriate kernel to the index function. Specifically, papers [56–59] introduced the regularisation terms and the kernel designing strategies for non-parametric system identification. Based on authors' experiences, for the investigation of the dynamics of cardiorespiratory response to exercise, the new kernel-based non-parametric approach should be the best option to greatly improve the robustness and accuracy.

The treadmill exercise is similar to human daily life running or walking status so it could be applied to analyse the mechanism of one's exercise. It is well documented that regular treadmill exercise can greatly improve the human cardiovascular system, e.g., increase total oxygen demand and consumption (the amount of increase depending on the size of the muscles used), and $\dot{V}O_2$ Max. Moreover, the treadmill is a good choice for exercise modelling because the model needs an accurate input to ensure a steady workload and exclude other effect factors. Some research [8] applied Heart Rate (HR) to make the analysis, but it can easily be affected by human motion or other aspects. In this way, other researchers choose

how the gas changes during the exercise as an index. Among the studies of cardiorespiratory response to exercise, researchers preferred to choose oxygen uptake as the index. Both linear and nonlinear static models [61, 97, 98] had been proposed based on the walking speed. Furthermore, some researchers modelled the $\dot{V}O_2$ response with a monoexponential curve [62, 76, 77]. In these studies, the oxygen uptake could indicate the respiratory gas exchange, energy providing situation, the energy saving phenomenon, the differential effect of training tense and other biological phenomenon. Some of the researchers had also recorded the $\dot{V}CO_2$ as an auxiliary data for analysis.

The above studies present different aspects of Kinematics and the pattern of gas exchange. However, $\dot{V}CO_2$ is uncommonly applied. What's more, the dynamic changing of the $\dot{V}CO_2$ and $\dot{V}O_2$ during the different periods of exercise and their relationship need a deeper investigation to get a comprehensive understand for human exercise mechanism. In this work, we apply the non-parametric modelling method [54, 67] to identify the relationship between $\dot{V}CO_2$ and the speed of the treadmill. The inputs of the $Speed-to-the-\dot{V}CO_2$ system are step functions (i.e., the onset period is from $3km/h$ to $8km/h$, and the offset is from $8km/h$ to $3km/h$). The exercise protocol of the treadmill speed is illustrated as in Fig. 4.1. We adopted the kernel-based estimation method for this modelling. The data were collected from 20 untrained participants in the treadmill exercise. After the identification, we make a statistical comparison between the onset period (from walking to running) of the speed and the offset period (from running to walking). Moreover, we analysed the relationship between the $\dot{V}O_2$ and the $\dot{V}CO_2$. The contributions of the part of work are listed as follows:

- The kernel-based non-parametric modelling approach has been applied to describe the dynamics of both $\dot{V}O_2$ and $\dot{V}CO_2$ responses to exercise.
- Based on comprehensively comparative numerical analyses, the SS kernel has been selected as the best kernel for the identification of dynamic response to exercise regarding the goodness-of-fit and parameter insensitivity.
- Based on the reliable experimental data acquired from twenty subjects, the dynamic models of the $\dot{V}O_2$ and $\dot{V}CO_2$ for exercise responses for both onset and offset of exercise have been identified.

- Comprehensively statistical analyses are performed to compare the dynamic characteristics of the onset and offset exercise responses for $\dot{V}O_2$ and $\dot{V}CO_2$, and several useful conclusions have been made to provide instructive guidance for the regulation of exercise intensity.

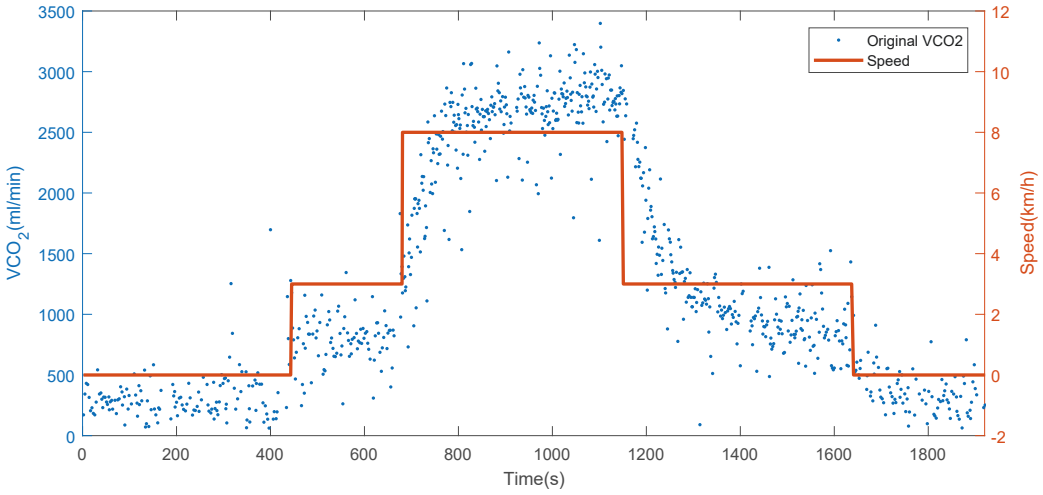

Fig. 4.1 Raw $\dot{V}CO_2$ and treadmill speed during the exercise.

4.2 Methods

According to previous studies, for the $\dot{V}O_2$ during exercise, the exponential function was applied to describe the dynamic performance [62, 76, 77]. Puente [62] demonstrated that the $\dot{V}CO_2$ could also be described by the same as:

$$\dot{V}CO_2(t) = \dot{V}CO_2^0 + R_A[1 - e^{-(t-T_D)/\tau}]. \tag{4.1}$$

where $\dot{V}CO_2(t)$ is the CO_2 output at time t, $\dot{V}CO_2^0$ is the initial value of CO_2 output, R_A is the response amplitude, T_D is the time delay, and τ is the time constant.

This function implies that Puente treated the model of $\dot{V}O_2$ response as a first-order dynamic system with constant time delay. However, for different individuals, the patterns of $\dot{V}CO_2$ responses to exercise are quite different based on our observations. Hence, the first order model would not be a good choice to use. In this study, as discussed in the introduction

section, we will adopt the non-parametric kernel-based modelling method to obtain a better result. Specifically, as one of the most commonly used non-parametric model, the finite impulse response (FIR), will be used to describe the characteristics of the system.

We first introduce the kernel-based estimation method in section 4.2.1 and then present the kernels we intend to select in section 4.2.2. The details of the experiment are presented in section 4.2.3 and the statistical methods are shown in section 4.2.4.

4.2.1 Kernel-Based Estimation Method for the Modelling of Finite Impulse Response

The data of carbon dioxide output and the speed of the treadmill are shown in Fig. 6.3, which indicates the step response of $\dot{V}CO_2$ regarding treadmill speed.

As previously mentioned, we will use non-parametric estimation based on kernel technique to build the $\dot{V}CO_2$ model for treadmill exercise. The relationship between the speed of the treadmill and the $\dot{V}CO_2$ can be considered as a single input single output (SISO) system. We consider the discrete case and assume the sampling time is t. Thus, the discrete time output calculated by impulse response can be expressed as (4.2):

$$y(t) = \sum_{\tau=0}^{\infty} u(t-\tau)g[\tau] + \varepsilon(t),\ t = 1,2,\ldots,N, \tag{4.2}$$

where $u(t)$ is the input, $y(t)$ is the output, $g(\tau)$ is the impulse response, $\varepsilon(t)$ is Gaussian white noise, and N is the total number of sampling.

The model output (predictor) is defined as:

$$P_t[g] = \sum_{\tau=0}^{\infty} u(t-\tau)g[\tau]. \tag{4.3}$$

Then the cost function regarding estimation error can be written as:

$$\hat{y}(t) = \sum_{t=1}^{N} (y(t) - P_t[g])^2. \tag{4.4}$$

In order to rewrite (4.2) in a vector form, we stack all the elements (row) in $y(t)$ and $u(t-\tau)$ to form the matrices $\boldsymbol{Y}$ and $\boldsymbol{\phi}$. Then the minimum value of the cost function can be solved by LS estimation or ML estimation. We define $g(\tau) = \boldsymbol{\theta} \in \mathbb{R}^m$, where the vector $\boldsymbol{\theta} \in \mathbb{R}^m$ contains the FIR coefficients. Then the LS estimation of the parameters $g(\tau)$ is:

$$\hat{\boldsymbol{\theta}} = \arg\min_{\boldsymbol{\theta}\in\mathbb{R}^m} \|\boldsymbol{Y} - \boldsymbol{\phi}\boldsymbol{\theta}\|^2. \tag{4.5}$$

However, the measurements of $\dot{V}CO_2$ from gas analyser contain various artifacts and are polluted by various noises. To regularise the estimation, a regularisation term can be added to (4.5). Regularisation approaches aim to put “soft" constraints on the structure $\boldsymbol{\theta}$ [57, 58]. We define $J_R(\boldsymbol{\theta})$ as the regularisation term, and it belongs to a Reproducing Kernel Hilbert Space (RKHS) $\mathscr{H}$. If we only consider FIR, the norm $\|g_{\boldsymbol{\theta}}\|_{\mathscr{H}}$ in the space $\mathscr{H}$ can be expressed via a quadratic form in (4.6), where $\boldsymbol{P}$ is a suitable kernel matrix:

$$J_R(\boldsymbol{\theta}) = \boldsymbol{\theta}^{\mathrm{T}} \boldsymbol{P}^{-1} \boldsymbol{\theta}. \tag{4.6}$$

The structure of $\boldsymbol{P}$ can account for different properties associated with prior information, which will be discussed in next subsection. The estimation of $\boldsymbol{\theta}$ can then be expressed as follow:

$$\begin{aligned} \hat{\boldsymbol{\theta}} &= \arg\min_{\boldsymbol{\theta}\in\mathbb{R}^m} \left(\|\boldsymbol{Y} - \boldsymbol{\phi}\boldsymbol{\theta}\|^2 + \gamma \boldsymbol{\theta}^{\mathrm{T}} \boldsymbol{P}^{-1} \boldsymbol{\theta} \right) \\ &= \left(\boldsymbol{P}\boldsymbol{\phi}^{\mathrm{T}}\boldsymbol{\phi} + \gamma I_m \right)^{-1} \boldsymbol{P}\boldsymbol{\phi}^{\mathrm{T}}\boldsymbol{Y}, \end{aligned} \tag{4.7}$$

where γ is a positive scalar, and $I_m \in \mathbb{R}^{m\times m}$ is an identity matrix with the dimension of $m \times m$.

4.2.2 Kernel Selection

The construction of kernel $\boldsymbol{P}$ is made up of two parts: the kernel structure design and hyper-parameter estimation. Many researchers have strived for kernel design [52–54, 67, 113]. Among them, the Stable Spline (SS) kernel, the Diagonal/ Correlated (DC) kernel, and the

Diagonal (DI) kernel have been well developed. Therefore, we select the following kernels for simulation study to achieve a better estimation of the impulse response of $\dot{V}CO_2$.

- SS kernel:

$$P(i,j) = \frac{c}{2}e^{-\beta min(i,j)} - \frac{c}{6}e^{-3\beta max(i,j)}, \tag{4.8}$$

  where $c \geq 0$, $0 \leq \beta < 1$.

- DC kernel:

$$P(i,j) = c\lambda^{\frac{i+j}{2}}\rho^{|i-j|}, \tag{4.9}$$

  where $c \geq 0$, $0 \leq \lambda < 1$, $\rho \leq 1$.

- DI kernel:

$$P(i,j) = \begin{cases} c\lambda^{i}, & \text{if} \quad i = j \\ 0, & \text{else} \end{cases} \tag{4.10}$$

  where $c \geq 0$, $0 \leq \lambda < 1$.

According to (4.1), the relationship between the CO_2 output and the treadmill speed can be approximately considered as a first order system. For this reason, we start the simulation study by using a first order system with different parameter settings. The detailed settings of the system are as follows:

$$Y(s) = \frac{K}{Ts+1}U(s), \tag{4.11}$$

where K is the steady state gain and follows the uniform distribution U(5, 15). T is the time constant and follows U(15, 25).

A step function is selected as the input $u(t)$, and the simulated output $y(t)$ is polluted by a Gaussian white noise with 1 dB Signal-Noise Ratio (SNR). The sampling time is selected as 1 second. The input $u(t)$ and output $y(t)$ of the simulated system are shown in Fig. 4.2.

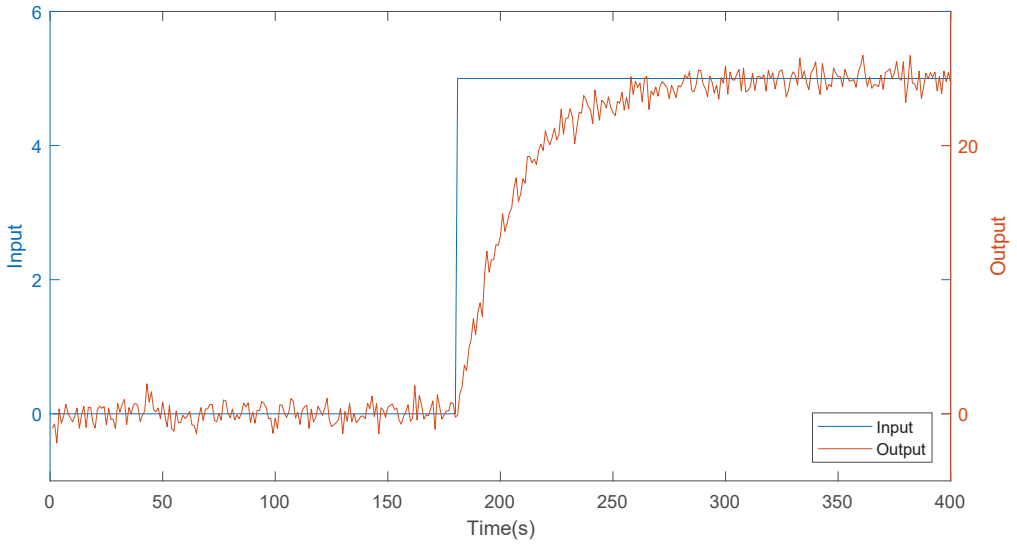

Fig. 4.2 An input and output pair of the simulated system.

4.2.3 Experiment

20 untrained healthy male subjects were asked to run on the treadmill. During the exercise, all data including $\dot{V}CO_2$ and $\dot{V}O_2$ are collected by a portable gas analyser-K4B2. The UTS Human Research Ethics Committee (UTS HREC 2009000227) had approved this experiment and the informed consent from all participants before the commencement of data collection was obtained. The statistical physical information of the participants is shown in Table 4.1.

Table 4.1 Information about the subjects

Information	Age($year$)	Height(cm)	Weight(kg)
Mean	46.4	176.6	91.2
Standard Deviation	5.68	4.40	11.37

Before the experiment, the subjects were asked to sit for five minutes and then stand for two minutes. The physical conditions and the environment settings were standardised for all participants. During the exercise, the participants first were walking at 3 km/h for four minutes and then running at 8 km/h for eight minutes followed by walking at 3 km/h for eight minutes before stopping. To exclude the impact of the subjects' weight on $\dot{V}CO_2$ and $\dot{V}O_2$, the $\dot{V}CO_2$ and $\dot{V}O_2$ were both divided by the weight (Kg) of each subject. The normalized $\dot{V}CO_2$ and $\dot{V}O_2$ are recorded as $\dot{V}_dCO_2$ and $\dot{V}_dO_2$.

4.2.4 Statistic

- The term “Time Index" as a reflection of response speed is introduced, which indicates the time when the output reaches the 75% of maximum.
- The *histogram* and *normal probability* are plotted in Matlab to present whether the gain and Time Index follow a normal distribution or not. *Paired T*-test is used for the one which follows and *Rank Sum* test is used for the one which does not follow. Generally, $P < 0.05$ was considered as statistically significant. Where $h = 0$ means we cannot determine the size of the two sets of data by mean value because the distinction is small. Meanwhile, the mean value can be used to make the comparison when $h = 1$ because the distinction is significant.
- The *correlation coefficient* between the estimated $\dot{V}_dCO_2$ and $\dot{V}_dO_2$ is calculated in order to know about the correlation between them. Normally, if the correlation coefficient is between ± 0.80 to ± 1.00, the two variables are highly correlated.
- We calculated the difference of Time Index ($\dot{V}_dCO_2$ minus $\dot{V}_dO_2$) in two periods to show whether it is all positive or not.

4.3 Results

In this section, we first present the simulation and kernel selection result in section 4.3.1. Then the modelling result for the onset and offset period is represented respectively in section 4.3.2 and 4.3.3. The IR and estimated $\dot{V}_dCO_2$ of both periods are also shown. Furthermore, we develop the comparison of onset vs offset and $\dot{V}_dCO_2$ vs $\dot{V}_dO_2$ from the aspect of the impulse response, step response and estimated output in section 4.3.4 and 4.3.5. Different statistic methods are employed for the analysis.

4.3.1 Simulation and Kernel Selection

At first, we use the LS method without kernel technique to perform the identification. The identified impulse response (IR) of the system is shown in Fig. 4.3. We can observe that

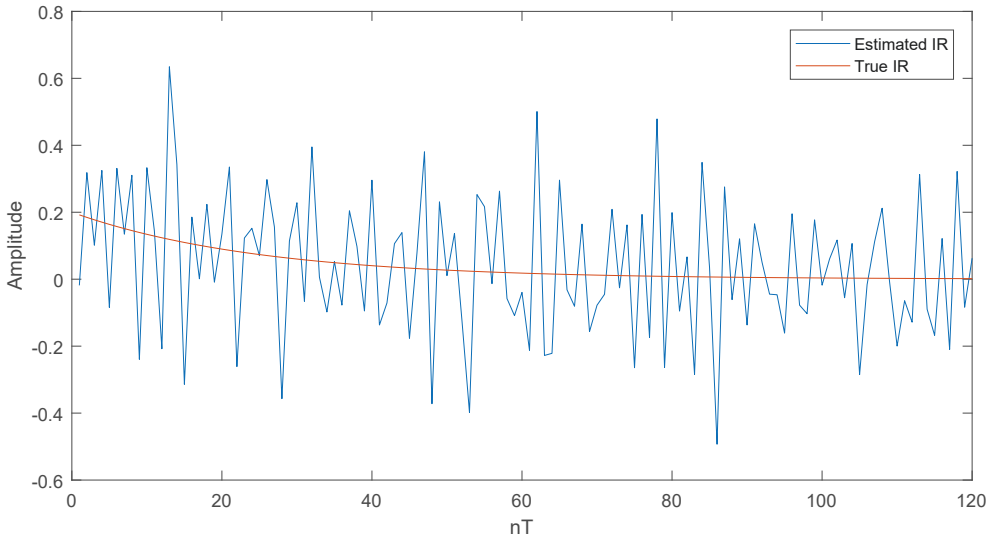

Fig. 4.3 The estimated IR by using the classical LS estimation.

the estimation error is big in the sense that the noise is amplified. Next, we will show the effectiveness of the kernel-based regularisation method. Then, we try to select the best parameters for each kernel and compare the sensitivity to parameters of the three kernels. The results are shown in Fig. 4.6.

After that, we tune the parameters partially according to the constraints introduced in [58] and make the final choice by the best results in our simulation. The selected optimal parameters of the kernels and the regulariser are listed below [52–54, 67, 113].

- SS kernel: $c = 1, \beta = 0.987$.
- DC kernel: $c = 0.3, \lambda = 0.999, \rho = 0.999$.
- DI kernel: $c = 0.3, \lambda = 0.95$.
- Regulariser: $\gamma = 4$.

We make a comparison between the true IR and the estimated IR based on the above-listed kernels. As we can see, the IR from SS kernel is closer to the true value compared to the others. At the same time, we compare the estimated output and the true output. We carry out the simulation for 20 times. One of the simulation results about IR and estimation is shown in Fig. 4.4.

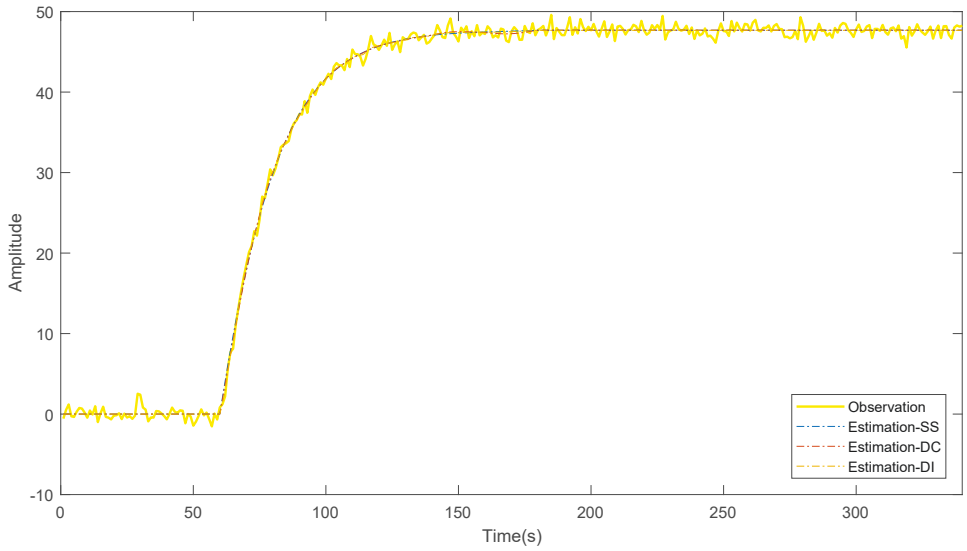

Fig. 4.4 Observation and estimation of three types kernels.

The goodness-of-fit of the estimated output is calculated by the fit ratio NRMSE (normalised root mean square error) which is defined as:

$$\text{Fit Ratio} = \left(1 - \frac{||\hat{Y}_N - Y_N||}{||Y_N - \text{mean}(Y_N)||}\right). \tag{4.12}$$

The averaged results are shown as follows and the simulation result is shown in Fig. 4.5.

- SS kernel: Average fit=0.9395.
- DC kernel: Average fit=0.9439.
- DI kernel: Average fit=0.9547.

Regarding the goodness-of-fit, the kernel-based methods outperformed the classical LS estimation. The three kernels have a similar fitness because the mean value of their fitness are between 0.93-0.96. Thus, we applied T-test to verify the significant difference of the goodness-of-fit. All the results show that $p < 0.0001$ which indicate they are of significant difference. That means the influence of different kernels on the results is significant. We could observe from the IR in Fig. 4.6 that the DI and DC kernel is over-fitted although they have a higher fitness. Moreover, the SS kernel has a more smooth IR and less sensitivity to the parameter. Thus, we choose the SS kernel to get a better IR estimation.

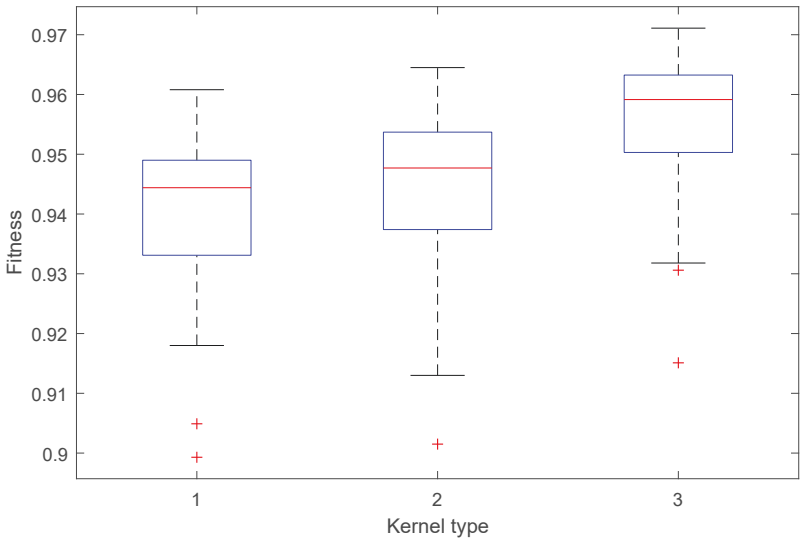

Fig. 4.5 Box plots of the estimations by using the SS, DC, DI kernels (from left to right).

4.3.2 Modelling of Onset Period

In this part, we selected the data from $t_1 = 501s$ to $t_2 = 900s$ (see Fig. 4.1) for the modelling of onset impulse response. The sampling rate of the $\dot{V}_dCO_2$ is irregular since the gas response recorded by K4B2 is breath by breath based. Thus, the raw data of $\dot{V}_dCO_2$ and $\dot{V}_dO_2$ have been interpolated and filtered by a median filter. For the recorded 400 observations, to remove the offset, the average value of the onset period for the initial 150 data is deducted. The order of the impulse response model is selected as 400.

The IR model can be expressed as:

$$\begin{aligned} y[n] &= g[1]u[n-1] + g[2]u[n-2] + \ldots + g[400]u[n-400] \\ &= \sum_{i=1}^{400} g[i]u[n-i]. \end{aligned} \tag{4.13}$$

After the pre-processing, we apply the kernel-based estimation method to estimate the IR model by using the SS kernel ($c = 1, \beta = 0.987, \gamma = 200$) as introduced in Section 4.2.

For the onset period of the treadmill exercise, the estimated impulse response of all participants (dotted line) and the average IR (bold line) are shown in Fig. 4.7.

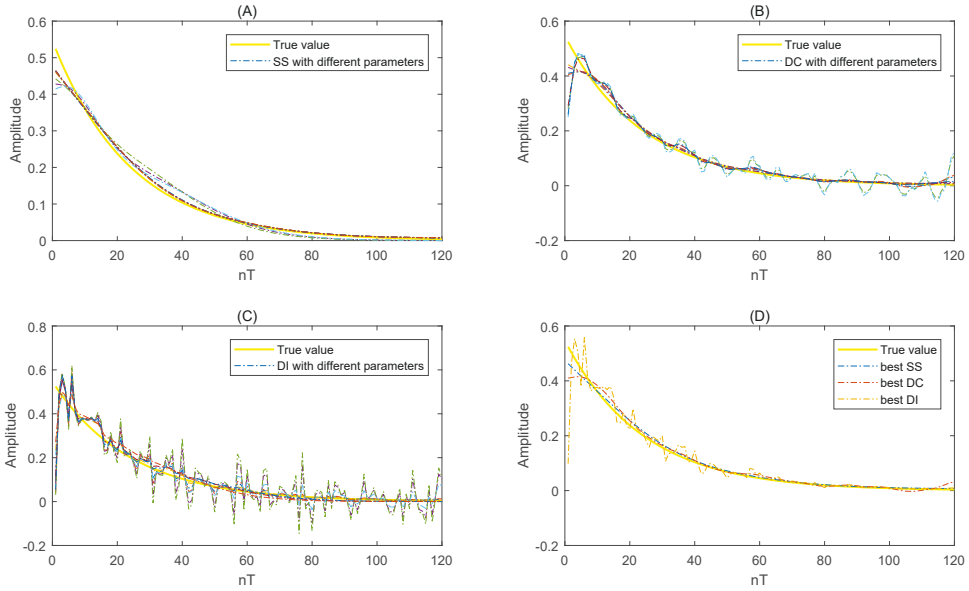

Fig. 4.6 Comparison results of the kernel with different parameters: (A) SS kernel with different parameters. (B) DC kernel with different parameters. (C) DI kernel with different parameters. (D) The comparison of the three kernels with well selected parameters and true IR.

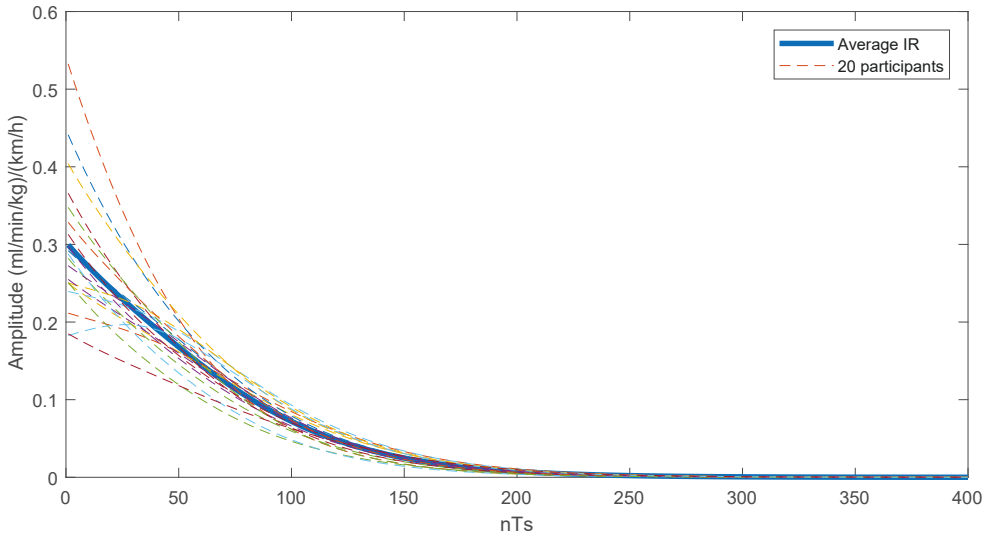

Fig. 4.7 Average IR and individual IR from 20 participants during the onset period of treadmill.

The response patterns are similar for most participants, but the individual differences do exist, which indicate that simply use of a first order model is not sufficient to describe

the dynamic response of $\dot{V}_dCO_2$. This is actually an advantage of adopting non-parametric modelling approach. The predicted $\dot{V}_dCO_2$ output marked (bold line) are compared with the measured $\dot{V}_dCO_2$ of each participant (dotted line) as shown in Fig. 4.8.

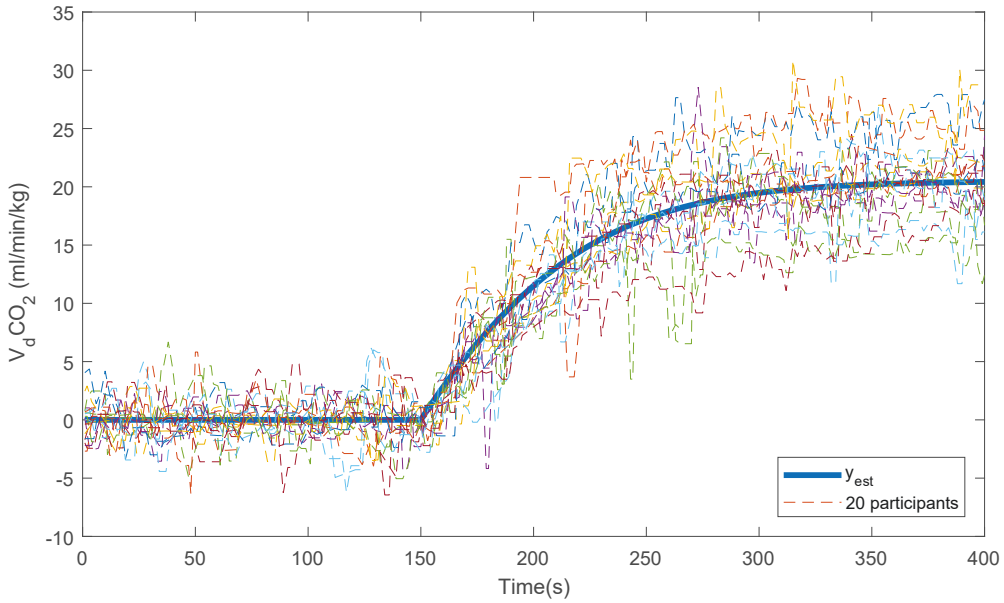

Fig. 4.8 Comparison between estimated $\dot{V}_dCO_2$ and measurements from 20 participants during the onset period.

It can be seen that the estimation fits well with the actual measurements regarding high goodness-of-fit.

4.3.3 Modelling of Offset Period

We select the data from t_1=901s to t_2=1300s for the modelling of offset period. Similar to the onset period, the original data are interpolated and filtered. The average value of the offset period for the initial 150 data is removed. The sampling time and the order of the impulse response model are selected as those of onset. The parameters of the kernel are also the same. The estimated impulse response of all participants (dotted line), as well as the, averaged IR (bold line) is shown in Fig. 4.9.

Again, most participants have a similar IR pattern, but some of them have a pattern which is quite different with the response of a first order system. The predicted $\dot{V}_dCO_2$ output (bold line) and the actual $\dot{V}_dCO_2$ of each participant (dotted line) are shown in Fig.4.10.

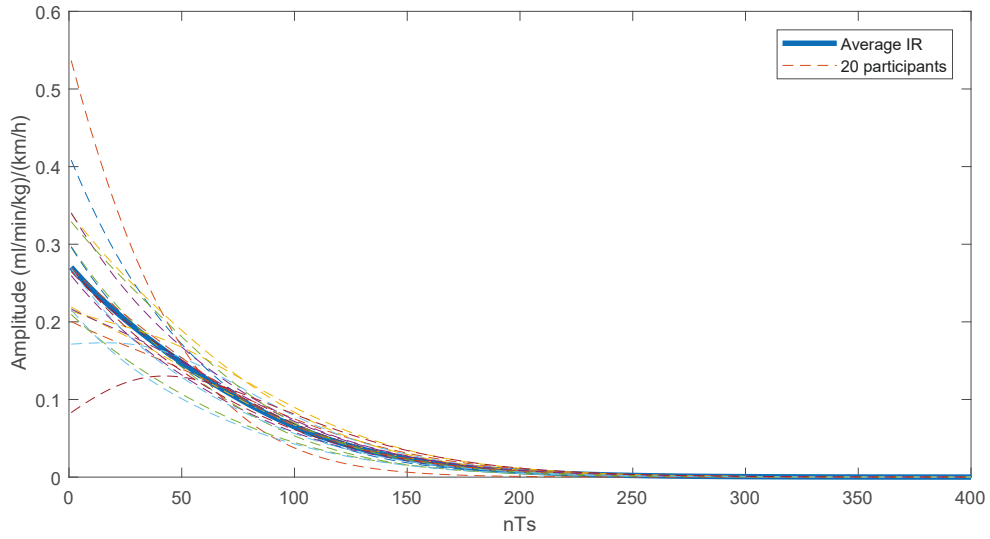

Fig. 4.9 Average IR and individual IR from 20 participants during the offset period of treadmill.

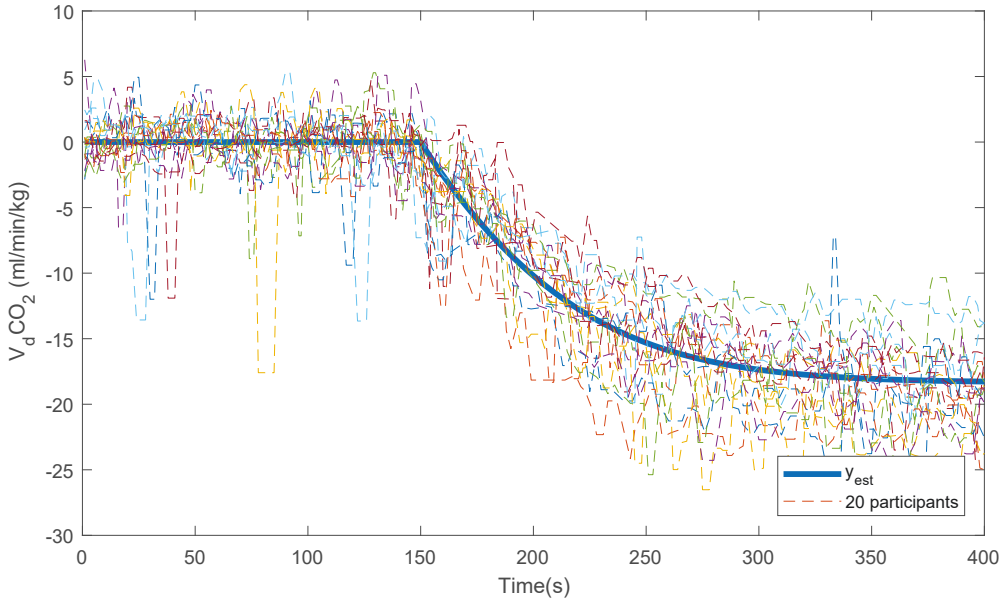

Fig. 4.10 Comparison between estimated $\dot{V}_d CO_2$ and measurements from 20 participants during the offset period of the treadmill.

4.3.4 Comparison between Onset and Offset Period

To see this difference in the response speed, we normalized the averaged estimation of $\dot{V}_dCO_2$ in onset and offset period, which is shown in Fig. 4.11.

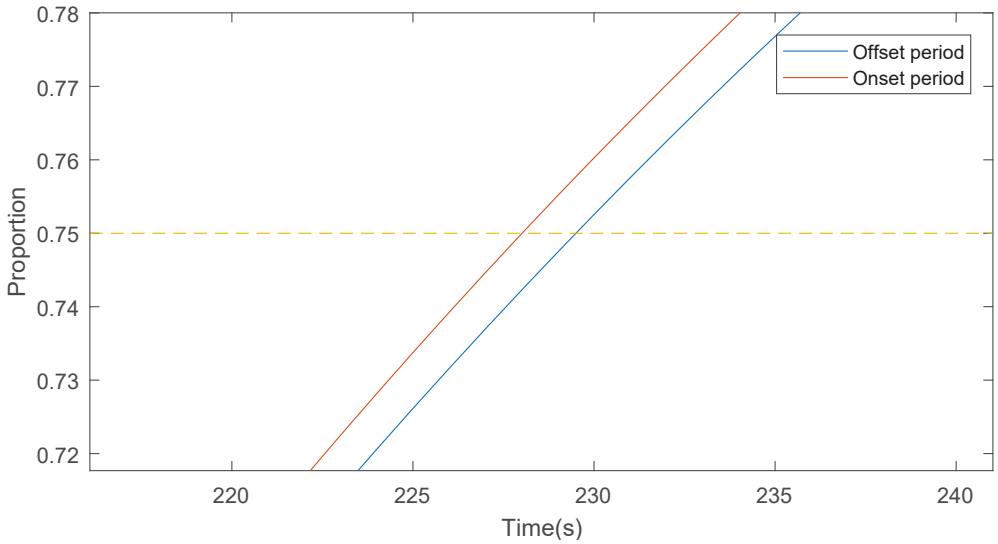

Fig. 4.11 The normalization of $\dot{V}_dCO_2$ in onset and offset period (Partial magnification).

To show the transient behaviors, e.g., the response time, the Step Response (SR) of each participant and the averaged SR are plotted both in onset and offset period. From the comparison of the average IR and SR between onset and offset period in Fig. 4.12, we find that the gain of the onset period is bigger than that of the offset. Meanwhile, the response speed for the IR and SR of the two periods are slightly different.

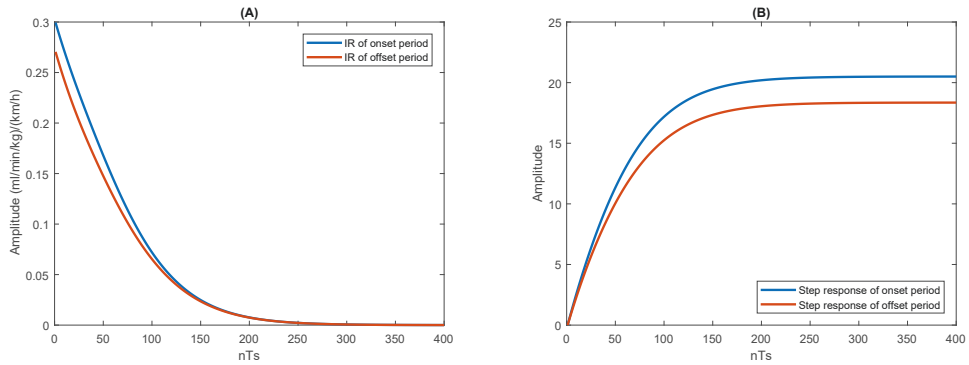

Fig. 4.12 Comparison between average IR and SR of $\dot{V}_dCO_2$ in onset period and offset period.

For a thorough individual analysis, we plot the gain and “Time Index" of each participant which is shown in Fig. 4.13.

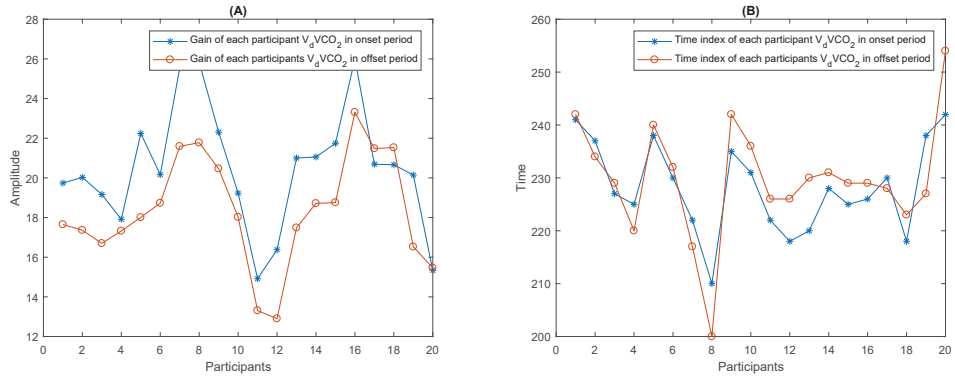

Fig. 4.13 The comparison of individual gain(A) and Time Index(B) of $\dot{V}_dCO_2$ in onset and offset.

The *histogram* and *normal probability* plotted in Matlab indicate that the individual Time Index follows the normal distribution while the individual gain does not strictly follow. Thus we applied *Paired* T-test for individual Time Index and test for individual gain using Matlab. The outcomes of the paired T-test and Ranks Sum test for Time index and Gain about $\dot{V}_dCO_2$ in onset and offset are shown in Table 4.2.

Table 4.2 The statistic test outcome of $\dot{V}_dCO_2$ in onset and offset

Item	Paired T-test	Rank sum test
Time Index	h=0, p=0.2539	–
Gain	–	h=1, p=0.0411

According to the outcomes (i.e. Table 4.2), the Time Index of onset and offset shows no significant difference. Jerzy’s research [76] reported a similar result about $\dot{V}O_2$. For the steady-state gain, we can compare the mean value of 20 participants, 20.50 for onset and 18.35 for offset. Compared to the offset period, the higher gain in the onset period indicates a higher ratio between output and input. In other words, the results of our study show that for the same speed change, human body exhales out more CO_2 in the onset than offset. We will give a detail explanation in the next section. Hunt’s research in Heart Rate (HR) modelling and control [8] also drew a similar conclusion for HR response.

4.3.5 Comparison of $\dot{V}_dCO_2$ and $\dot{V}_dO_2$

Various comparisons, including IR, SR, and estimated output for $\dot{V}_dCO_2$ and $\dot{V}_dO_2$, for both onset period and offset period, are shown in Fig. 4.14 and Fig. 4.15, where clearly show that the changing of carbon dioxide is dynamically correlated to the changing of oxygen, during onset and offset exercise.

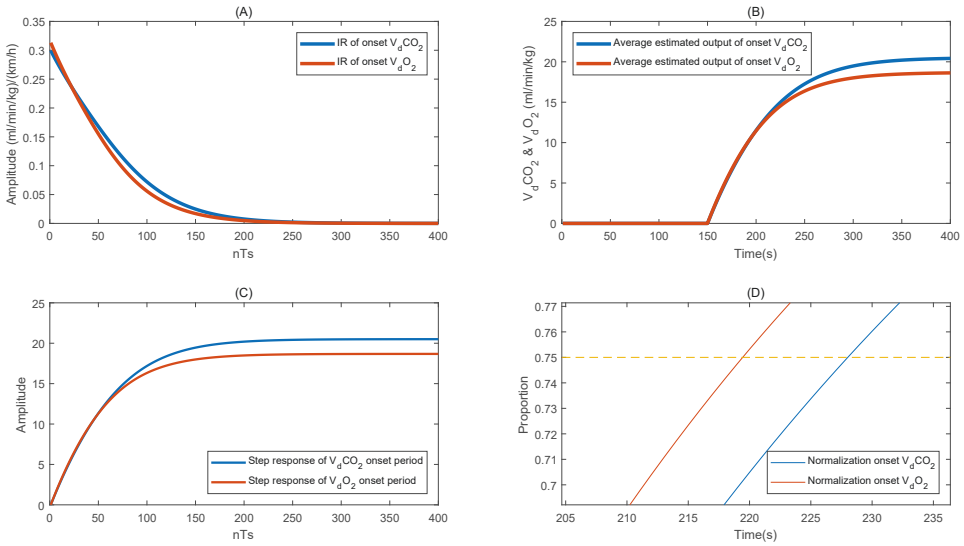

Fig. 4.14 (A)Comparison between average IR of $\dot{V}_dCO_2$ and $\dot{V}_dO_2$ during onset period. (B)Comparison between average estimation output of $\dot{V}_dCO_2$ and $\dot{V}_dO_2$ during onset period. (C)Comparison between average SR of $\dot{V}_dCO_2$ and $\dot{V}_dO_2$ during onset period. (D)The normalization of estimated $\dot{V}_dCO_2$ and $\dot{V}_dO_2$ in onset period (Partial magnification).

As the calculated correlation coefficient is 0.9991 in onset period and 0.9990 in offset period respectively, the high correlation between these two variables can be confirmed.

That means in some cases, the $\dot{V}_dO_2$ can be approximately estimated by $\dot{V}_dCO_2$, even in the transient period, or vice versa. This may be helpful to simplify the experimental procedure, as well as to reduce the cost of equipment maintenance. For example, for the gas collection during the experiment, it is often the case that the assessment of the exhaled gas components (with more carbon dioxide) is simpler than that of the inhaled gas (with more oxygen), i.e., the measurement of carbon dioxide output is more convenient than that of oxygen uptake. Then, if it is necessary, the measurement of $\dot{V}_dO_2$ can be bypassed, but estimated by using $\dot{V}_dCO_2$ instead to reduce the cost.

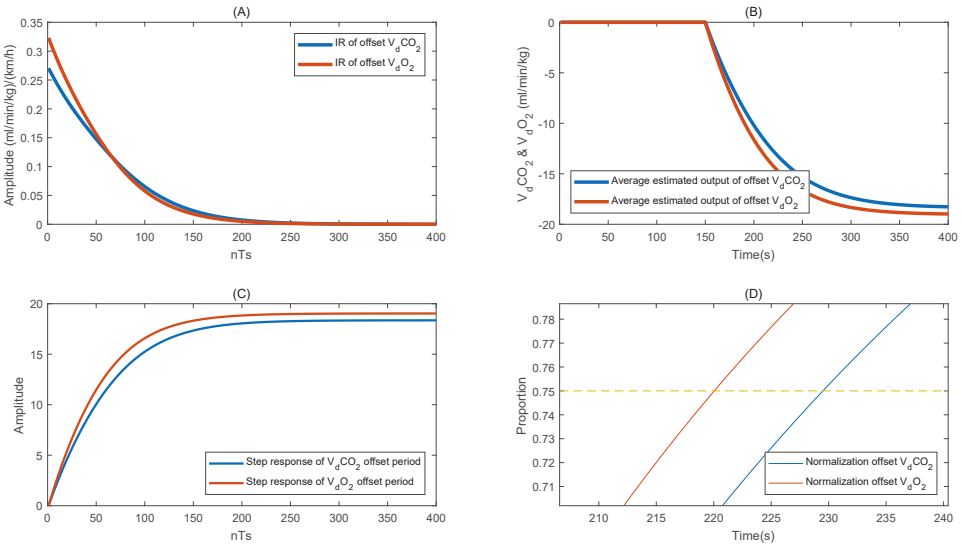

Fig. 4.15 (A)Comparison between average IR of $\dot{V}_dCO_2$ and $\dot{V}_dO_2$ during offset period. (B)Comparison between average estimation output of $\dot{V}_dCO_2$ and $\dot{V}_dO_2$ during offset period. (C)Comparison between average SR of $\dot{V}_dCO_2$ and $\dot{V}_dO_2$ during offset period. (D)The normalization of estimated $\dot{V}_dCO_2$ and $\dot{V}_dO_2$ in offset period (Partial magnification).

To show interpersonal differences, the gain and Time Index of each participant in onset and offset period are shown in Fig. 4.16 and Fig. 4.17. The histogram and normal probability of them are plotted in Matlab to decide which test methods will be applied.

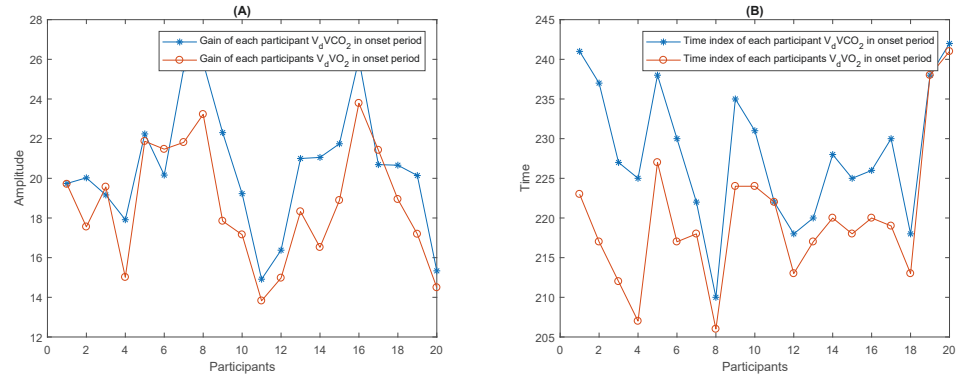

Fig. 4.16 The comparison of individual gain (A) and Time Index (B) between $\dot{V}_dCO_2$ and $\dot{V}_dO_2$ in onset.

Similar to the last subsection, we applied Paired T-test for individual Time Index and Rank Sum test for individual gain (using Matlab) according to whether they follow the normal distribution or not. The outcomes are shown in Table 4.3 and Table 4.4.

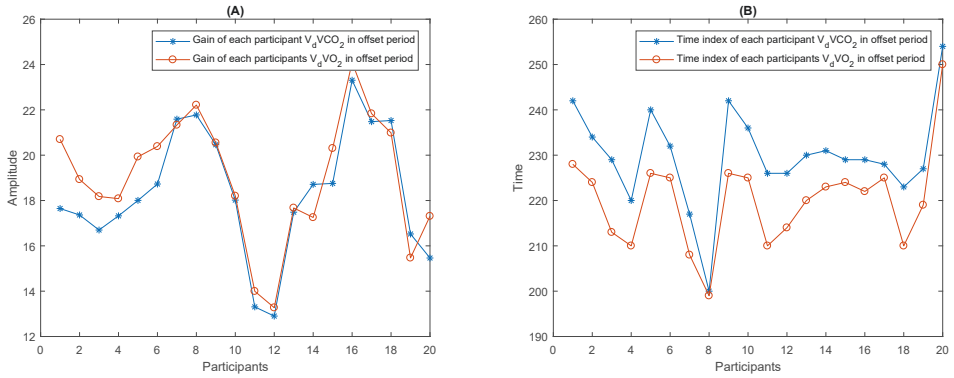

Fig. 4.17 The comparison of individual gain (A) and Time Index (B) between $\dot{V}_dCO_2$ and $\dot{V}_dO_2$ in offset .

According to the above outcomes, the gain of $\dot{V}_dCO_2$ and $\dot{V}_dO_2$ in both periods shows no significant difference. Then for the Time Index of the two periods, we can compare the mean value of 20 participants, 228.15 for $\dot{V}_dCO_2$ and 219.80 for $\dot{V}_dO_2$ in onset; 229.75 for $\dot{V}_dCO_2$ and 220.05 for $\dot{V}_dO_2$ in offset. It indicates that the $\dot{V}_dO_2$ shows a quicker response speed in both periods.

To further verify the conclusion, the difference of Time Index ($\dot{V}_dCO_2$ minus $\dot{V}_dO_2$) in two periods are calculated. As the differences are all positive, it further validated the conclusion.

Table 4.3 The statistic test outcome of $\dot{V}_dCO_2$ and $\dot{V}_dO_2$ in the onset

Item	Paired T-test	Rank Sum test
Time Index	h=1, p=6.96×10^{-6}	–
Gain	–	h=0, p=0.0720

Table 4.4 The statistic test outcome of $\dot{V}_dCO_2$ and $\dot{V}_dO_2$ in the offset

Item	Paired T-test	Rank Sum test
Time Index	h=1, p=6.54×10^{-6}	–
Gain	–	h=1, p=0.3942

4.4 Discussion

In this section, we attempt to explain the results from a physiological point of view. The explanation about the similarity and difference between onset vs. offset and $\dot{V}_dCO_2$ vs. $\dot{V}_dO_2$ are illustrated respectively in Subsection 4.1 and 4.2.

Aerobic respiration produces carbon dioxide and water, resulting in the releasing of energy and generating large amounts of Adenosine Triphosphate (ATP, also known as adenine nucleoside triphosphate). ATP transports chemical energy within cells for metabolism. Under normal circumstances, only considering the case of glucose for energy, in aerobic breathing, the product is carbon dioxide and water. The total reaction of aerobic respiration is shown in Eq. (4.14). The concept of Respiratory Quotient [114] (referred as RQ or R, the $\dot{V}CO_2$ divided by $\dot{V}O_2$ in local tissue) was presented, which is equal to 1 when glucose is the only available source for energy according to Eq. (4.14). Every litre of oxygen will produce one litre of carbon dioxide and the volume ratio of carbon dioxide and oxygen is 1 [115, 116]:

$$\begin{aligned} &C_6H_{12}O_6 + 6O_2 + 6H_2O \overset{enzyme}{\longrightarrow} \\ &6CO_2 + 12H_2O + large\ amount\ of\ energy. \end{aligned} \tag{4.14}$$

Based on the above background about aerobic respiration, the results and their physiological explanations are summarized as follows.

4.4.1 Comparison between Onset and Offset Period of $\dot{V}_dCO_2$

- The Time Index of $\dot{V}_dCO_2$ in onset is similar to offset and the gain of $\dot{V}_dCO_2$ in onset is bigger than offset.

As we observed, for the same speed change, the carbon dioxide output in onset is more than offset. The reason behind this observation is the fact that ATP is the “molecular currency" for intracellular energy transfer, storage as well as transfer chemistry energy. With the increasing of the exercise intensity, the human body has to consume more ATP in onset period than that of in offset period. Human body provides ATP and produces carbon dioxide

by respiration. Thus, the participants produce more carbon dioxide in onset period than offset for the same speed changing rate. This observation is also related to the “oxygen debt" [65, 82, 117], which is first proposed by Hill [16]. The “debt” occurs during the onset period because the stored credits are expended.

4.4.2 Comparison of $\dot{V}_dCO_2$ and $\dot{V}_dO_2$

- Similarity: The $\dot{V}_dCO_2$ and $\dot{V}_dO_2$ are significantly related, and the gains of $\dot{V}_dCO_2$ and $\dot{V}_dO_2$ are similar in both periods.

The similar gain and correlation coefficient of $\dot{V}_dCO_2$ and $\dot{V}_dO_2$ also work in concert with the respiration formula as Eq. (4.14).

- Difference: The Time Index of $\dot{V}_dCO_2$ is bigger than that of $\dot{V}_dO_2$ in both periods, so the $\dot{V}_dO_2$ shows a quicker response speed.

The different Time Index means a different gas delivery rate. The Fig. 3 in Williams’s research [80] shows the same result. For their half-time constant, oxygen uptake is smaller than carbon dioxide elimination. This is also related to the O_2 debt and excess CO_2 and respond to the Subsection 4.1. The Fig. 2 of Karlman’s research [82] also shows that the R is over 1 which is same to our results and explain it by a buffer system.

4.5 Conclusion

This study investigates the onset and offset dynamics of cardiorespiratory response to treadmill exercise. In order to detect the characteristic differences during onset and offset exercise, a recently developed non-parametric modelling method based on l^2-norm kernel regularisation has been applied to identify the impulse responses of the carbon dioxide output ($\dot{V}_dCO_2$) and oxygen uptake ($\dot{V}_dO_2$) responses. By well-designed kernel-based regularisation term, this approach can handle the data with short records and low SNR (Signal-to-Noise-Ratio), and orderly fit the experimental data. In terms of the fitness for the experimental data from twenty healthy subjects, the stable spline (SS) kernel achieves a reliable estimation of the

impulse response for both $\dot{V}_dCO_2$ and $\dot{V}_dO_2$. Based on the identified impulse response model, various statistical comparisons are developed and the comparison results are explained from physiological perspective. The bigger gain of $\dot{V}_dCO_2$ in onset demonstrates the human's ATP storage during the relaxing status. Meanwhile, the quicker response speed of $\dot{V}_dCO_2$ in both periods explains why there is a delay due to the conversion from O_2 to CO_2. We believe the kernel-based non-parametric modelling approach together with the developed impulse response models will significantly improve our understanding of human cardiorespiratory response to exercise, and provide instructive guidance for the regulation of exercise intensity to ensure the efficiency and safety during training and rehabilitation exercise.

Chapter 5

Non-Parametric Dynamical Model of Cardiorespiratory Responses of Stairs Exercise

5.1 Introduction

Aerobic exercise is a type of exercise performed at a moderate level of intensity for an extended period of time. Among the various forms of aerobic exercise, the interval training exercise, e.g., the ascending-descending switching exercise, is one of the most commonly used protocols for trainers seeking to enhance cardiovascular fitness. The regular stairs exercise is a proper method to demonstrate the effects of the interval training exercise owing to several advantages. These include improving cardiovascular fitness, consuming calories, convenience and low-cost [4–6]. The intensity of the stairs exercise can be adjusted by the exercise phase (ascending or descending) without causing any discomfort to the participants [7]. Portable sensors enable us to conveniently measure the Heart Rate (HR) of participants in order to ensure that the exercise is conducted under aerobic conditions [7, 9, 10]. The respiratory information, such as voluntary ventilation, oxygen uptake ($\dot{V}O_2$) or carbon dioxide output ($\dot{V}CO_2$), is also commonly used to assess the metabolism demands [62, 63, 69–71]. In addition, unlike HR, the respiratory information is not affected by the participants' emotion and hence a more accurate assessment result is guaranteed. The Maximum Heart Rate

(HR_{max}) is the highest HR that an individual can achieve without causing severe problems through exercise stress [10]. Considering the linear relationship between the HR and $\dot{V}O_2$, HR_{max} [11, 12] has been recognised as an indicator to detect the exercise intensity [13]. One representative formula of HR_{max} is introduced in Robert's research [78] as shown in Eq. (6.3):

$$HR_{max} = 205.8 - 0.685 \times age, \tag{5.1}$$

where, *age* indicates the age of the participant.

For the past four decades, $\dot{V}O_2$ and $\dot{V}CO_2$ have been measured at various sports laboratories by the means of the gas analyser [14, 100]. The energy consumption, HR, $\dot{V}O_2$ and $\dot{V}CO_2$ keeps increasing until participants reach the peak level in terms of going upstairs (ascending). When going downstairs (descending), these figures decrease to form a valley [7]. The phase of the stairs exercise (ascending or descending) can be considered as a square signal if we describe the ascending and descending as two numerical indicators. The above physiological signals, such as HR, $\dot{V}O_2$ and $\dot{V}CO_2$, change with the phase. This means that the human cardiovascular system can be described as a dynamic model wherein the input is the phase and the output is the physiological signal.

One of the challenges for the modelling of the human physiological variable is the fact that the stimulation of the input is often limited. This prevents the use of models with high-dimensional parameters, as they usually lead to ill-posed inverse problems. Recently, the intrinsical ill-posed problem is circumvented with kernel-based regularisation methods, which also admit a Bayesian interpretation. In particular, a non-parametric modelling approach is proposed, in which the impulse response is modelled as a zero-mean Gaussian process. In this way, prior information is introduced in the identification process by assigning a kernel covariance [52, 53, 57]. When the structure of the system cannot be determined or it is too complicated to be described by a simple parametric model, the non-parametric modelling method is the preferable choice [55, 56]. Furthermore, the development of the wearable equipment, such as the $K4b^2$, makes it possible to record large amounts of data compared to the limited amount of data that was recorded in the past. The traditional modelling method achieves good fitness with a limited amount of data, while the non-parametric model accommodates a large dataset. The non-parametric model with the kernel-based regularisation approach has been applied by several researchers to system identification

with different demands [54, 58, 60]. This has achieved high accuracy and robust system identification when it has been applied to the dynamics of physiological information responses to the exercise phase within a well-designed kernel strategy and regularisation term.

Our study focuses on the dynamic relationship between the exercise phase and the $\dot{V}O_2$. The non-parametric model has been applied due to the uncertain structure of the model. Different types of fixed-order models have been used for the purpose of comparison. The continuously changing protocol for the stairs exercise provides more stimulation for the system, utilised as prior information for the tuning of the kernel covariance. The results demonstrate that the non-parametric model could achieve better performance under different conditions, i.e. different exercise phases and different participants. The identification results from the non-parametric model display a consistently high level of accuracy, and this illustrates that the non-parametric model is compatible. The variant structure of the phase-oxygen uptake system is also demonstrated. In addition, experimental results justify the conclusion that has been drawn.

The remainder of this work is organized as follows. Section 5.2 introduces the non-parametric model with the kernel-based regularisation, the experiment, the pre-processing and verification approach. The identification and comparison results are presented in Section 5.3. Then, we analyse and discuss the results in Section 5.4. Finally, the conclusion is drawn in Section 5.5.

5.2 Methods

5.2.1 Experiment

During the stairs exercise experiment, 10 participants' exercise information, including HR and exercise phase (ascending or descending), is collected by a self-designed mobile phone application. In addition, the physiological information is collected by the portable gas analyser-Cosmed $K4b^2$ (Cosmed, Italy) [118]. The scenario of the experiment, the $K4b^2$ and the interface of the self-developed mobile phone application are shown in Fig. 5.1. The UTS Human Research Ethics Committee (UTS HREC 2009000227) approved these experiments

and informed consent was obtained from all participants before commencement of data collection.

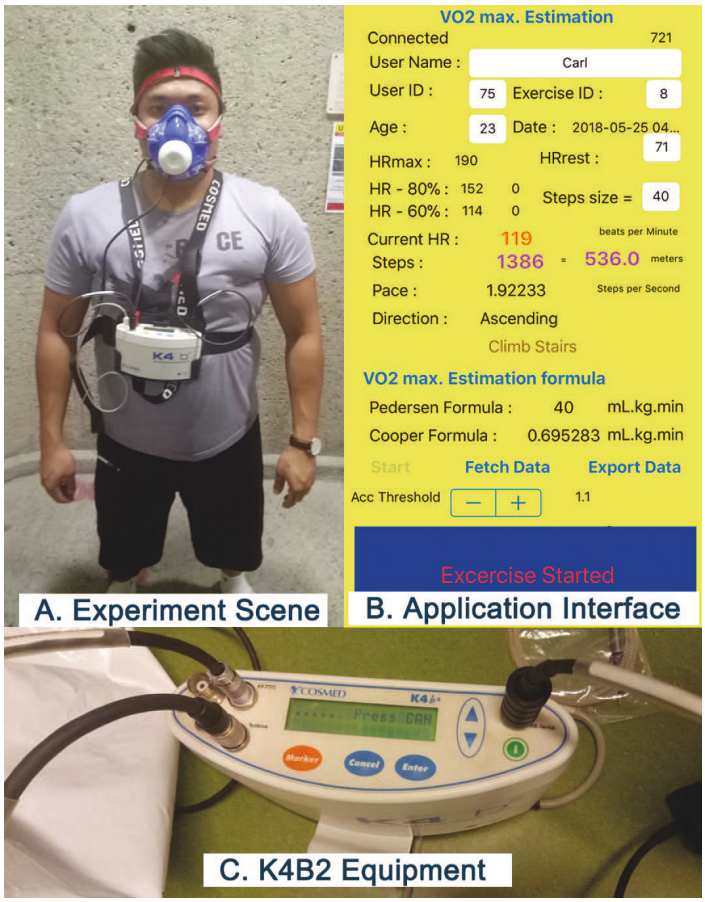

Fig. 5.1 The Scene, Application Interface and Equipment of the Stairs Experiment.

The mobile phone is placed on the ankle of participants during going upstairs and downstairs. The exercise phase is acquired from the measurements of the Inertial Measurement Unit (IMU) data. During the exercise, ten untrained (non-athletes) and healthy (no records of motor skill disorder, cardiac-respiratory disorder or related medications history) are instructed to maintain their HR within the range from 60% to 80% of their HR_{max}. When their HR starts to exceed 80% of HR_{max} during the ascending phase, the participants are instructed to go downstairs. Once their HR is below 60% of HR_{max} during the descending phase, the participants are instructed to go upstairs. The range of the HR guarantees the exercise is in an aerobic circumstance and the model will not change dramatically and stay in a linear range. Also, this protocol ensures that all the physiological signals are constantly and randomly changing without the participants feeling uncomfortable. Meanwhile, the

respiration data, such as $\dot{V}O_2$ and $\dot{V}CO_2$, are collected by the portable gas analyser-$K4b^2$ during the participants' stairs exercise. Each experiment lasts 12 minutes. An entire period during the exercise is defined as from the beginning of the ascending period to the end of the descending period. In that case, most participants completed the experiment within two to four periods in around 12 minutes. The statistical physical information of the participants is shown in Table 5.1.

Table 5.1 Information about the Participants (n=10)

Information	Age($year$)	Height(cm)	Mass(kg)	HR_{max}	$60\%HR_{max}$	$80\%HR_{max}$
Mean	26.2	171.2	83.6	187.8	112.6	150.2
Standard Deviation	6.75	0.42	2.95	4.64	2.95	3.79

The $\dot{V}O_2$ is divided by the mass (kg) for each participant to exclude the impact of the participant's mass on breath information. The normalized $\dot{V}O_2$ are recorded as $\dot{V}_dO_2$. The phase of the exercise is described as 2 when the participants are ascending (go upstairs) and as 1 when descending (go downstairs). The phase and measured ($\dot{V}_dO_2$) of one representative participant are shown in Fig. 5.2.

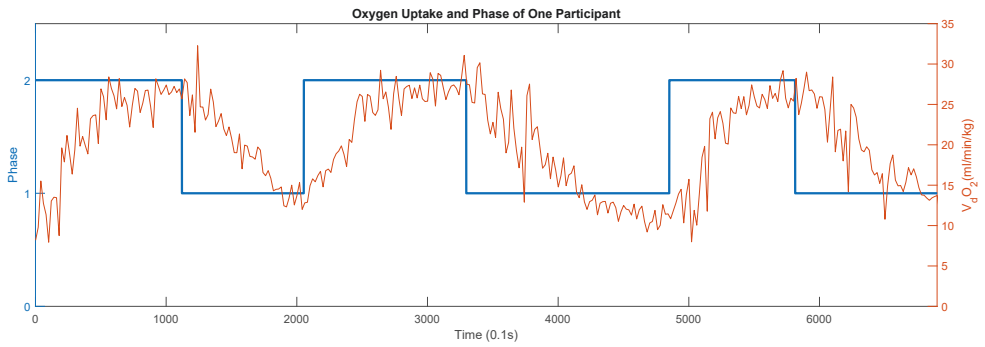

Fig. 5.2 Measured $\dot{V}_dO_2$ and Exercise Phase of One Participant during Stairs Exercise.

5.2.2 Kernel-based Non-parametric Modelling

The kernel-based non-parametric estimation method introduced in the Chapter 4 is also applied to build the phase-$\dot{V}O_2$ model in this part of work. Similarly, the relationship between exercise phase (input) and $\dot{V}_dO_2$ (output) is described as a single input single output (SISO) system. The exercise phase which varies between ascending and descending could be

considered as a square input. The output can be calculated by impulse response. Accordingly, the matrix form to describe the system can be written as an FIR model:

$$\boldsymbol{Y} = \boldsymbol{\phi}\boldsymbol{\theta} + \boldsymbol{\varepsilon}. \tag{5.2}$$

where $\boldsymbol{\phi}$ is the input, $\boldsymbol{Y}$ is the output, $\boldsymbol{\varepsilon}$ is the Gaussian white noise, and the vector $\boldsymbol{\theta} \in \mathbb{R}^m$ contains the Finite Impulse Response (FIR) coefficients.

The estimation of $\boldsymbol{\theta}$ can be solved by LS estimation as [57]:

$$\hat{\boldsymbol{\theta}} = \arg\min_{\boldsymbol{\theta}\in\mathbb{R}^m} \|\boldsymbol{Y} - \boldsymbol{\phi}\boldsymbol{\theta}\|^2. \tag{5.3}$$

As the input of this system is a square signal, and therefore the above equation could be inappropriate for modelling the $\dot{V}_dO_2$ impulse response (especially when m is big). Often the measurements of $\dot{V}_dO_2$ contain various artifacts. In order to regularise the estimation and guarantee the validity of the obtained model, the regularisation term $J_R(\boldsymbol{\theta})$, which belongs to a Reproducing Kernel Hilbert Space (RKHS) $\mathscr{H}$, is also added to Eq. (5.3):

$$J_R(\boldsymbol{\theta}) = \boldsymbol{\theta}^{\mathrm{T}}\boldsymbol{P}^{-1}\boldsymbol{\theta}, \tag{5.4}$$

where $\boldsymbol{P}$ is a suitable kernel matrix.

Finally, the estimation of $\boldsymbol{\theta}$ is described as:

$$\hat{\boldsymbol{\theta}} = \arg\min_{\boldsymbol{\theta}\in\mathbb{R}^m} \left(\|\boldsymbol{Y} - \boldsymbol{\phi}\boldsymbol{\theta}\|^2 + \gamma\boldsymbol{\theta}^{\mathrm{T}}\boldsymbol{K}^{-1}\boldsymbol{\theta} \right), \tag{5.5}$$

where γ is a positive scalar.

Eq. (5.5) could be adapted as the following description:

$$\hat{\boldsymbol{\theta}} = \left(\boldsymbol{P}\boldsymbol{\phi}^{\mathrm{T}}\boldsymbol{\phi} + \gamma I_m\right)^{-1}\boldsymbol{P}\boldsymbol{\phi}^{\mathrm{T}}\boldsymbol{Y}, \tag{5.6}$$

where $I_m \in \mathbb{R}^{m\times m}$ is an identity matrix with the dimension of $m \times m$.

For the kernel part, we select the Stable Spline (SS) kernel from various kernels to achieve a better performance of FIR model and a more accurate estimation of $\dot{V}_dO_2$ based on previous study [119, 120]. The SS kernel is described as follows:

$$\boldsymbol{P}(i,j) = \frac{c}{2}e^{-\beta \min(i,j)} - \frac{c}{6}e^{-3\beta \max(i,j)}, \tag{5.7}$$

where $c \geq 0$, $0 \leq \beta < 1$.

The parameters γ, c and β in this identification method need to be well-tuned. The tuning is based on Alessandro and Tianshi's studies [58, 121] and we intend to select the best combination of the parameters. The principle of tuning is to find the best fitness between the real $\dot{V}_dO_2$ and estimated $\dot{V}_dO_2$ under the premise of ensuring a smooth Impulse Response (IR) and avoiding over-fit. Above all, we choose $\gamma = 200$, $c = 1$ and $\beta = 0.9985$ after tuning.

5.2.3 Pre-processing, Identification Strategy and Verification

Due to the individual differences, the total number and length of one entire period are different for each participant. In that case, the results of the identification fitness are affected by these factors. Table 5.2 presents the total number of periods of each participant and makes a summary.

Table 5.2 Quantity of Participants with Different Number of Exercise Periods.

Periods	Participants Quantity
2	6
3	4

According to Table 5.2, we make a comparison of the fitness of the filtered $\dot{V}_dO_2$ estimation when the number of periods is 0.5, 1, 2, as all the participants have at least two entire exercise periods. This estimation is conducted by the non-parametric model method, which is introduced in Section 5.2.2. After the identification, we applied the Wilcoxon Rank Sum Test to illustrate the significant difference of the IR results with different number of periods as the results does not follow the normal distribution.

In order to demonstrate the benefit of this method and study model structure of the exercise phase- $\dot{V}_dO_2$ system, the system identification toolbox in MATLAB is applied to

make a comparative identification. The fixed-order model including first, second and third-order are implemented in MATLAB. The goodness of fit of estimated output is calculated by the fit ratio NRMSE (normalised root mean square error):

$$NRMSE = \left(1 - \frac{||\hat{Y}_N - Y_N||}{||Y_N - (\bar{Y_N})||}\right). \tag{5.8}$$

where N is total number of sampling, Y_N is the real data (reference), $\hat{Y_N}$ is the estimated Y_N and $\bar{Y_N}$ is the mean value of Y_N.

To verify the changing of the system structure throughout the entire exercise and demonstrate the benefit of the non-parametric model when we focus on the whole exercise period, the IR model and three kinds of fixed-order models identified from previous period, are applied to estimate the output of the next period for each participant. The goodness of fit is the primary indicator in this stage to study the estimation performance of these approaches.

5.3 Results

This section shows the identification results and the fitness of different models in a different situation. The results about Wilcoxon Rank Sum Test and variance is used to demonstrate the significant difference of the IR from different periods and verify the stability of different models. The verification results about the changing structure for different periods are also presented.

Three representative identification results by non-parametric model of each number of periods are shown in Fig. 5.3, Fig. 5.4, Fig. 5.5, which contains the impulse response and the estimated output ($\dot{V}_d O_2$) from half, one and two periods.

The boxplot to describe the fitness results from non-parametric model of a different number of periods for all participants is presented in Fig. 5.6.

The results from one and two periods are focused for the next step study as the IR of them perform stable in the end as shown in Fig. 5.5. We calculated the estimated output fitness of 10 participants which are from different methods, including non-parametric model, first-order, second-order and third-order model. The comparison results is shown in Fig. 5.7. The fitness from four methods of each participant is represented separately. For the second-order and

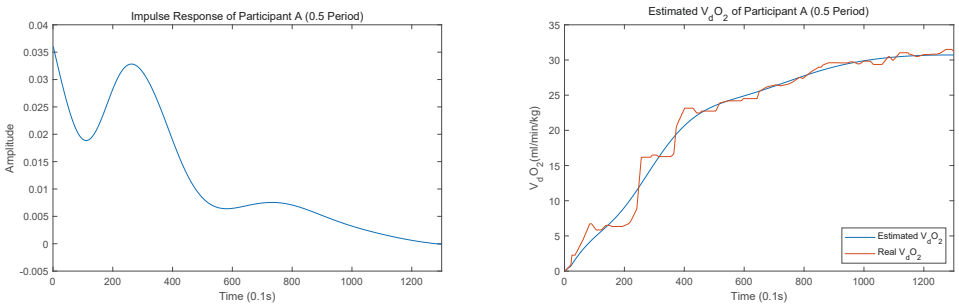

Fig. 5.3 Impulse Response and Estimated ($\dot{V}_dO_2$) of Three Participants (0.5 period).

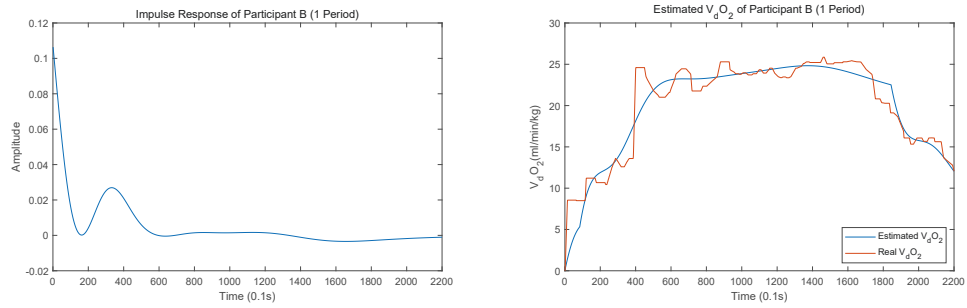

Fig. 5.4 Impulse Response and Estimated ($\dot{V}_dO_2$) of Three Participants (1 period).

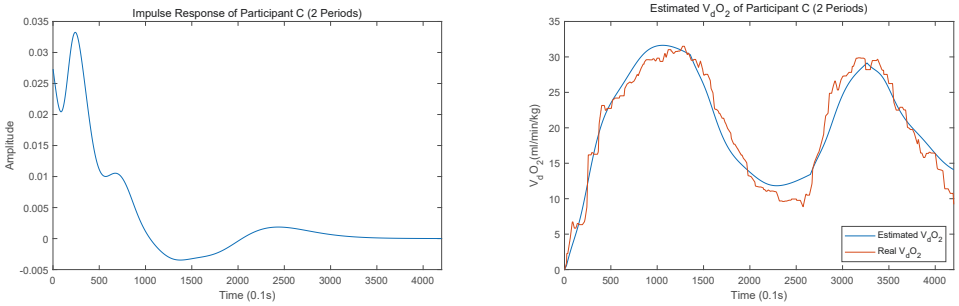

Fig. 5.5 Impulse Response and Estimated ($\dot{V}_dO_2$) of Three Participants (2 periods).

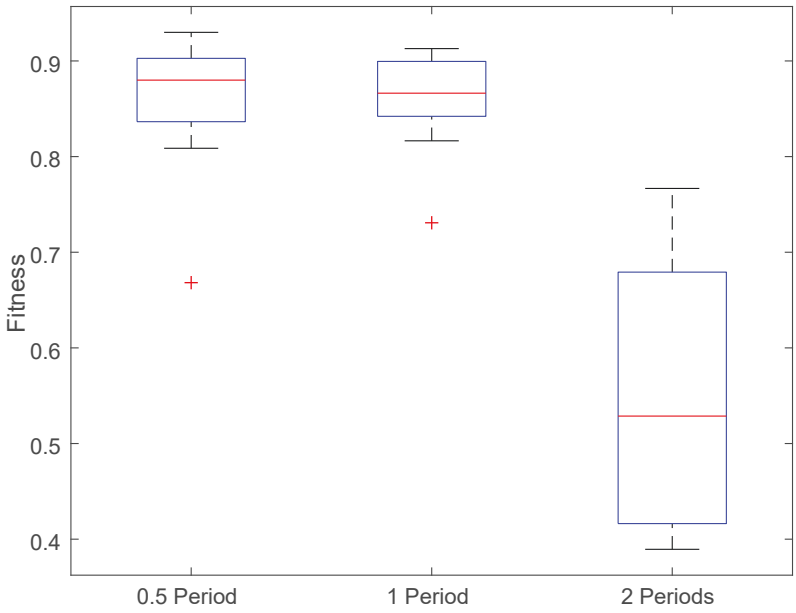

Fig. 5.6 Fitness of Estimated Output of Different Number of Periods from Non-parametric Model.

third-order model, some results of fitness show a quite concussive or peculiar performance, which means the non-parametric and first-order model is more stable than higher-order model for this system.

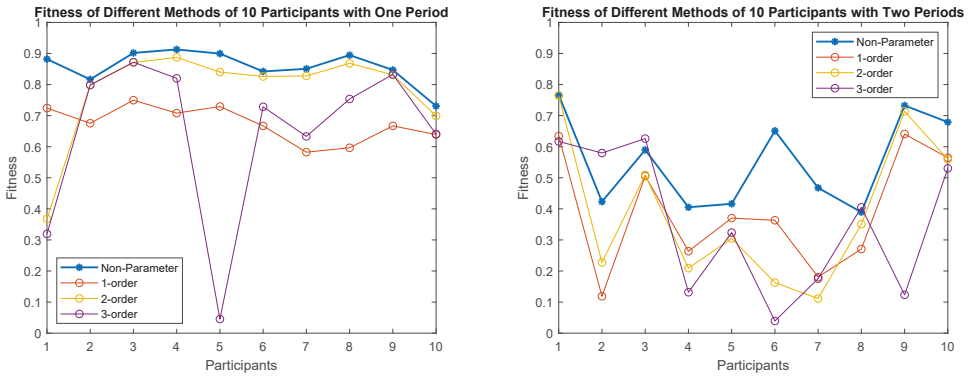

Fig. 5.7 Fitness of Different Methods of 10 Participants with One Period or Two Periods.

The variance of the fitness by different models indicates the stability of the model which is shown in Table 5.3. We could find that the non-parametric model exhibits the smallest variance in both one period and two periods, which means that this model is more stable and

suitable for different situations. Moreover, the first, second and third-order show different performance as the number of periods change.

Table 5.3 The Variance of Fitness by Different Model Method in One or Two periods.

Model Type	One Period	Two Periods
First-order	0.0031	0.0350
Second-order	0.0239	0.0539
Third-order	0.0695	0.0514
Non-parametric	0.0030	0.0218

In order to demonstrate the significant difference between the different number of periods, we apply Wilcoxon Rank Sum Test on IR because it does not follow a normal distribution. The IR of the same participants with the different number of periods are compared and the results are shown in Table 5.4. Generally, $P < 0.05$ is considered as statistically significant. All the P value means $h = 1$, which also means that all the distinctions of IR (different number of periods with the same participants) are significant. This also illustrates that the system model of a different period is quite different.

Table 5.4 Rank Sum Test of Same Participants' IR with Different Numbers of Periods.

Participant	Half vs One	One vs Two	Half vs Two
1	P=2.42^{-215}	P=2.38^{-214}	P=0
2	P=1.73^{-240}	P=1.11^{-129}	P=0
3	P=5.17^{-113}	P=4.22^{-258}	P=0
4	P=2.36^{-131}	P=5.09^{-208}	P=0
5	P=2.26^{-184}	P=6.31^{-98}	P=0
6	P=1.26^{-214}	P=2.70^{-110}	P=0
7	P=1.68^{-273}	P=1.82^{-114}	P=0
8	P=0	P=7.66^{-20}	P=0
9	P=9.23^{-225}	P=7.90^{-38}	P=0
10	P=4.90^{-317}	P=2.14^{-10}	P=0

When extending the identification period, the fitness is significantly decreased as shown in Fig. 5.6 and Fig. 5.7. We intend to verify the structure of the system is changing with periods and demonstrate the non-parametric method is more stable. Therefore, the impulse response model acquired from the non-parametric modelling approach and the first-order, second-order, third-order model in the previous period is implemented to estimate the output

in the next period for each participant. The verification fitness of the estimation is shown in Fig. 5.8.

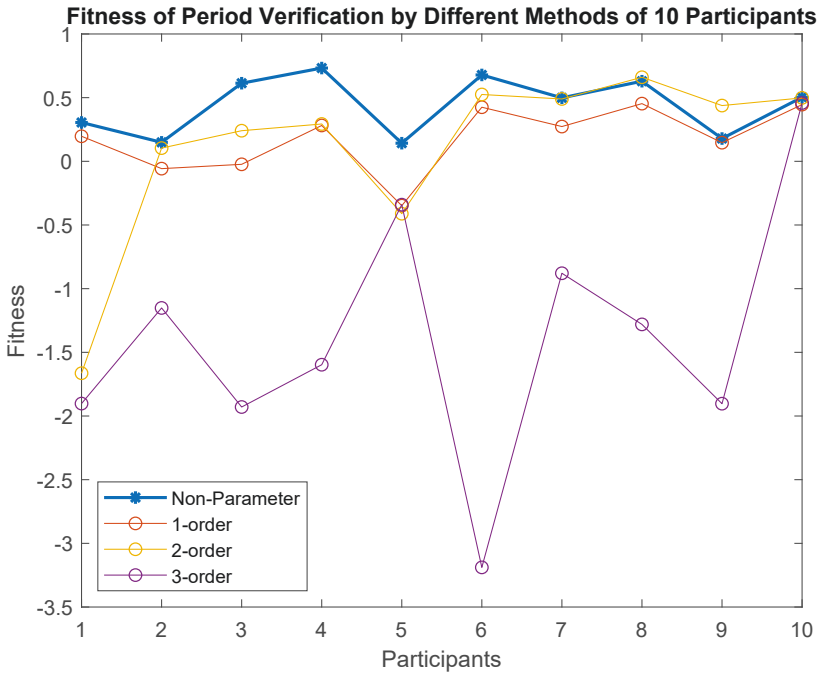

Fig. 5.8 The Fitness of Period Verification by Different Model Method.

The initial point of the first period is ensured to be consistent with the next period when the verification is conducted. According to the results in Fig. 5.6, Fig. 5.7 and Table 5.3, the fitness of the estimation output in next period decline when using the IR model from the previous model. In addition, Fig. 5.8 illustrates that the IR model from the non-parametric model is with robustness when the identification period changes. The summarization is displayed in Fig. 5.9 which combined the results from Fig. 5.7 and Fig. 5.8. The results of different models (non-parametric model, first-order model, second-order model, third-order model) for different periods (one period, two periods and previous period model verification for next period) are directly shown in Fig. 5.9, and demonstrate that the non-parametric model performs better than the other three models in different situation.

5.4 Discussion

In this section, the results are analysed and explained as follows.

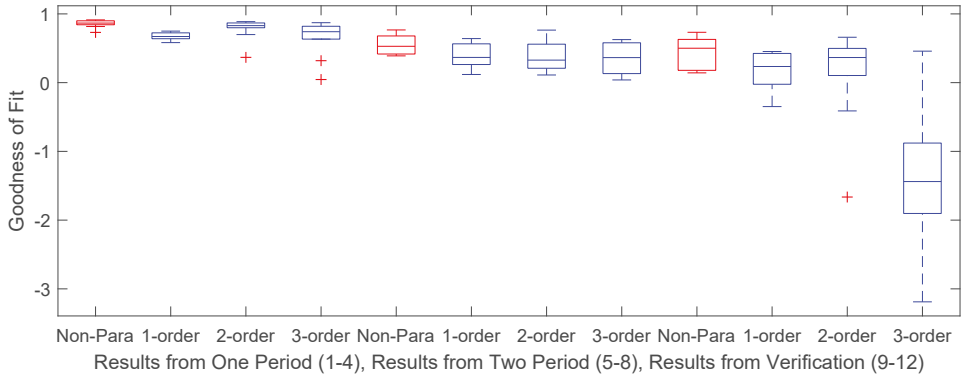

Fig. 5.9 The Boxplot for Fitness from Different Models and Different Periods.

1. From the perspective of the periods comparison in Fig. 5.6, the fitness of two periods is significantly lower than those of half or one period when the model of two periods is described by one stable IR model as shown in Fig. 5.7. Table 6.5 illustrates that the IR model is quite different when the number of periods is different. Furthermore, the testing part is conducted to support this point. Comparing Fig. 5.8 with the left figure in Fig. 5.7, it is concluded that the IR model from the previous period is not particularly suitable for the next period as the fitness level is lower. In all of the above results, the model of the system changes with different exercise periods. In the next step, we plan to apply an online modelling approach, which could adjust the system structure over time in order to do the identification.

2. As for the structure of the system order, the comparison between the non-parametric model and the fixed-order model illustrates that the structure of the model is variant. The examples of IR model in Fig. 5.5 also illustrate this conclusion. The continuously changing protocol for the stairs exercise provides more stimulation for the system, utilised as prior information for the tuning of the kernel covariance. Commonly, the system in previous articles [62, 66, 95] comes from a single onset or offset period experiment and is considered as a first-order system. However, the first-order system is not suitable when the input and output of the system become complicated as in our experiment. Moreover, the individual difference in our previous study [66] also supports the diversity of the model due to the complexity of the participants' respective motions and respiratory systems. The continuously changing protocol for the stairs exercise in our study provides more stimulation for the system which is also an

important aspect. As the participants' HR_{max} is maintained in the range of 60% to 80%, the maximum range of stimulation is provided. The input signals from the stairs exercise have significant strength and duration, and the uncertainty of the stochastic input can increase the index of the information matrix.

3. In terms of the above demonstration, the advantages of the non-parametric model are obvious. The fitness comparison in Fig. 5.7 and variance comparison in Table 5.3 indicate that the non-parametric model is more stable for different participants and different numbers of periods. When the first, second and third-order models are applied to identify the system model, the best fitness for different participants is obtained from different models. In addition, for some participants, the fitness is quite low when using these three kinds of model. This illustrates that the system could not be described as a fixed-order model. In contrast, the fitness from the non-parametric model performs well for all of the participants. As for the verification results in Fig. 5.8, the model from the previous period using the non-parametric model also performs better in the next period. The summarized performance of different models in different periods shown in Fig. 5.9 also directly and clearly demonstrates the higher fitness of the non-parametric model. The above aspects indicate that the non-parametric model is suitable for the system when the structure is complicated and changing. The reason is that the amount of information is sufficient when the non-parametric model is applied to fully utilise the priori information. The priori information in the kernel provides a foundation to estimate the structure of the system and provides the capacity to accommodate the complexity of the model.

5.5 Conclusion

The non-parametric model is applied to investigate the dynamics of $\dot{V}O_2$ responding to stairs exercise. The self-designed application and $K4b^2$ gas analyser provide a reliable technique to record $\dot{V}O_2$ data and exercise phase. The protocol of the experiment guarantees a continuous and random changing $\dot{V}O_2$ and the exercise phase. The identification results of different numbers of periods are compared to illustrate the variation model of the system. Experimental results indicate that the model from the previous period is no longer suitable

for the next period. The fixed-order model includes three types of order which are conducted as comparison approaches to demonstrate the benefits of using the non-parametric modelling approach. It can be concluded that the non-parametric model is more stable and compatible for different participants in different periods. The complexity of human respiratory systems, as well as individual differences, would be worth exploring in more depth in future research.

Chapter 6

Prediction of Cardiorespiratory Response to Treadmill Exercise Using Non-parametric Modelling with Optimised Kernel-Parameter Selection

6.1 Introduction

Aerobic exercise is a physical exercise which mainly depends on the aerobic energy-generating process [3]. The oxygen inhaled by the human body is equal to the demands during exercise and reaches a physiological balance. Aerobic exercise depends primarily on oxygen uptake, the intensity of which is related to respiratory information. The oxygen uptake ($\dot{V}O_2$) or carbon dioxide output ($\dot{V}CO_2$) are widely used to analyse the mechanism of the human body during exercise [72–75]. Due to the linear relationship between respiratory information (e.g. $\dot{V}O_2$ and $\dot{V}CO_2$) and heart rate (HR), the maximum heart rate (HR_{max}) [11, 12] is recognised as a key indicator for detecting exercise intensity [13]. It is recommended that the HR_{max} should be kept in a proper range to ensure that the working peripheral muscles are supplied with enough oxygen.

Among the research that spans across the three decades, $\dot{V}O_2$ and $\dot{V}CO_2$ have been measured at various sports physiological laboratories using the gas analyser [51]. With the

development of new technology, the automated portable gas analysis system has been used in several sports fields for energy consumption assessment [14]. $\dot{V}O_2$ and $\dot{V}CO_2$ analysis during exercise have been significantly developed in different ways. Hill [122] and Wasserman [79] demonstrated the logarithmic equation of $\dot{V}O_2$ and $\dot{V}CO_2$. Based on this equation, the $\dot{V}O_2$ and $\dot{V}CO_2$ modelling for aerobic exercise has been developed to estimate the steady status and dynamic response during one simple phase of exercise. The respiration reaction system is described as a first or higher order time-invariant system in the respective research of Hill and Wasserman. The classical system identification methods, e.g. Least Square, Maximum Likelihood and Prediction Error Method, are broadly used in modelling the first or higher order time-invariant system. However, an important issue in identification is how to design the experiment to ensure sufficient stimulation for the modelling of the system. The input signals need enough intensity and duration when participants are involved in the experiment. On the other hand, the signal applied to the human body should be carefully chosen to ensure safety. Considering the following two aspects, the conflicts of the goals can be successfully resolved.

The first aspect is to apply the non-parametric method for identification. System structure information used in model complexity selection is a crucial step in modelling. However, when the information is insufficient to determine the parametric model structure, the system dynamics could be described by non-parametric models instead of the commonly used fixed-order linear time-invariant models[55, 56]. In addition, the non-parametric model has the advantage when the system is in a state of massive information. Furthermore, the well-designed kernel strategies and regularisation terms can dramatically improve the accuracy and robustness of the modelling [57–59]. The other aspect is to select an appropriate input with sufficient stimulation for the model. Various dynamic physiological signals are used in respiratory modelling, such as HR , $\dot{V}O_2$ and $\dot{V}CO_2$, during walking, running [61–63], or treadmill exercise [8, 64–66]. However, the physiological signal in these studies reaches a steady platform that shows an identical trend as a step response input. With this in mind, we designed an appropriate protocol for the stairs exercise to make the signal continuously change to ensure sufficient stimulation.

In this study, the kernel-based non-parametric method to identify how the $\dot{V}O_2$ or $\dot{V}CO_2$ response to treadmill speed is developed. Different with the previous section, two approaches are compared in the selection of the kernel parameter in this methodology. One approach

is numerical simulation which has been proposed in our previous paper [66], and the other approach is selecting the parameters of the kernel in the regularisation term based on identification results when using data from the stairs experiment. During the stairs exercise, the energy consumption, heart rate, and minute ventilation volume will increase until it reaches a peak when people go upstairs (ascending). When going downstairs (descending), these figures will decrease to form a valley. The exercise phase and the physiological signal change continuously during this experiment. The selected parameters of the kernel ensure a consistent stability for the purpose of treadmill exercise identification. After the parameters selection and identification by the non-parametric method, the experimental results and the goodness-of-fit (NRMSE) comparison demonstrate that the non-parametric method is more suitable in order to identify how the $\dot{V}O_2$ or $\dot{V}CO_2$ responds to treadmill speed according to accuracy and flexibility. It should be emphasized that the system model in our research is no longer a simple onset or offset structure which can be described as a linear model. According to the complexity and the massive information in the system, the non-parametric model is chosen as the identification approach. Furthermore, the parameter from the stairs experiment is also proven to be a better choice, since it provides enough stimulation and diversified input.

The remainder of this part of work is organized as follows. Section 6.2 introduces the non-parametric model with the kernel-based regularisation, the experiment, and the parameter selection. The identification and comparison results are presented in Section 6.3. Then the analysis and discussion about results are presented in Section 6.4. Finally, the conclusion is drawn in Section 6.5.

6.2 Methods

In this section, we illustrate the non-parametric modelling method that is applied for the $\dot{V}O_2$ and $\dot{V}CO_2$ identification during the treadmill exercise. The experiment is introduced afterward, which contains the stairs experiment and treadmill experiment. Two different selection methods for the parameters of kernel including the numerical simulation and tuning from stairs experiment are also introduced for the non-parametric modelling of treadmill exercise.

6.2.1 Non-parametric Modelling of Finite Impulse Response Based on Kernel

The non-parametric modelling method based on kernel, which is introduced in Chapter 4 and 5, is conducted to discern how the $\dot{V}O_2$ or $\dot{V}CO_2$ reacts to treadmill speed. Under the discrete case, the relationship between treadmill speed (input) and $\dot{V}O_2$ or $\dot{V}CO_2$ (output) is also considered as a single input single output (SISO) system which can be calculated by impulse response.

The estimation of $\boldsymbol{\theta}$ is obtained and adapted as Eq. (6.1):

$$\hat{\boldsymbol{\theta}} = \left(\boldsymbol{P}\boldsymbol{\phi}^{\mathrm{T}}\boldsymbol{\phi} + \gamma I_m\right)^{-1}\boldsymbol{P}\boldsymbol{\phi}^{\mathrm{T}}\boldsymbol{Y}, \tag{6.1}$$

where γ is a positive scalar and $I_m \in \mathbb{R}^{m\times m}$ is an identity matrix with the dimension of $m \times m$.

The priori information in kernel matrix $\boldsymbol{P}^{-1}$ could help the estimated $\hat{\boldsymbol{\theta}}$ provide a better and smoother result when compared to least square estimation [57].

Based on our previous work [66], the Stable Spline (SS) kernel which is shown in Eq. (6.2), demonstrates a better performance than the other kernels based on the aspects of accuracy, sensitivity, stability and smoothness.

$$P(i,j) = \frac{c}{2}e^{-\beta min(i,j)} - \frac{c}{6}e^{-3\beta max(i,j)}, \tag{6.2}$$

where $c \geq 0$, $0 \leq \beta < 1$.

The SS kernel inherits all the approximation capabilities of the spline curve by construction [57][123] and is intrinsically stable. The SS kernel represents the least committing priors when smoothness and stability is the sole information on $\boldsymbol{\theta}$.

6.2.2 Experiment

Two experiments, namely “stairs experiment" and “treadmill experiment ", which are introduced in Chapter 4 and 5, are also conducted in this part of work due to the different command. In summary, the set-up of the two experiments, hardware and the application interface are shown in Fig. 6.1. For the two experiments, the $\dot{V}CO_2$ and $\dot{V}O_2$ were both

divided by the weight (Kg) for each participant to exclude the impact of the participant's weight on breath information. The normalized $\dot{V}CO_2$ and $\dot{V}O_2$ are recorded as $\dot{V}_dCO_2$ and $\dot{V}_dO_2$. The participants are recruited randomly. These two experiments (stairs experiment and treadmill experiment) recruited different participants (random difference in age, height and HR_{max}) to ensure the fairness of the comparison for the two kernel parameters selection methods.

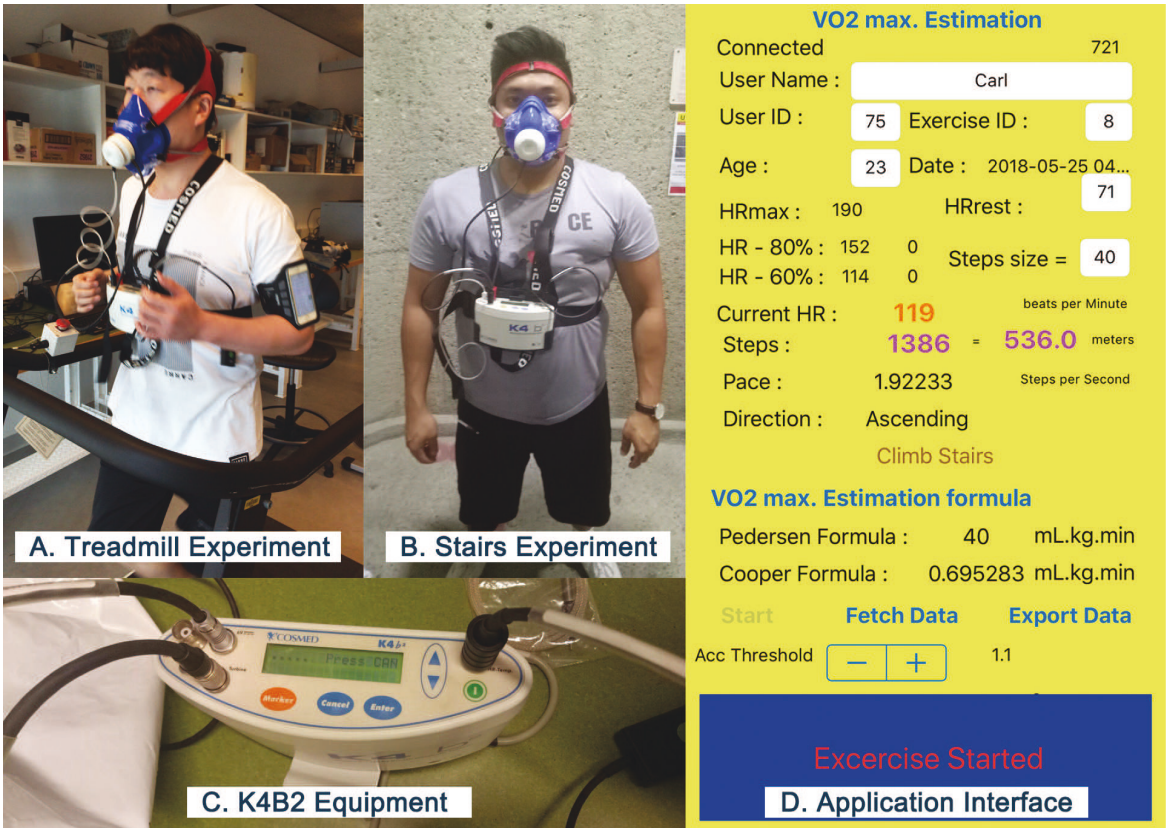

Fig. 6.1 Scenes of Experiments, the Equipment and Application Interface.

Table 6.1 Information about the 15 Participants in Stairs Experiment

Information	Age $(year)$	Height (cm)	Mass (kg)	HR_{max}	$60\%HR_{max}$	$80\%HR_{max}$
Mean	29.60	172.60	83.00	185.40	111.10	148.30
Standard Deviation	7.60	3.40	5.39	5.25	4.28	3.35

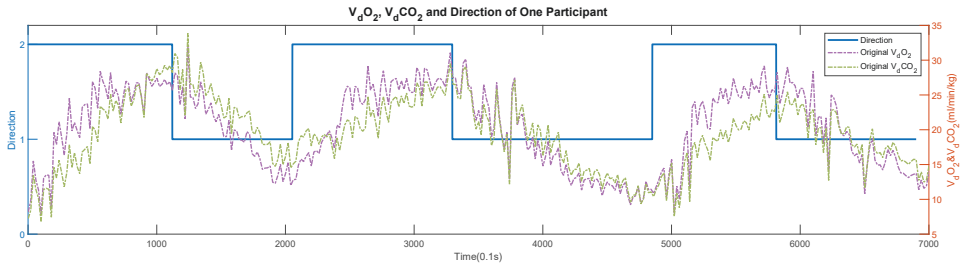

Fig. 6.2 Measured $\dot{V}_dO_2$, $\dot{V}_dCO_2$ and Exercise Direction of One Participant during Stairs Experiment.

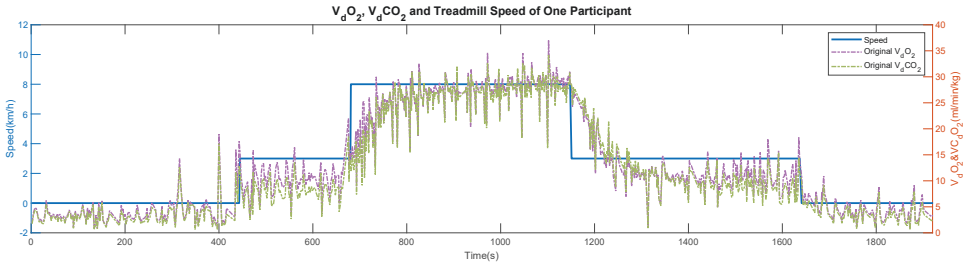

Fig. 6.3 Measured $\dot{V}_dO_2$, $\dot{V}_dCO_2$ and Speed of One Participant during the Treadmill Experiment.

Table 6.2 Information about the 20 Participants in Treadmill Experiment

Information	Age ($year$)	Height (cm)	Mass (kg)	HR_{max}	$60\%HR_{max}$	$80\%HR_{max}$
Mean	46.40	176.60	91.20	173.60	104.16	138.88
Standard Deviation	5.68	4.40	11.37	5.53	3.32	4.42

Stairs Experiment

The stairs experiment is about HR maintaining between the range of 60% to 80% of the participants' HR_{max} during the stairs exercise. In this experiment, HR_{max} is calculated as [78]:

$$HR_{max} = 205.8 - 0.685 \times age \tag{6.3}$$

A self-designed mobile application is used to collect the various information from 15 untrained (non-athletes) and healthy (no records of motor skill disorder, cardiac-respiratory disorder or related medications history) male participants, including HR, steps, and direction (upstairs or downstairs). The mobile phone is placed on the ankle of participants. The Inertial Measurement Unit (IMU) data could represent the direction of the movement. Meanwhile,

the breath data including $\dot{V}_dO_2$ and $\dot{V}_dCO_2$ are collected by a portable gas analyser- Cosmed $K4b^2$ (Cosmed, Italy) [118]. The basic biological information of the participants is shown in Table 6.1.

The participants are instructed to go upstairs and downstairs continuously for 12 minutes. The experiment starts by collecting data while going upstairs. Once the participants' HR exceeds 80% of HR_{max}, they are instructed to go downstairs. When their HR is under 60% of HR_{max}, they are asked to go upstairs again. The $\dot{V}O_{2max}$ is monitored to ensure the lactate threshold $VT2$ will not be reached. There will be $2-4$ complete periods (one whole period is from the beginning of upstairs exercise to the end of downstairs exercise) for an entire exercise routine for all participants. The direction of the exercise is described as 1 when the participants are ascending (go upstairs), and 2 when descending (go downstairs). A sample of the direction and measured $\dot{V}_dCO_2$ and $\dot{V}_dO_2$ from one participant is shown in Fig. 6.2. The $\dot{V}_dCO_2$ or $\dot{V}_dO_2$ are filtered by median filter to remove the artifacts before identification. This experiment ensures a continuously changing input (direction) and output ($\dot{V}_dCO_2$ or $\dot{V}_dO_2$) for guaranteing a sufficient stimulation in kernel parameter selection part.

Treadmill Experiment

The treadmill experiment is about a jogging exercise on treadmill. The $\dot{V}_dCO_2$ and $\dot{V}_dO_2$ data is also recorded by the $K4b^2$ when the 20 untrained (non-athletes) and healthy (no records of motor skill disorder) males, who are not the same individuals as the stairs experiment, are jogging on the treadmill following an exercise protocol. The physical information of the participants is shown in Table 6.2.

The protocol of this experiment is shown in Fig. 6.3. The participants first walk at 3 km/h for four minutes, and then run at 8 km/h for eight minutes, followed by another walk at 3 km/h for eight minutes before stopping.

6.2.3 Parameter Selection

The parameters of the kernel are a vital part to determine the estimated model structure. Two different methods are applied to select the parameters c and β in SS kernel as shown in Eq. (6.2). The first method is numerical simulation and the second method is parameter tuning in

the stairs experiment. The most appropriate parameters are selected to the non-parametric modelling for the treadmill experiment.

We apply the fit ratio NRMSE (normalised root mean square error) to obtain the goodness of fit of estimated output, which is represented as follow:

$$NRMSE = \left(1 - \frac{||\hat{Y}_N - Y_N||}{||Y_N - mean(Y_N)||}\right), \tag{6.4}$$

where N is total number of sampling, Y_N is the real data (reference) and $\hat{Y_N}$ is the estimated Y_N.

Parameters Selected from Numerical Simulation

Our simulation begins with a first-order system to describe the relationship between the O_2 uptake or CO_2 output and the treadmill speed according to the description of $\dot{V}_dCO_2$ and $\dot{V}_dO_2$ in previous study [62][66] as shown in Eq. (6.5):

$$V(t) = V_0 + R_A[1 - e^{-(t-T_D)/\tau}]. \tag{6.5}$$

where $V(t)$ is the $\dot{V}_dO_2$ or $\dot{V}_dCO_2$ at time t, V_0 is the initial value of $\dot{V}_dO_2$ or $\dot{V}_dCO_2$, R_A is the response amplitude, T_D is the time delay, and τ is the time constant.

Thus, the system is set as Eq. (6.6):

$$Y(s) = \frac{K}{Ts+1}U(s), \tag{6.6}$$

where K that follows the uniform distribution U(5, 15) is the steady gain, and T which follows U(15, 25) is the time constant.

The input of the system $u(t)$ is set to be the same trend as the stairs experiment to ensure a similar stimulation. The simulated output $y(t)$ is polluted by a Gaussian white noise with 1 dB Signal-Noise Ratio (SNR). The sampling time is selected as 1 second.

The parameter c and β in Eq. (6.2) of the SS kernel mentioned in Section 6.2.1 are the primary targets of tuning. After tuning the parameters in the simulation [121], we selected the following combination of $c = [100\ 200\ 300]$ and $\beta = [0.95\ 0.987\ 0.99]$ and the samples

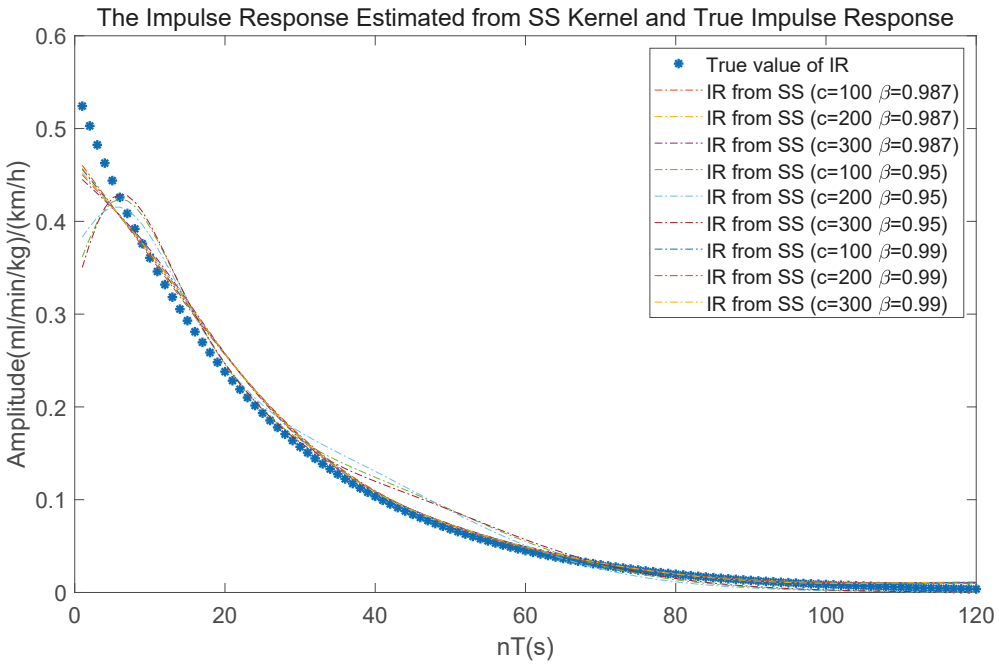

Fig. 6.4 Impulse Response from SS kernel Compared to the True Value of Impulse Response in the Simulation.

of the IR model are shown in Fig. 6.4. After the statistics of fitness and the observation of IR smoothness and stability, the best combination is $c = 200$ and $\beta = 0.987$.

Parameters Tuning from Stairs Experiment

As mentioned above, the continuously changing data in stairs experiment could ensure a enough stimulation for the system. Therefore, the identification for $\dot{V}_d CO_2$ and $\dot{V}_d O_2$ in the stairs experiment is aimed to select the most appropriate parameters and compare the selection process. We choose one period from each participant to do the identification. The identification is also conducted by non-parametric method. After the preliminary range selection, we find that when β is in the range of $0.9975 - 0.999$, the fitness shows better results. Then we make further statistics about the fitness of the parameters in this range. Table 6.3 represents the fitness level of stairs experiment identification results (10 out of 15 participants) ($> 60\%$). The results from these 10 participants are chosen to construct the model for the kernel parameters selection. Finally, we decided that $c = 200$ which is same

Table 6.3 The Fitness of Different Parameter β for $\dot{V}_dO_2$ and $\dot{V}_dCO_2$ about the Stairs Experiment Identification for Ten Participants.

Sub.	$\dot{V}_dO_2$				
β	**0.9975**	**0.9978**	**0.998**	**0.9985**	**0.999**
1	68.91%	73.16%	75.34%	76.91%	76.40%
2	66.64%	66.74%	66.53%	65.42%	63.85%
3	81.95%	82.11%	82.30%	82.00%	81.16%
4	76.89%	79.36%	80.36%	80.46%	79.41%
5	65.30%	69.06%	71.94%	76.95%	76.98%
6	63.07%	64.16%	64.69%	64.69%	63.27%
7	75.83%	76.25%	76.11%	75.17%	73.34%
8	76.66%	77.49%	77.58%	76.70%	74.85%
9	66.27%	66.29%	66.36%	67.85%	69.41%
10	63.84%	65.42%	66.26%	66.79%	65.41%
Best	0	2	2	1	2
Sub.	$\dot{V}_dCO_2$				
β	**0.9975**	**0.9978**	**0.998**	**0.9985**	**0.999**
1	73.26%	73.82%	74.66%	75.93%	75.45%
2	66.68%	66.46%	66.29%	65.21%	63.42%
3	80.69%	80.91%	81.23%	81.67%	81.18%
4	81.55%	81.68%	81.70%	81.19%	80.23%
5	76.96%	77.90%	78.26%	77.99%	76.41%
6	64.45%	64.72%	64.68%	64.25%	63.04%
7	77.51%	77.30%	76.98%	76.29%	74.50%
8	77.15%	77.92%	78.12%	77.29%	75.32%
9	66.30%	66.30%	66.31%	67.85%	69.45%
10	67.58%	67.16%	66.93%	65.8%	64.54%
Best	3	0	4	2	1

* "Sub." means the ten participants.

** "Best" indicates the number of participants which achieve the best fitness when using this value of parameter-β.

with the simulation, and $\beta = 0.998$, which is marked as red in Table 6.3, according to its university for most participants' $\dot{V}_d CO_2$ and $\dot{V}_d O_2$.

6.2.4 Statistical Analysis

In order to verify that the fitness of the models is significantly different between the two parameters selecting approaches, the statistical analysis is necessary. After the fitness of identification results from treadmill experiment by different parameters selecting approaches is calculated, the histogram and normal probability of the fitness is plotted in Matlab to determine whether the fitness follows a normal distribution. As the results of normality shows, the Wilcoxon Rank Sum test is used because the fitness does not follow normal distribution. Generally, $p < 0.05$ means $h = 1$, and the fitness is considered as statistically significant.

6.3 Results

In this section, the identification results about the $\dot{V}_d O_2$ and $\dot{V}_d CO_2$ in the treadmill experiment are discussed. The comparison between estimation fitness when using the parameter β from stairs experiment and simulation are also be presented.

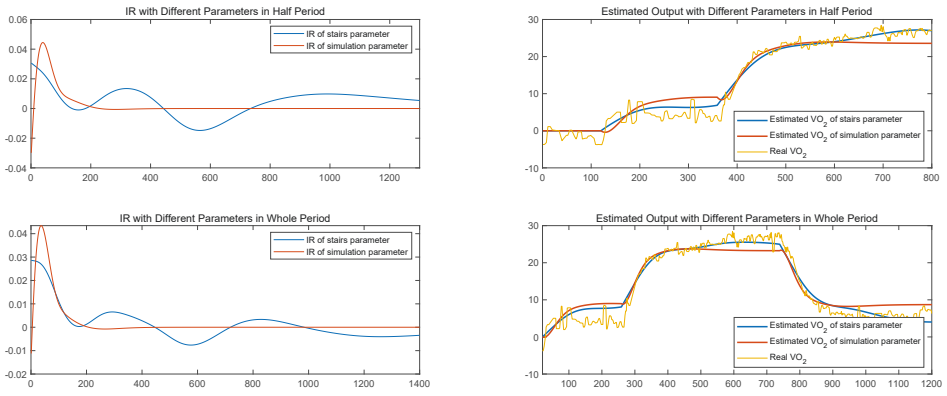

Fig. 6.5 IR and Estimated $\dot{V}_d O_2$ Comparison with Different Parameters in Whole Period and Half Period of Participant A.

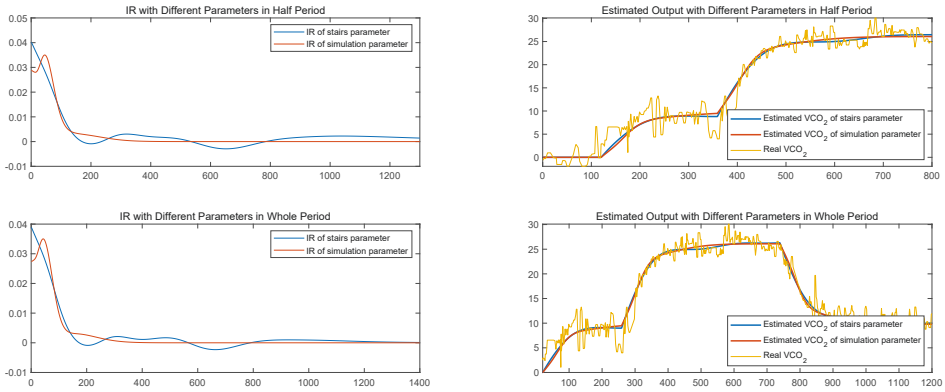

Fig. 6.6 IR and Estimated $\dot{V}_d CO_2$ Comparison with Different Parameters in Whole Period and Half Period of Participant A.

We applied the non-parametric model identification method for both the ascending period and entire period of $\dot{V}_d O_2$ and $\dot{V}_d CO_2$ in the treadmill experiment. The impulse response and the estimated results (ascending period and entire period) of $\dot{V}_d O_2$ and $\dot{V}_d CO_2$ from one representative participant are shown in Fig. 6.5 and Fig. 6.6. Based on the IR in these two figures, the model is more flexible when the parameter β from stairs experiment is used. Furthermore, the estimated output is closer to the real output both for $\dot{V}_d O_2$ and $\dot{V}_d CO_2$ during both ascending and entire period.

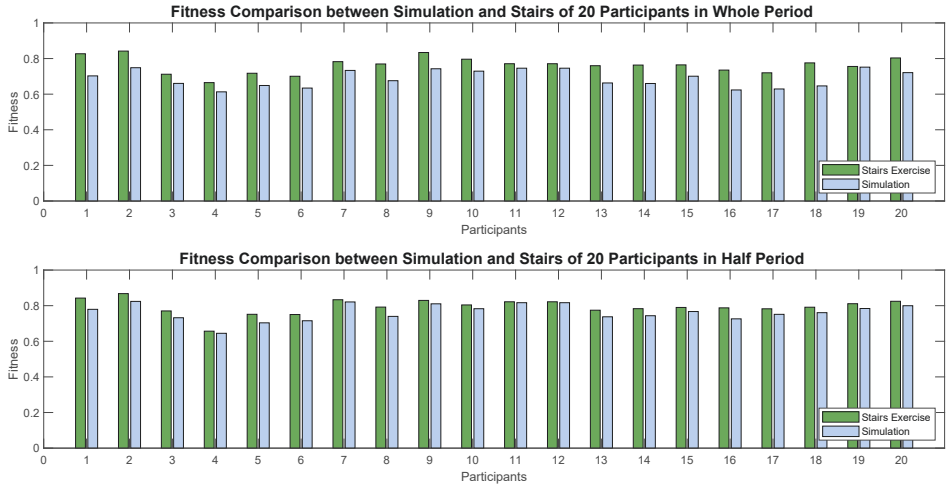

Fig. 6.7 Estimated $\dot{V}_d O_2$ Fitness Comparison between Simulation and Stairs of 20 Participants in Whole Period and Ascending Period.

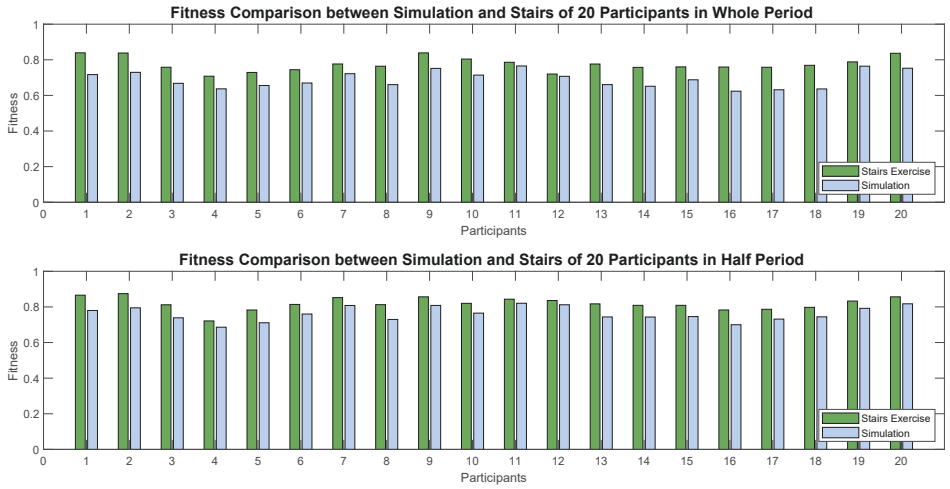

Fig. 6.8 Estimated $\dot{V}_d CO_2$ Fitness Comparison between Simulation and Stairs of 20 Participants in Whole Period and Ascending Period.

To investigate the quality of the parameter β from both the stairs experiment and the simulation, a comparison is established for estimated fitness during the onset period and the whole onset-offset period in treadmill experiment, which is shown in Fig. 6.7 and Fig. 6.8. The figures illustrate that all the output estimation fitness when using the parameter β from the stairs experiment is higher than using the parameter β from the simulation for both $\dot{V}_d O_2$ or $\dot{V}_d CO_2$. The fitness improvement by kernel parameters from stairs experiment compared with parameters from numerical simulation are summarized in Table 6.4.

Table 6.4 The Improvement of Estimation Fitness Using Kernel Parameters from Stairs Experiment.

Comparison	Improvement
$\dot{V}_d O_2$ in Half Period	4.18%
$\dot{V}_d O_2$ in One Period	11.00%
$\dot{V}_d CO_2$ in Half Period	7.63%
$\dot{V}_d CO_2$ in One Period	12.60%

The histogram and normal probability of the $\dot{V}_d O_2$ and $\dot{V}_d CO_2$ estimation fitness during treadmill experiment shown in Fig. 6.9 include the estimation fitness using parameters from simulation or stairs experiment during half or one period, which demonstrate that the identification fitness is commonly higher when using the parameter selected from the stairs exercise than numerical simulation. The Wilcoxon Rank Sum test is applied because the

estimation fitness does not follow the normal distribution. As the Wilcoxon Rank Sum test results shown in Table 6.5, all four outputs satisfy with the general condition, indicating that the results is statistically significant.

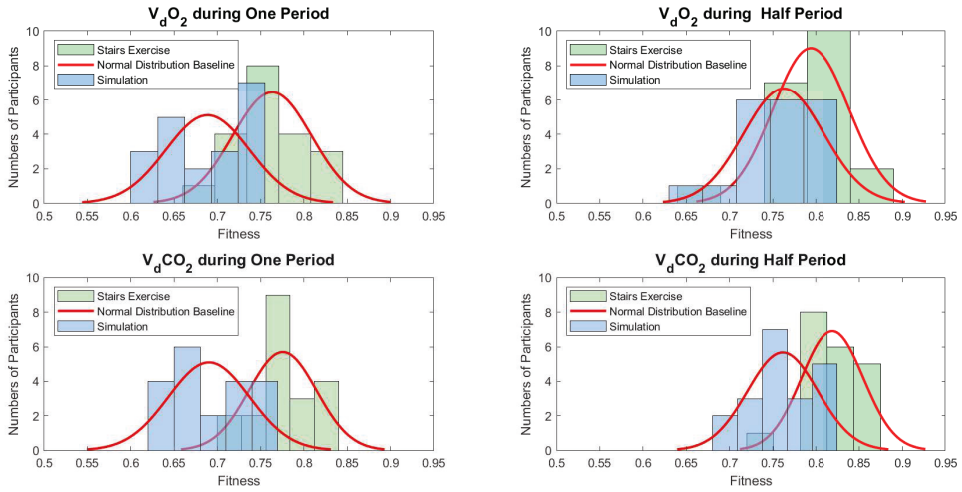

Fig. 6.9 $\dot{V}_dO_2$ and $\dot{V}_dCO_2$ Estimation Fitness for One Period/ Half Period by Parameter from Simulation/ from Stairs Experiment.

Table 6.5 Wilcoxon Rank Sum Test of Estimation Fitness Comparison when Using β from Simulation and Stairs Experiment.

Output	p value	h
$\dot{V}_dO_2$ in Half Period	p=1.55^{-2}	h=1
$\dot{V}_dO_2$ in One Period	p=5.24^{-5}	h=1
$\dot{V}_dCO_2$ in Half Period	p=1.44^{-4}	h=1
$\dot{V}_dCO_2$ in One Period	p=8.60^{-6}	h=1

6.4 Discussion

The regularisation term within the kernel matrix plays a significate role in identification. Accordingly, the parameter of the kernel should be selected carefully. For the impulse response estimation, the kernel $\boldsymbol{P}$ possesses a large condition number which leads to numerical problems, such as failure or inaccuracy of the Cholesky decomposition of $\boldsymbol{P}$ [121]. Compared with the numerical computation method in Gulob and Van Loan's study [124], this problem could be tackled in an active way based on our priori information about $\boldsymbol{P}$ in the impulse

response estimation. If the parameters of the kernel that controls the decaying rate of $\boldsymbol{P}$ are very small, the kernel may have a large condition number. Under this circumstance, the extra constraint on these parameters should be enforced in order to guarantee the tolerably large condition number which is designed to avoid numerical problems. To reach such a goal, the selected value from the stairs experiment is compared with the value from the simulation to create a more appropriate constraint for the parameter β of the kernel. The extra constraints limit the search region of the parameters. The research of Chen, Ohlsson et al.[52] demonstrates that the extra constraints do not cause the performance issues in the regularised least squares estimation.

The advantage of using the non-parametric modelling method when the system structure is uncertain as opposed to the classical linear modelling method [65, 72, 75], was presented in various ways. The impulse response of the model generated by the two approaches illustrates the characteristics of a non-first-order system and this is demonstrated directly in Fig. 6.5. By contrast, the IR model using the parameter β from the stairs experiment fluctuates to a greater extent than the simulation. The oxygen uptake identification results of the stairs experiment using the linear model from Jan's paper (Table 2) [75] showed a mean fitness of 62.5%. The fitness results using the non-parametric model in this work, as shown in Table 6.3, are 6.21% higher. As the non-parametric model is applied, the amount of information is sufficient to fully utilise the priori information and this ensures the complexity of the IR model for estimation. The priori information in the kernel provides the support to estimate the structure of the system. In addition, the regularisation term contains the kernel matrix which eliminates the possibility of overfitting.

The structure of the system under the protocol in our experiments is of higher complexity than the first-order system or time-invariant system and this is demonstrated by the identification results. In the simulation, we acquired the parameter β under the assumption that the system is a first-order system based on the previous study [62]. Our previous study [66] also revealed that in the single ascending or descending period, the system is close to a first-order system, but there are still exceptions because of the individual difference. However, in this research, the physiological information contains two periods of ascending $(0-3-8km/h)$ or a whole period with ascending and descending $(3-8-3km/h)$. This means that the information is not enough to determine the structure of the system which is more complicated than a single onset or offset period. Thus, we can achieve ideal results when we use the

non-parametric model. We can also demonstrate that the system is no longer a first-order system or that it doesn't vary when the period changes. The higher improvement in terms of estimation in one period, as shown in Table 6.4, also demonstrates that the non-parametric model is effective for the complicated system.

The fitness of identification results is higher in Fig. 6.7-Fig. 6.9 when using the parameter β from the stairs experiment, which is also demonstrated by the fitness comparison in Table 6.4. As well, the estimated output in Fig. 6.5 shows that the estimation when using the parameter β from the stairs experiment observes some slight changing trends in relation to the $\dot{V}_dO_2$ or $\dot{V}_dCO_2$. The reason for the higher fitness is that sufficient stimulation is important for the modelling. Data from the stairs experiment ensures that there is sufficient input, which is a continuously changing step response for the system. The direction switching strategy guarantees the randomness of the input. The selection of the participants' HR_{max} from the 60% to 80% range is designed to ensure a maximum range of stimulation. The uncertainty of a random input could make the information matrix substantial in a limited time. The input signals from the stairs experiment are of enough intensity and duration. The dynamic relationship between the exercise phase and $\dot{V}_dO_2$ or $\dot{V}_dCO_2$ during the stairs experiment is obvious enough because of their continuously changing nature. By contrast, the frequently changing treadmill speed can make the participants uncomfortable. However, this shortcoming does not exist in the stairs experiment. Accordingly, this is the reason for using the stairs experiment for the parameters selection.

6.5 Conclusion

To make a summarize, we applied the kernel-based non-parametric method to identify the dynamics of $\dot{V}_dO_2$ and $\dot{V}_dCO_2$ responses to treadmill speed. In order to guarantee a sufficient stimulation for modelling, the parameter β selected from the stairs experiment is constructed and compared with β from simulation. The data from the stairs experiment is collected by a self-designed application, and this experiment protocol ensures a continuously changing input and physiological signal. The results demonstrate the benefits of using the non-parametric modelling method when the system structure cannot be described by a simple model. The fitness comparison also illustrates that when using the parameter β from the

stairs experiment, the estimation results are better than the ones from the simulation. This is because the switching protocol provides a sufficient level of random stimulation and the stairs experiment provides continuously changing data.

Chapter 7

Conclusions and Future Work

7.1 Conclusions

In this section, we firstly summarise the contributions of the dissertation and secondly, we conclude the thesis. The research in this dissertation addresses several challenging physiological assessment problems with respect to static nonlinear modelling and dynamic linear modelling problem. The main contributions of this thesis are as follows:

- The physiological assessment which focused on the cardiorespiratory responses to the exercise phase is comprehensively studied in this work. To meet different demands in the assessment procedure, different modelling methods are proposed. For the purpose of detecting the exercise phase in our experiment, the static nonlinear modelling method is proposed in IMU sensor calibration. As to the aspect of modelling the relationship between the physiological signal and exercise, the dynamic linear modelling method is developed.

- The Inclination based Calibration is proposed to calibrate the IMU sensor based on the fact that the angle between the local magnetic field and gravity is constant. This method can accurately estimate the coefficients of the magnetometers model by simply using a linear Least Square estimator. The advantage of this method is low computational cost and no divergence problems.

- The non-parametric modelling approach with a kernel-based regularisation term is developed in this work. This modelling approach is applied in studying the relationship between the oxygen uptake and carbon dioxide output during aerobic exercise, and the different performances of different exercise phases. Through these aspects of results analysis, the advantage of non-parametric modelling is proved in different ways, such as accuracy, stability and compatibility.

- The kernel matrix in the regularisation term of the non-parametric model is significant in the identification results. Hence, the different selection approaches of the parameters in the kernel matrix are compared in this study. The proper kernel and parameters are selected for the identification part regarding the goodness-of-fit and parameter insensitivity.

- The experiment protocol is well designed to meet the demands in studying the changing structure with the different phases of the exercise. With this experiment protocol and the non-parametric model, sufficient stimulation for the system is ensured and the dynamic models of the physiological signal for exercise responses for different exercise phases are identified.

- The analysis results, such as the difference between the static nonlinear model and dynamic linear model, the relationship between different physiological signal, the various performances of the exercise phase, the importance of the experiment protocol, provide comprehensive instructive guidance for strategic exercise design, athletic assessment, exercise enhancement and health monitoring.

In Chapter 1, a brief introduction to the related works and a brief overview of interesting problems in the related topics is provided.

In Chapter 2, some basic knowledge of physiological assessment and related topics are reviewed. Particularly, the in-field calibration method and experimental design in static nonlinear modelling, the cardiorespiratory signal modelling, the development of wearable devices and the development of non-parametric modelling in dynamic linear modelling, etc., are reviewed.

In Chapter 3, A practical algorithm named Inclination based Calibration (I-Calibration) is developed to calibrate the tri-axial magnetometers. This algorithm is based on the fact that

the angle between the local magnetic field and gravity is constant. As opposed to existing in-field calibration methods, the newly proposed I-Calibration can accurately estimate the coefficients of the magnetometers model by simply using a linear Least Square estimator. Both 6-parameter and 9-parameter mathematical methods associated with the 12-observation experimental design are proposed for the calibration procedure. The problem is finally formulated as a linear least square problem based on the measured magnetic value and calibrated acceleration value. Extensive numerical simulations demonstrate the effectiveness of the I-Calibration. The algorithm performs well on both the simulation study and practical experiment. It also proves that the I-Calibration is robust to the mismatch of the frames of TAs and TMs. Real-time experiments are also performed to compare the performance of the proposed I-Calibration and the M-Calibration. The experimental results demonstrate the two calibration methods are similar effective in terms of calibration accuracy. To investigate the significance of the accuracy of the acceleration value, a contrast study is applied in the simulation and experimental procedure. It demonstrates that the acceleration data should be calibrated well to ensure the effectiveness of the Inclination based Calibration algorithm. As the I-Calibration method is a single-calculation linear method, with low computational costs and no divergence problems, it would be more suitable for real-time in-field calibration for wearable devices with limited computational power.

In Chapter 4, we investigate the onset and offset dynamics of the cardiorespiratory response to treadmill exercise. In order to detect the characteristic differences during the onset and offset exercise, a recently developed the non-parametric modelling method based on the l^2-norm kernel regularisation has been applied to identify the impulse responses of the carbon dioxide output ($\dot{V}_dCO_2$) and oxygen uptake ($\dot{V}_dO_2$) responses. Through the means of a well-designed kernel-based regularisation term, this approach can handle the data which has short records and a low SNR (Signal-to-Noise-Ratio), and it can orderly fit the experimental data. In terms of the fitness for the experimental data from twenty healthy subjects, the stable spline (SS) kernel achieves a reliable estimation of the impulse response for both $\dot{V}_dCO_2$ and $\dot{V}_dO_2$. Based on the identified impulse response model, various statistical comparisons are developed and the comparison results are explained in terms of the physiological perspective. The bigger gain of $\dot{V}_dCO_2$ in onset demonstrates the human ATP storage during the relaxing status. Meanwhile, the quicker response speed of $\dot{V}_dCO_2$ in both periods explains why there is a delay due to the conversion from O_2 to CO_2. We believe the kernel-based non-parametric

modelling approach together with the developed impulse response models will significantly improve our understanding of human cardiorespiratory response to exercise, and provide instructive guidance for the regulation of exercise intensity to ensure efficiency and safety during the training and rehabilitation exercise.

In Chapter 5, the non-parametric model is applied to investigate the dynamics of $\dot{V}O_2$ responding to the stairs exercise. The self-designed application and $K4b^2$ gas analyser provide a reliable technique to record $\dot{V}O_2$ data and the exercise phase. The protocol of the experiment guarantees a continuous and random changing $\dot{V}O_2$ and the exercise phase. The identification results of a different number of periods are compared to illustrate the variation model of the system. Experimental results indicate that the model from the previous period is no longer suitable for the next period. The fixed-order model including three types of order are conducted as comparison approaches to demonstrate the benefit of using the non-parametric modelling approach. It can be concluded that the non-parametric model is stable and compatible for different participants in different periods. The complexity of human respiratory systems, as well as individual differences, are worth further in-depth research.

In Chapter 6, the kernel-based non-parametric method is also applied to identify the dynamics of $\dot{V}_dO_2$ and $\dot{V}_dCO_2$ responses to treadmill speed. In order to guarantee a sufficient stimulation of modelling, the parameter β selected from the stairs experiment is constructed and compared with β from the simulation. The data from the stairs experiment and this experiment protocol ensures a continuously changing input and physiological signal. The results demonstrate the benefits of using the non-parametric modelling method when the system structure cannot be described by a simple model. The fitness comparison also illustrates that when using the parameter β from the stairs experiment, the estimation results are better than the ones from the simulation because of the sufficiently random stimulation provided by the switching protocol and the continuously changing data of the stairs experiment.

7.2 Future work

Interesting directions for future work are detailed below.

- In Chapter 3, to further improve the effectiveness of the two proposed methods, the I-Calibration can be used to select the initial conditions, then the M-Calibration could be applied by using the well-selected initial values to ensure the convergence of the M-Calibration. In addition, the non-parametric model with kernel regularisation term could be implemented in the calibration method when the parameters of the model are more than nine. This method can omit the step of linearising the nonlinear model.

- In Chapter 4, the kernel-based non-parametric modelling approach together with the developed impulse response models could be investigated with more experiment data to understand the human cardiorespiratory response to exercise and provide instructive guidance for the regulation of exercise intensity to ensure efficiency and safety during training and rehabilitation exercise [125].

- In Chapter 5, owing to the changing structure of the physiological signal-exercise phase system [126], the complexity of human respiratory systems, as well as individual differences, it be worthwhile exploring these areas in more depth in future research.

- In Chapter 6, the next step in terms of research would be to apply an online modelling approach, which could adjust the system structure over time, to do the identification. [56, 127, 128].

References

[1] P. J. Maud and G. E. Longmuir, "A survey of health-fitness evaluation centers.," *Public Health Reports*, vol. 98, no. 1, p. 30, 1983.

[2] P. J. Maud and C. Foster, *Physiological assessment of human fitness*. Human Kinetics, 2006.

[3] S. A. Plowman and D. L. Smith, *Exercise physiology for health fitness and performance*. Lippincott Williams & Wilkins, 2013.

[4] J. Ilmarinen, R. Ilmarinen, A. Koskela, O. Korhonen, P. Fardy, T. Partanen, and J. Rutenfranz, "Training effects of stair-climbing during office hours on female employees," *Ergonomics*, vol. 22, no. 5, pp. 507–516, 1979.

[5] N. Butts, C. Dodge, and M. McAlpine, "Effect of stepping rate on energy costs during stairmaster exercise.," *Medicine and science in sports and exercise*, vol. 25, no. 3, pp. 378–382, 1993.

[6] C. A. Boreham, W. F. Wallace, and A. Nevill, "Training effects of accumulated daily stair-climbing exercise in previously sedentary young women," *Preventive Medicine*, vol. 30, no. 4, pp. 277–281, 2000.

[7] K. C. Teh and A. R. Aziz, "Heart rate, oxygen uptake, and energy cost of ascending and descending the stairs," *Medicine & Science in Sports & Exercise*, vol. 34, no. 4, pp. 695–699, 2002.

[8] K. J. Hunt, S. E. Fankhauser, and J. Saengsuwan, "Identification of heart rate dynamics during moderate-to-vigorous treadmill exercise," *Biomedical engineering online*, vol. 14, no. 1, p. 117, 2015.

[9] R. A. Cooper, T. L. Fletcher-Shaw, and R. N. Robertson, "Model reference adaptive control of heart rate during wheelchair ergometry," *IEEE transactions on control systems technology*, vol. 6, no. 4, pp. 507–514, 1998.

[10] H. Tanaka, K. D. Monahan, and D. R. Seals, "Age-predicted maximal heart rate revisited," *Journal of the American College of Cardiology*, vol. 37, no. 1, pp. 153–156, 2001.

[11] M. L. Pollock, G. A. Gaesser, J. D. Butcher, J.-P. Després, R. K. Dishman, B. A. Franklin, and C. E. Garber, "Acsm position stand: the recommended quantity and quality of exercise for developing and maintaining cardiorespiratory and muscular

fitness, and flexibility in healthy adults," *Med Sci Sports Exerc*, vol. 30, no. 6, pp. 975–991, 1998.

[12] E. T. Howley, "Type of activity: resistance, aerobic and leisure versus occupational physical activity," *Medicine & Science in Sports & Exercise*, vol. 33, no. 6, pp. S364–S369, 2001.

[13] S. M. Fox III and J. S. Skinner, "Physical activity and cardiovascular health," *The American journal of cardiology*, vol. 14, no. 6, pp. 731–746, 1964.

[14] J. McLaughlin, G. King, E. Howley, D. Bassett Jr, and B. Ainsworth, "Validation of the cosmed k4 b2 portable metabolic system," *International journal of sports medicine*, vol. 22, no. 04, pp. 280–284, 2001.

[15] B. Henning, R. Löfgren, and L. Sjöström, "Chamber for indirect calorimetry with improved transient response," *Medical and Biological Engineering and Computing*, vol. 34, no. 3, pp. 207–212, 1996.

[16] A. V. Hill, C. Long, and H. Lupton, "Muscular exercise, lactic acid, and the supply and utilisation of oxygen," *Proceedings of the Royal Society of London. Series B, Containing Papers of a Biological Character*, vol. 97, no. 681, pp. 84–138, 1924.

[17] A. M. Sabatini, C. Martelloni, S. Scapellato, and F. Cavallo, "Assessment of walking features from foot inertial sensing," *IEEE Transactions on biomedical engineering*, vol. 52, no. 3, pp. 486–494, 2005.

[18] R. Brugarolas, T. Latif, J. Dieffenderfer, K. Walker, S. Yuschak, B. L. Sherman, D. L. Roberts, and A. Bozkurt, "Wearable heart rate sensor systems for wireless canine health monitoring," *IEEE Sensors Journal*, vol. 16, no. 10, pp. 3454–3464, 2015.

[19] P. Li, R. Meziane, M. J.-D. Otis, H. Ezzaidi, and P. Cardou, "A smart safety helmet using imu and eeg sensors for worker fatigue detection," in *2014 IEEE International Symposium on Robotic and Sensors Environments (ROSE) Proceedings*, pp. 55–60, IEEE, 2014.

[20] O. Postolache, J. M. D. Pereira, V. Viegas, L. Pedro, P. S. Girão, R. Oliveira, and G. Postolache, "Smart walker solutions for physical rehabilitation," *IEEE Instrumentation & Measurement Magazine*, vol. 18, no. 5, pp. 21–30, 2015.

[21] V. Renaudin, M. H. Afzal, and G. Lachapelle, "Complete triaxis magnetometer calibration in the magnetic domain," *Journal of sensors*, vol. 2010, 2010.

[22] P. Guo, H. Qiu, Y. Yang, and Z. Ren, "The soft iron and hard iron calibration method using extended kalman filter for attitude and heading reference system," in *2008 IEEE/ION Position, Location and Navigation Symposium*, pp. 1167–1174, IEEE, 2008.

[23] M. Glueck, D. Oshinubi, P. Schopp, and Y. Manoli, "Real-time autocalibration of mems accelerometers," *IEEE Transactions on Instrumentation and Measurement*, vol. 63, no. 1, pp. 96–105, 2013.

[24] J. L. Crassidis, K.-L. Lai, and R. R. Harman, "Real-time attitude-independent three-axis magnetometer calibration," *Journal of Guidance, Control, and Dynamics*, vol. 28, no. 1, pp. 115–120, 2005.

[25] J. Fang, H. Sun, J. Cao, X. Zhang, and Y. Tao, "A novel calibration method of magnetic compass based on ellipsoid fitting," *IEEE Transactions on Instrumentation and Measurement*, vol. 60, no. 6, pp. 2053–2061, 2011.

[26] W. Koo, S. Sung, and Y. J. Lee, "Error calibration of magnetometer using nonlinear integrated filter model with inertial sensors," *IEEE Transactions on Magnetics*, vol. 45, no. 6, pp. 2740–2743, 2009.

[27] L. Ye and S. W. Su, "Optimum experimental design applied to mems accelerometer calibration for 9-parameter auto-calibration model," in *2015 37th Annual International Conference of the IEEE Engineering in Medicine and Biology Society (EMBC)*, pp. 3145–3148, IEEE, 2015.

[28] R. Alonso and M. D. Shuster, "Complete linear attitude-independent magnetometer calibration," *Journal of the Astronautical Sciences*, vol. 50, no. 4, pp. 477–490, 2002.

[29] I. Markovsky, A. Kukush, and S. Van Huffel, "Consistent least squares fitting of ellipsoids," *Numerische Mathematik*, vol. 98, no. 1, pp. 177–194, 2004.

[30] J. F. Vasconcelos, G. Elkaim, C. Silvestre, P. Oliveira, and B. Cardeira, "Geometric approach to strapdown magnetometer calibration in sensor frame," *IEEE Transactions on Aerospace and Electronic systems*, vol. 47, no. 2, pp. 1293–1306, 2011.

[31] D. Gebre-Egziabher, G. H. Elkaim, J. David Powell, and B. W. Parkinson, "Calibration of strapdown magnetometers in magnetic field domain," *Journal of Aerospace Engineering*, vol. 19, no. 2, pp. 87–102, 2006.

[32] W. Gander, G. H. Golub, and R. Strebel, "Least-squares fitting of circles and ellipses," *BIT Numerical Mathematics*, vol. 34, no. 4, pp. 558–578, 1994.

[33] D. Y. Kim, B. K. Kim, S. H. Park, K. S. KI, H. S. Shin, J. A. Na, Y. J. Kim, and Y. S. Choi, "Method for calculating the angle of inclination of magnetic field in a sensor coordination system," Mar. 2 2017. US Patent App. 15/132,545.

[34] M. Kok, J. D. Hol, T. B. Schön, F. Gustafsson, and H. Luinge, "Calibration of a magnetometer in combination with inertial sensors," in *2012 15th International Conference on Information Fusion*, pp. 787–793, IEEE, 2012.

[35] R. S. Methodology, "Process and product optimization using designed experiments," *Myers, RH and Montgomery, DC, John Wiely & Sons, New York*, 1995.

[36] A. Atkinson, A. Donev, and R. Tobias, *Optimum experimental designs, with SAS*, vol. 34. Oxford University Press, 2007.

[37] R. H. Myers, D. C. Montgomery, and C. M. Anderson-Cook, *Response surface methodology: process and product optimization using designed experiments*. John Wiley & Sons, 2016.

[38] D. C. Montgomery, *Design and analysis of experiments*. John wiley & sons, 2017.

[39] R. Mehra, "Optimal input signals for parameter estimation in dynamic systems–survey and new results," *IEEE Transactions on Automatic Control*, vol. 19, no. 6, pp. 753–768, 1974.

[40] J. Lopez-Fidalgo and S. A. Garcet-Rodríguez, "Optimal experimental designs when some independent variables are not subject to control," *Journal of the American Statistical Association*, vol. 99, no. 468, pp. 1190–1199, 2004.

[41] K. Chaloner and I. Verdinelli, "Bayesian experimental design: A review," *Statistical Science*, pp. 273–304, 1995.

[42] C. R. Rojas, J. S. Welsh, G. C. Goodwin, and A. Feuer, "Robust optimal experiment design for system identification," *Automatica*, vol. 43, no. 6, pp. 993–1008, 2007.

[43] S. Asprey and S. Macchietto, "Designing robust optimal dynamic experiments," *Journal of Process Control*, vol. 12, no. 4, pp. 545–556, 2002.

[44] M. Patan and D. UcińSki, "Configuring a sensor network for fault detection in distributed parameter systems," *International Journal of Applied Mathematics and Computer Science*, vol. 18, no. 4, pp. 513–524, 2008.

[45] A. I. Khuri and S. Mukhopadhyay, "Response surface methodology," *Wiley Interdisciplinary Reviews: Computational Statistics*, vol. 2, no. 2, pp. 128–149, 2010.

[46] D. M. Wardrop and R. H. Myers, "Some response surface designs for finding optimal conditions," *Journal of statistical planning and inference*, vol. 25, no. 1, pp. 7–28, 1990.

[47] L. Ye and S. W. Su, "Experimental design for the calibration of tri-axial magnetometers," in *2015 9th International Conference on Sensing Technology (ICST)*, pp. 711–715, IEEE, 2015.

[48] S. Mukhopadhyay and P. Sircar, "Parametric modelling of ecg signal," *Medical and Biological Engineering and computing*, vol. 34, no. 2, pp. 171–174, 1996.

[49] L. Lu, L. Hamzaoui, B. Brown, B. Rigaud, R. Smallwood, D. Barber, and J. Morucci, "Parametric modelling for electrical impedance spectroscopy system," *Medical and Biological Engineering and Computing*, vol. 34, no. 2, pp. 122–126, 1996.

[50] C.-C. Lin, C.-M. Chen, I.-F. Yang, and T.-F. Yang, "Automatic optimum order selection of parametric modelling for the evaluation of abnormal intra-qrs signals in signal-averaged electrocardiograms," *Medical and Biological Engineering and Computing*, vol. 43, no. 2, pp. 218–224, 2005.

[51] B. Henning, R. Löfgren, and L. Sjöström, "Chamber for indirect calorimetry with improved transient response," *Medical and Biological Engineering and Computing*, vol. 34, no. 3, pp. 207–212, 1996.

[52] T. Chen, H. Ohlsson, and L. Ljung, "On the estimation of transfer functions, regularizations and gaussian processes—revisited," *Automatica*, vol. 48, no. 8, pp. 1525–1535, 2012.

[53] G. Pillonetto, A. Chiuso, and G. De Nicolao, "Prediction error identification of linear systems: a nonparametric gaussian regression approach," *Automatica*, vol. 47, no. 2, pp. 291–305, 2011.

[54] G. Pillonetto and G. De Nicolao, "A new kernel-based approach for linear system identification," *Automatica*, vol. 46, no. 1, pp. 81–93, 2010.

[55] H. Leeb and B. M. Pötscher, "Model selection and inference: Facts and fiction," *Econometric Theory*, vol. 21, no. 1, pp. 21–59, 2005.

[56] T. Chen, M. S. Andersen, L. Ljung, A. Chiuso, and G. Pillonetto, "System identification via sparse multiple kernel-based regularization using sequential convex optimization techniques," *IEEE Transactions on Automatic Control*, vol. 59, no. 11, pp. 2933–2945, 2014.

[57] G. Pillonetto, F. Dinuzzo, T. Chen, G. De Nicolao, and L. Ljung, "Kernel methods in system identification, machine learning and function estimation: A survey," *Automatica*, vol. 50, no. 3, pp. 657–682, 2014.

[58] A. Chiuso, T. Chen, L. Ljung, and G. Pillonetto, "Regularization strategies for nonparametric system identification," in *Decision and Control (CDC), 2013 IEEE 52nd Annual Conference on*, pp. 6013–6018, IEEE, 2013.

[59] T. Chen and L. Ljung, "On kernel design for regularized lti system identification," *arXiv preprint arXiv:1612.03542*, 2016.

[60] T. Chen, "On kernel design for regularized lti system identification," *Automatica*, vol. 90, pp. 109–122, 2018.

[61] W. Van der Walt and C. Wyndham, "An equation for prediction of energy expenditure of walking and running.," *Journal of Applied Physiology*, vol. 34, no. 5, pp. 559–563, 1973.

[62] L. Puente-Maestu, M. Sanz, P. Sanz, J. R. De Ona, J. Rodriguez-Hermosa, and B. Whipp, "Effects of two types of training on pulmonary and cardiac responses to moderate exercise in patients with copd," *European Respiratory Journal*, vol. 15, no. 6, pp. 1026–1032, 2000.

[63] D. Abe, K. Yanagawa, and S. Niihata, "Effects of load carriage, load position, and walking speed on energy cost of walking," *Applied ergonomics*, vol. 35, no. 4, pp. 329–335, 2004.

[64] S. W. Su, L. Wang, B. G. Celler, and A. V. Savkin, "Oxygen uptake estimation in humans during exercise using a hammerstein model," *Annals of biomedical engineering*, vol. 35, no. 11, pp. 1898–1906, 2007.

[65] Y. Zhang, A. Haddad, S. W. Su, B. G. Celler, A. J. Coutts, R. Duffield, C. E. Donges, and H. T. Nguyen, "An equivalent circuit model for onset and offset exercise response," *Biomedical engineering online*, vol. 13, no. 1, p. 145, 2014.

[66] H. Yu, L. Ye, G. R. Naik, R. Song, H. T. Nguyen, and S. W. Su, "Nonparametric dynamical model of cardiorespiratory responses at the onset and offset of treadmill exercises," *Medical & biological engineering & computing*, pp. 1–15, 2018.

[67] G. Pillonetto and G. De Nicolao, "Kernel selection in linear system identification part i: A gaussian process perspective," in *Decision and Control and European Control Conference (CDC-ECC), 2011 50th IEEE Conference on*, pp. 4318–4325, IEEE, 2011.

[68] B. J. Whipp, J. A. Davis, F. Torres, and K. Wasserman, "A test to determine parameters of aerobic function during exercise," *Journal of Applied Physiology*, vol. 50, no. 1, pp. 217–221, 1981.

[69] S. F. Loy, L. M. Conley, E. R. Sacco, W. J. Vincent, G. J. Holland, E. G. Sletten, and P. R. Trueblood, "Effects of stairclimbing on vo2max and quadriceps strength in middle-aged females.," *Medicine and science in sports and exercise*, vol. 26, no. 2, pp. 241–247, 1994.

[70] S. W. Su, B. G. Celler, A. V. Savkin, H. T. Nguyen, T. M. Cheng, Y. Guo, and L. Wang, "Transient and steady state estimation of human oxygen uptake based on noninvasive portable sensor measurements," *Medical & biological engineering & computing*, vol. 47, no. 10, p. 1111, 2009.

[71] R. A. Cooper, F. Baldini, W. Langbein, R. Robertson, P. Bennett, and S. Monical, "Prediction of pulmonary function in wheelchair users," *Spinal Cord*, vol. 31, no. 9, p. 560, 1993.

[72] B. J. Whipp, S. A. Ward, N. Lamarra, J. A. Davis, and K. Wasserman, "Parameters of ventilatory and gas exchange dynamics during exercise," *Journal of Applied Physiology*, vol. 52, no. 6, pp. 1506–1513, 1982.

[73] K. Wasserman, J. E. Hansen, D. Y. Sue, W. W. Stringer, and B. J. Whipp, *Principles of exercise testing and interpretation: including pathophysiology and clinical applications*, vol. 206. Lippincott Williams & Wilkins Philadelphia, 1999.

[74] D. R. Bassett and E. T. Howley, "Limiting factors for maximum oxygen uptake and determinants of endurance performance," *Medicine and science in sports and exercise*, vol. 32, no. 1, pp. 70–84, 2000.

[75] J. Riedo and K. J. Hunt, "Feedback control of oxygen uptake during robotics-assisted end-effector-based stair climbing," *Systems Science & Control Engineering*, vol. 5, no. 1, pp. 142–155, 2017.

[76] J. A. Zoladz, B. Grassi, J. Majerczak, Z. Szkutnik, M. Korostyński, M. Grandys, W. Jarmuszkiewicz, and B. Korzeniewski, "Mechanisms responsible for the acceleration of pulmonary vo2 on-kinetics in humans after prolonged endurance training," *American Journal of Physiology-Regulatory, Integrative and Comparative Physiology*, vol. 307, no. 9, pp. R1101–R1114, 2014.

[77] D. Polle and A. Jones, "Towards an understanding of the mechanistic bases of vo2 kinetics: summary of key points raised in chapters 2—11," *Oxygen Uptake Kinetics in Sport, Exercise and Medicine*, pp. 294–328, 2007.

[78] R. A. Robergs and R. Landwehr, "The surprising history of the" hrmax= 220-age" equation," *Journal of Exercise Physiology Online*, vol. 5, no. 2, pp. 1–10, 2002.

[79] K. Wasserman, B. J. Whipp, S. Koyl, and W. Beaver, "Anaerobic threshold and respiratory gas exchange during exercise.," *Journal of applied physiology*, vol. 35, no. 2, pp. 236–243, 1973.

[80] W. E. Berg, "Individual differences in respiratory gas exchange during recovery from moderate exercise," *American Journal of Physiology-Legacy Content*, vol. 149, no. 3, pp. 597–610, 1947.

[81] K. Wasserman and M. B. McIlroy, "Detecting the threshold of anaerobic metabolism in cardiac patients during exercise," *The American journal of cardiology*, vol. 14, no. 6, pp. 844–852, 1964.

[82] S. N. Koyal, W. L. Beaver, *et al.*, "Anaerobic threshold and respiratory gas exchange during exercise," *J appl Physiol*, vol. 35, no. 82, p. 236, 1973.

[83] M. Galdston and A. Wollack, "Oxygen and carbon dioxide tensions of alveolar air and arterial blood in healthy young adults at rest and after exercise," *American Journal of Physiology-Legacy Content*, vol. 151, no. 2, pp. 276–281, 1947.

[84] H. Schmidt, N. R. Rypkema, and E. Fischell, "Submerged vehicle localization system and method," July 4 2019. US Patent App. 16/237,463.

[85] A. K. Bourke, P. Van De Ven, M. Gamble, R. O'Connor, K. Murphy, E. Bogan, E. McQuade, P. Finucane, G. ÓLaighin, and J. Nelson, "Assessment of waist-worn tri-axial accelerometer based fall-detection algorithms using continuous unsupervised activities," in *2010 Annual International Conference of the IEEE Engineering in Medicine and Biology*, pp. 2782–2785, IEEE, 2010.

[86] T. Lei, A. A. Mohamed, and C. Claudel, "An imu-based traffic and road condition monitoring system," *HardwareX*, vol. 4, p. e00045, 2018.

[87] M. H. Afzal, V. Renaudin, and G. Lachapelle, "Assessment of indoor magnetic field anomalies using multiple magnetometers," in *ION GNSS*, vol. 10, pp. 21–24, 2010.

[88] M. Kayton and W. R. Fried, *Avionics navigation systems*. John Wiley & Sons, 1997.

[89] S.-h. P. Won and F. Golnaraghi, "A triaxial accelerometer calibration method using a mathematical model," *IEEE Transactions on Instrumentation and Measurement*, vol. 59, no. 8, pp. 2144–2153, 2009.

[90] R. O. Kuehl and R. Kuehl, "Design of experiments: statistical principles of research design and analysis," 2000.

[91] L. Ye, S. W. Su, *et al.*, "Experimental design and its posterior efficiency for the calibration of wearable sensors," *Journal of Intelligent Learning Systems and Applications*, vol. 7, no. 01, p. 11, 2015.

[92] S. W. Su, L. Wang, B. G. Celler, A. V. Savkin, and Y. Guo, "Identification and control for heart rate regulation during treadmill exercise," *IEEE Transactions on biomedical engineering*, vol. 54, no. 7, pp. 1238–1246, 2007.

[93] S. W. Su, L. Wang, B. G. Celler, A. V. Savkin, and Y. Guo, "Modelling and control for heart rate regulation during treadmill exercise," in *Engineering in Medicine and Biology Society, 2006. EMBS'06. 28th Annual International Conference of the IEEE*, pp. 4299–4302, IEEE, 2006.

[94] H. Witte, F. Liese, S. Glaser, and D. Hoyer, "Results of modelling and physiological examination of movement-related heart-rate reactions in neonates," *Medical and Biological Engineering and Computing*, vol. 26, no. 6, pp. 599–604, 1988.

[95] E. Magosso and M. Ursino, "Cardiovascular response to dynamic aerobic exercise: A methematical model," *Medical and Biological Engineering and Computing*, vol. 40, no. 6, pp. 660–674, 2002.

[96] A. S. Tafreshi, J. Okle, V. Klamroth-Marganska, and R. Riener, "Modeling the effect of tilting, passive leg exercise, and functional electrical stimulation on the human cardiovascular system," *Medical & biological engineering & computing*, vol. 55, no. 9, pp. 1693–1708, 2017.

[97] A. C. of Sports Medicine, *Guidelines for exercise testing and prescription*. Williams & Wilkins, 1991.

[98] D. Abe, K. Yanagawa, and S. Niihata, "Effects of load carriage, load position, and walking speed on energy cost of walking," *Applied ergonomics*, vol. 35, no. 4, pp. 329–335, 2004.

[99] C. Wenzel, K. Golka, F. Klimmer, J. Rutenfranz, and H. Wenzel, "Volume calibration of various gasmeters using a modified tissot spirometer," *European journal of applied physiology and occupational physiology*, vol. 61, no. 5-6, pp. 380–385, 1990.

[100] R. Duffield, B. Dawson, H. Pinnington, and P. Wong, "Accuracy and reliability of a cosmed k4b2 portable gas analysis system," *Journal of Science and Medicine in Sport*, vol. 7, no. 1, pp. 11–22, 2004.

[101] V. Y. Skvortzov, H.-K. Lee, S. Bang, and Y. Lee, "Application of electronic compass for mobile robot in an indoor environment," in *Proceedings 2007 IEEE International Conference on Robotics and Automation*, pp. 2963–2970, IEEE, 2007.

[102] M. Kangas, A. Konttila, I. Winblad, and T. Jamsa, "Determination of simple thresholds for accelerometry-based parameters for fall detection," in *2007 29th Annual International Conference of the IEEE Engineering in Medicine and Biology Society*, pp. 1367–1370, IEEE, 2007.

[103] J. Chen, K. Kwong, D. Chang, J. Luk, and R. Bajcsy, "Wearable sensors for reliable fall detection," in *2005 IEEE Engineering in Medicine and Biology 27th Annual Conference*, pp. 3551–3554, IEEE, 2006.

[104] A. A. Kaufman, R. O. Hansen, and R. L. Kleinberg, *Principles of the magnetic methods in geophysics*. Elsevier, 2009.

[105] V. Renaudin, M. H. Afzal, and G. Lachapelle, "New method for magnetometers based orientation estimation," in *IEEE/ION Position, Location and Navigation Symposium*, pp. 348–356, IEEE, 2010.

[106] I. Frosio, F. Pedersini, and N. A. Borghese, "Autocalibration of mems accelerometers," *IEEE Transactions on Instrumentation and Measurement*, vol. 58, no. 6, pp. 2034–2041, 2008.

[107] L. Ye, Y. Guo, and S. W. Su, "An efficient autocalibration method for triaxial accelerometer," *IEEE Transactions on Instrumentation and Measurement*, vol. 66, no. 9, pp. 2380–2390, 2017.

[108] M. Kok and T. B. Schön, "Magnetometer calibration using inertial sensors," *IEEE Sensors Journal*, vol. 16, no. 14, pp. 5679–5689, 2016.

[109] E. L. Renk, M. Rizzo, W. Collins, F. Lee, and D. S. Bernstein, "Calibrating a triaxial accelerometer-magnetometer-using robotic actuation for sensor reorientation during data collection," *IEEE Control Systems Magazine*, vol. 25, no. 6, pp. 86–95, 2005.

[110] E. L. Renk, W. Collins, M. Rizzo, F. Lee, and D. S. Bernstein, "Optimization-based calibration of a triaxial accelerometer-magnetometer," in *Proceedings of the 2005, American Control Conference, 2005.*, pp. 1957–1962, IEEE, 2005.

[111] C. C. Foster and G. H. Elkaim, "Extension of a two-step calibration methodology to include nonorthogonal sensor axes," *IEEE Transactions on Aerospace and Electronic Systems*, vol. 44, no. 3, pp. 1070–1078, 2008.

[112] J. C. Springmann and J. W. Cutler, "Attitude-independent magnetometer calibration with time-varying bias," *Journal of Guidance, Control, and Dynamics*, vol. 35, no. 4, pp. 1080–1088, 2012.

[113] T. Chen, H. Ohlsson, G. C. Goodwin, and L. Ljung, "Kernel selection in linear system identification part ii: A classical perspective," in *Decision and Control and European Control Conference (CDC-ECC), 2011 50th IEEE Conference on*, pp. 4326–4331, IEEE, 2011.

[114] F. Peronnet, D. Massicotte, *et al.*, "Table of nonprotein respiratory quotient: an update," *Can J Sport Sci*, vol. 16, no. 1, pp. 23–29, 1991.

[115] P. Rich, "The molecular machinery of keilin's respiratory chain," 2003.

[116] L. Stryer, "Biochemistry, 1995," *Newyork, NY: WH Freeman and Co, Fourth Google Scholar*, 1995.

[117] N. M. Beltz, F. T. Amorim, A. L. Gibson, J. M. Janot, L. Kravitz, C. M. Mermier, N. Cole, T. A. Moriarty, T. P. Nunez, S. Trigg, *et al.*, "Hemodynamic and metabolic responses to self-paced and ramp-graded exercise testing protocols," *Applied Physiology, Nutrition, and Metabolism*, no. 999, pp. 1–8, 2018.

[118] H. C. Pinnington, P. Wong, J. Tay, D. Green, and B. Dawson, "The level of accuracy and agreement in measures of feo2, feco2 and ve between the cosmed k4b2 portable, respiratory gas analysis system and a metabolic cart," *Journal of Science and Medicine in Sport*, vol. 4, no. 3, pp. 324–335, 2001.

[119] G. Pillonetto and G. De Nicolao, "Kernel selection in linear system identification part i: A gaussian process perspective," in *Decision and Control and European Control Conference (CDC-ECC), 2011 50th IEEE Conference on*, pp. 4318–4325, IEEE, 2011.

[120] T. Chen, H. Ohlsson, G. C. Goodwin, and L. Ljung, "Kernel selection in linear system identification part ii: A classical perspective," in *Decision and Control and European Control Conference (CDC-ECC), 2011 50th IEEE Conference on*, pp. 4326–4331, IEEE, 2011.

[121] T. Chen and L. Ljung, "Implementation of algorithms for tuning parameters in regularized least squares problems in system identification," *Automatica*, vol. 49, no. 7, pp. 2213–2220, 2013.

[122] A. Hill and C. Long, "Muscular exercise, lactic acid, and the supply and utilisation of oxygen," *Ergebnisse der Physiologie*, vol. 24, no. 1, pp. 43–51, 1925.

[123] K. E. Atkinson, "On the order of convergence of natural cubic spline interpolation," *SIAM Journal on Numerical Analysis*, vol. 5, no. 1, pp. 89–101, 1968.

[124] G. H. Golub and C. F. Van Loan, "Johns hopkins studies in the mathematical sciences," 1996.

[125] P. H. Charlton, T. Bonnici, L. Tarassenko, D. A. Clifton, R. Beale, and P. J. Watkinson, "An assessment of algorithms to estimate respiratory rate from the electrocardiogram and photoplethysmogram," *Physiological measurement*, vol. 37, no. 4, p. 610, 2016.

[126] P.-B. Wieber, "Trajectory free linear model predictive control for stable walking in the presence of strong perturbations," in *2006 6th IEEE-RAS International Conference on Humanoid Robots*, pp. 137–142, IEEE, 2006.

[127] S. Bonettini, A. Chiuso, and M. Prato, "A scaled gradient projection method for bayesian learning in dynamical systems," *SIAM Journal on Scientific Computing*, vol. 37, no. 3, pp. A1297–A1318, 2015.

[128] G. Prando, D. Romeres, and A. Chiuso, "Online identification of time-varying systems: A bayesian approach," in *2016 IEEE 55th Conference on Decision and Control (CDC)*, pp. 3775–3780, IEEE, 2016.

Appendix A

List of Main Variables

Table A.1 List of Main Variables.

Variables	Description
$\dot{V}O_2$	Oxygen Uptake
$\dot{V}CO_2$	Carbon Dioxide Output
ECG	Electrocardiogram
EMG	Electromyogram
EEG	Electroencephalogram
IMU	Inertial Measurement Unit
I-Calibration	Inclination based Calibration
M-Calibration	Magnitude based Calibration
HR	Heart Rate
HR_{max}	Maximum Heart Rate
TAs	Tri-Axial Accelerometers
TMs	Tri-Axial Magnetometers
TGs	Tri-Axial Gyroscopes
IMU	Inertial Measurement Unit
MEMS	Micro Electro Mechanical Systems
DoE	Design of Experiment
FIM	Fisher Information Matrix
CCD	Central Composite Design
BBD	Box-Behnken Design

$\dot{V}O_2^0$	Initial Value of O_2 Output
R_A	Response Amplitude
T_D	Time Delay
τ	Time Constant
AHRS	Attitude and Heading Reference Systems
MAD	Magnetic Anomaly Detection
$\mathbf{M^m}$	measurement magnetic value
$\mathbf{M^r}$	local magnetic field
$\mathbf{M^c}$	calibrated magnetic value
$\mathbf{M^s}$	simulated magnetic value
$\mathbf{A^m}$	measured acceleration
$\mathbf{A^r}$	acceleration field
$\mathbf{A^c}$	calibrated acceleration value
$\mathbf{A^s}$	simulated acceleration value
$\mathbf{G_s}$	scale factors
$\mathbf{G_e}$	nonorthogonality and misalignment of the sensors
$\mathbf{G}$	simplified matrix from $\mathbf{G_s G_e}$
β_M and β_I	unknown parameter vector
$\mathbf{X_M}$ and $\mathbf{X_I}$	observation matrix
L	constant for I-Calibration
φ	tolerance angle
H_M	calibrated magnitude value by M-Calibration
H_I	calibrated magnitude value by I-Calibration
H_0	raw magnitude value
SD	standard deviation
MAD	mean absolute deviation
MAV	mean absolute value
IR	impulse response
FIR	Finite Impulse Response
SR	Step response
$\boldsymbol{\theta}$	FIR coefficients
$\boldsymbol{P}$	kernel matrix
SS	Stable Spline kernel
DC	Diagonal/ Correlated kernel
DI	Diagonal kernel
$\dot{V}_d CO_2$	$\dot{V}CO_2$ normalized by weight
$\dot{V}_d O_2$	$\dot{V}O_2$ normalized by weight
NRMSE	normalised root mean square error